TECHNISCHE UNIVERSITÄT DRESDEN

Loss of *lrrk2* impairs dopamine catabolism, cell proliferation, and neuronal regeneration in the zebrafish brain

DISSERTATION
zur Erlangung des akademischen Grades

Doctor of Philosophy (Ph.D.)

vorgelegt der Fakultät Mathematik und Naturwissenschaften
der Technische Universität Dresden

von

Stefano Suzzi

geboren am 8. August 1988 in Gaeta, Italien

Gutachter:
Prof. Dr. Michael Brand, TUD
Prof. Dr. Gerd Kempermann, TUD

Eingereicht am .... Tag der Verteidigung: ....

FORSAN ET HÆC OLIM MEMINISSE IVVABIT

Virgil, *Aeneid*, I.203

Abstract

Mutations in the leucine-rich repeat kinase 2 (*LRRK2*) gene are a major genetic cause of Parkinson's disease (PD), which is why modelling PD by replicating their effects in animal models attracts great interest. However, the exact mechanisms of pathogenesis are still unclear. While a gain-of-function hypothesis generally receives consensus, there is evidence supporting an alternative loss-of-function explanation. Yet, neither overexpression of the human wild-type LRRK2 protein or its pathogenic variants, nor *Lrrk2* knockout recapitulates key aspects of human PD in rodent models. Furthermore, there is conflicting evidence from morpholino knockdown studies in zebrafish regarding the extent of zygotic developmental abnormalities.

Because reliable null mutants may be useful to infer gene function, and because the zebrafish is a more tractable laboratory vertebrate system than rodents to study disease mechanisms *in vivo*, clustered regularly interspaced short palindromic repeats (CRISPR)/CRISPR-associated protein-9 nuclease (Cas9) genomic editing was used to delete the $\sim$60-kbp-long zebrafish *lrrk2* locus containing the entire open reading frame. Constitutive removal of both the maternal and the zygotic *lrrk2* function (*mzLrrk2* individuals) causes a pleomorphic phenotype in the larval brain at 5 days post-fertilisation (dpf), including increased cell death, delayed myelination, and reduced and morphologically abnormal microglia/leukocytes. However, the phenotype is transient, spontaneously attenuating or resolving by 10 dpf, and the mutants are viable and fertile as adults. These observations are mirrored by whole-larva transcriptome data, revealing a more than eighteen-fold drop in the number of differentially expressed genes in *mzLrrk2* larvae from 5 to 10 dpf. Additionally, analysis of spontaneous swimming activity shows hypokinesia as a predictor of Lrrk2 protein deficiency in larvae, but not in adult fish.

Because the catecholaminergic (CA) neurons are the main clinically relevant target of PD in humans, the CA system of larvae and adult fish was analysed on both cellular and metabolic level. Despite an initial developmental delay at 5 dpf, the CA system is structurally intact at 10 dpf and later on in adult fish aged 6 and 11 months. However, monoamine oxidase (Mao)-dependent degradation of biogenic amines, including dopamine, is increased in older fish, possibly suggesting impaired synaptic transmission or a leading cause of cell damage in the long term.

Furthermore, decreased mitosis rate in the larval brain was found, in the anterior portion only at 5 dpf, strongly and throughout the whole organ at 10 dpf. Conceivably, *lrrk2* may have a more general role in the control of cell proliferation during early development and a more specialised one in the adult stage, possibly conditional, for example upon brain damage. Because the zebrafish can regenerate lost neurons, it represents a unique opportunity to elucidate the endogenous processes that may counteract neurodegeneration in a predisposing genetic back-

ground. To this aim, the regenerative potential of the adult telencephalon upon stab injury was tested in *mzLrrk2* fish. Indeed, neuronal proliferation was reduced, suggesting that a complete understanding of Lrrk2 biology may not be fully appreciated without recreating challenging scenarios.

To summarise, the present results demonstrate that loss of *lrrk2* has an early effect on zebrafish brain development that is later often compensated. Nonetheless, perturbed aminergic catabolism, and specifically increased Mao-dependent aminergic degradation, is reported for the first time in a *LRRK2* knockout model. Furthermore, a link between Lrrk2 and the control of basal cell proliferation in the brain, which may become critical under challenging circumstances such as brain injury, is proposed. Future directions should aim at exploring which brain cell types are specifically affected by the *mzLrrk2* hypoproliferative phenotype and the resulting consequences on a circuitry level, particularly in very old fish (i.e., over 2 years of age).
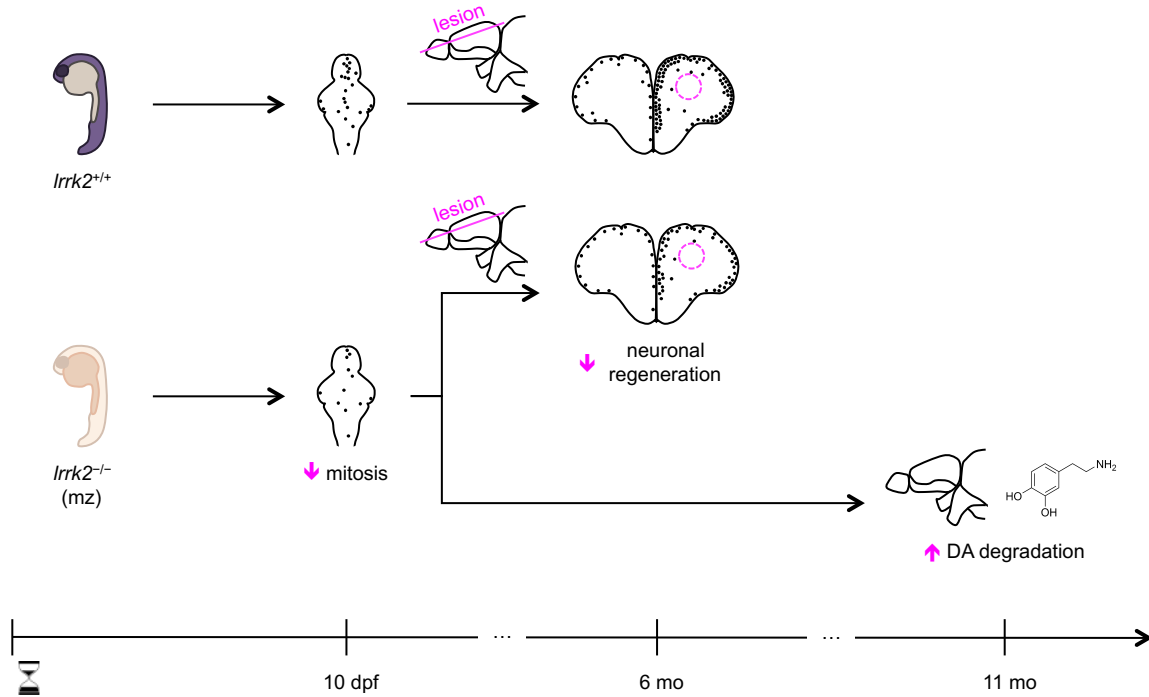

Figure 1: Overview of the main findings. Removal of both maternal and zygotic *lrrk2* (mz) determines reduced mitosis rate in the larval brain and defective neuronal regeneration upon stab in the adult telencephalon. Older fish also display perturbed aminergic catabolism, most prominently increased dopamine degradation.

Acknowledgements

Contents

List of Figures

List of Tables

Preface

The present dissertation has been written to fulfil the graduation requirements of the Technische Universität (TU) Dresden and is ultimately based on my original work conducted from November 2012 to April 2017 in Michael Brand laboratory, Biotechnology Center TU Dresden (BIOTEC)/DFG-Center for Regenerative Therapies TU Dresden (CRTD), Dresden, Germany.

None of the text is taken directly from previously published articles. Parts of the text interpolate material from the manuscript entitled "Loss of *lrrk2* impairs dopamine catabolism, cell proliferation, and neuronal regeneration in the zebrafish brain" authored by Stefano Suzzi (BIOTEC/CRTD), Reiner Ahrendt (BIOTEC/CRTD), Stefan Hans (BIOTEC/CRTD), Svetlana Semenova (Neuroscience Center, Institute of Biomedicine/Anatomy, University of Helsinki, Helsinki, Finland), Saygın Bilican (BIOTEC/CRTD), Shady Sayed (BIOTEC/CRTD), Sylke Winkler (Max Planck Institute of Molecular Cell Biology and Genetics, Dresden, Germany), Sandra Spieß (BIOTEC/CRTD), Jan Kaslin (BIOTEC/CRTD; present address: Australian Regenerative Medicine Institute, Monash University, Clayton, Australia), Pertti Panula (Neuroscience Center, Institute of Biomedicine/Anatomy, University of Helsinki, Helsinki, Finland), and Michael Brand (BIOTEC/CRTD). As of today, 17 Sep, 2017, the manuscript is under revision at a prominent journal; a preprint is available on bioRxiv at the following link: `http://www.biorxiv.org/content/early/2017/08/01/140608`.

My research project has been developed together with and under the supervision of Michael Brand. Experimental support has been provided as henceforth acknowledged.

Fish care has been provided by the Fish Facility (BIOTEC/CRTD).

The *lrrk2*$^{\text{tud115}}$ and *lrrk2*$^{\text{tud113}}$ zebrafish alleles herein described have been designed by Stefan Hans. The founder fish for the *tud115* line have been generated by Christopher Spiegel (BIOTEC/CRTD) and Sandra Spieß; the founder fish for the *tud113* line have been generated by Sandra Spieß.

Sectioning of the adult zebrafish heads used for this dissertation has been carried out by the Histology Facility (BIOTEC).

The anti-Claudin k antibody was provided by Michel Reimer (CRTD); the anti-L-Plastin antibody was provided by Michael J. Redd (Department of Pathology, University of Utah, Salt Lake City, Utah, USA).

All microscopes used were provided by the Light Microscopy Facility (BIOTEC/CRTD).

High performance liquid chromatography and immunoblotting were performed by Svetlana A. Semenova and Pertti Panula.

The behavioural data herein analysed have been generated by Saygın Bilican and Shady Sayed. The syringe pump used for assessment of the olfactory response

Introduction

Clinical signs of limb tremor and postural instability have been known since ancient times, but it is only at the onset of the 19th century that a "shaking palsy" was first recognised by James Parkinson and later more thoroughly characterised by Jean-Martin Charcot[1]. Today, Parkinson's disease (PD, OMIM entry 168600) is one of the most common movement disorders, affecting approximately seven million people globally, with incidence between 8 and 18 per 100,000 persons-years[2]. Typically associated with ageing, the onset usually occurs after the age of 60, but it may be earlier in individuals with family history[3]; women may experience a two-year later onset and a milder phenotype than men[4]. PD patients are characterised by a motor syndrome comprising resting tremor, rigidity, postural instability, and bradykinesia, or slowness of movement. However, pathology is highly variable and not even only motoric: sensory, sleep, neuropsychiatric, and cognitive problems may also occur, alone or in combination, at different stages of disease[5]. On a neuropathological level, PD is characterised by one invariant feature that is the loss of dopaminergic (DA) neurons in the *substantia nigra pars compacta*. It is estimated that DA neuronal loss amounts to 30% by the time motor symptoms appears, though higher percentages are also proposed[6]. A common feature is the presence of Lewy bodies, abnormal protein aggregates associated with several neurodegenerative disorders, mainly composed of α-synuclein and ubiquitin[7]. In particular, Lewy body pathology is better correlated with non-motor symptoms[8]. It shall also be noted that PD is a multisystem disorder and, although relatively less understood, non-DA dysfunction seems to play an important pathophysiological role as well, particularly in the prodromic stages of disease[9].

Lengthening of the average human life and demographic ageing make the prevalence of PD worldwide destined to increase and this renders PD one of the most serious health urgencies of modern societies. Current treatments are only symptomatic as incapable of stopping neurons to die[10]. Although several genetic conditions and risk factors have been widely investigated and the molecular mechanisms of neuropathology are being day-by-day elucidated, in most cases PD is idiopathic, as no specific cause can be attributed[11]. Moreover, a reliable *in vivo* model displaying comprehensive PD pathology is lacking. This does not mean that present models are limited beyond translational research. On the contrary, much of what is currently known about disease mechanisms and progression would have hardly been established otherwise. Animal models are indispensable when it comes to dissect out what mechanisms are impacted in the early stages of the disease and how the diseased brain responds to therapeutics. Rather, their limited translational amenability is chiefly due to an unfocused definition of their range

of validity combined with the paucity of preclinical studies in humans[12].

In the following section, the general criticalities of modelling PD in animals will be illustrated, with particular emphasis on genetic models. For reasons of consistency with the scopes of the present work, and not to lessen their importance[13,14], *in vitro* models will not be considered.

1.1 Modelling PD: the Sisyphean task

Current PD animal models span from invertebrates to mammals. Although the DA system, the most clinically relevant target of PD, is fundamentally conserved in all chordates[15], humans are the only species where PD naturally occurs. The reason may lie in the functional flexibility of the DA system, resulting in a remarkable degree of diversification even within mammals[15]. Because there is no natural animal counterpart of human PD, the only way to study PD-like features in animals is to generate induced models. This can be achieved either chemically or genetically.

Historically, chemical models were the first to be introduced and are still widely used nowadays[16]. Commonly, but not exclusively, used DA neurotoxins are 6-hydroxydopamine (6-OHDA), 1-methyl-4-phenyl-1,2,3,6-tetrahydropyridine (MPTP), rotenone, and paraquat. However useful to investigate the consequences of DA neuronal loss and test (mainly symptomatic) treatments, chemical models present several limitations, the most important of which are (*i*) the acuteness and transiency of key features, compared to the slow and chronic progression of human PD, and (*ii*) the comparability and reproducibility of reported phenotypes, as different drugs have different mechanisms of actions, elicit different effects, and different species or even strains of the same species have different susceptibility[17].

Genetic models take advantage of mutations in a number of genes being responsible for monogenic forms of hereditary and sporadic PD[18]. One of these is *LRRK2*, the leading theme of the present work, reviewed in detail further below (see 1.2). Here it will suffice to highlight that PD has an impressive genetic heterogeneity, emerged mainly via linkage analysis[19], with up to twenty loci (termed "*PARK*") so far identified, distributed over nine autosomal and one sex (X) chromosomes; there is also evidence for contributing mitochondrial mutations (OMIM entry 556500). PD-associated autosomal mutations are the majority, with some being recessive, others (like the ones in *LRRK2*) dominant. To complicate the picture further, several genetic or environmental modifiers can influence the phenotypic onset and strength[20–22]. Mechanistically, these mutations cause either a gain of toxic function (GOF) or loss of a protective function (LOF). These effects can be mimicked in animal models in several ways; the most popular include: to achieve GOF, the generation of knockin models overexpressing the (typically human) wild-type or mutant gene product of interest; to achieve LOF, the generation of knockout models or the induction of transient knockdown. Hypomorphic rather than amorphic phenotypes may sometimes be useful as more closely mimicking the effects of inhibitor drugs. Recently, viral vectors have been used to drive the expression/induce conditional knockout of PD-associated genes in a regionally-

controlled manner[23]. Despite the tantamount advances in the genome editing field and the generation of a wealth of models, so far no one develops a degenerative phenotype sufficiently comparable to human PD.

1.1.1   GOF and LOF models: general caveats

Promises and drawbacks of established genetic models for PD have been reviewed in detail elsewhere[24,25]. Here their limitations from a more general point of view will be discussed. A critical issue concerns the choice of the animal model. No matter the degree of homology with humans, even slight dissimilarities between orthologous genes of interest, network of interactions, cellular and extracellular milieux can make disease-causing mutations work simply differently in the model. Furthermore, because almost all of the genetic approaches used are effective since early development, compensatory mechanisms in embryos/juveniles may attenuate vulnerability in adults. Inducible models could overcome this inconvenience, but they may display discrepancies depending on age at/duration of induction.

Methodological considerations are not secondary; for more details on the advantages and drawbacks of different techniques to interfere with/modify gene function, dedicated reviews are referred to[26–28]. For GOF models, a major problem is the very construction of the transgene. Depending on the strategy used, the animal may either express the transgene in all of its cells, or be chimeric. While in the latter case the model might better reflect sporadic pathology[29], it would be more difficult to analyse due to phenotypic variability. In order to more closely model disease, transgene knockin should be performed in a null background. On the contrary, in all models the transgene is merely added while leaving the endogenous, wild-type counterpart intact, and without controlling the integration site. Another problem is the choice of the promoter. Very strong and ubiquitous promoters artificially enhance the expression of the mutant product everywhere in the organism, whereas the slowness of PD onset and progression in humans would rather suggest gradually mounting and anatomically confined effects. On the other hand, cell-specific promoters make it hard to dissect out non cell-autonomous mechanisms.

For LOF models, the major concern is the genomic context of the disrupting mutation. Large deletions and subsequent chromosomal rearrangements may introduce dramatic changes in the topology of cis-regulatory elements, for example via enhancer adoption[30]. Small insertions/deletions can disrupt inter- or intragenic non-coding RNA genes or be bypassed via alternative splicing. Stability of prematurely-stopped RNAs or presence of downstream alternative in-frame translation initiation sites may give rise to truncated protein products with residual or even new functions. More frequently, mutant RNAs undergo nonsense-mediated decay[31]. However, constitutive production of mutant RNAs highjacks RNA quality control systems, normally preventing the accumulation of randomly occurring nonfunctional RNAs, but also deputed to a gamut of other cell homeostatic functions[32]. As a result, artificially occurring nonfunctional RNAs might cause toxicity via cellular stress, rather than pure LOF. Knockdown strategies are even more ambiguous, as their efficacy depends on gene dosage. Transient knockdown on a

post-transcriptional level have the additional problem of the route of administration to cells, which limits its application on complex animals like mammals. A last but not least *memento* is maternal effects. Very well known in invertebrates, particularly drosophila, but relatively little investigated in vertebrates, despite the spur from recent maternal-effect screens in zebrafish[33], this aspect is typically overlooked in mammalian (and not only) models.

Whatever strategy is chosen, it is imperative to verify the specificity of putative phenotypes to exclude potential off-target effects. For GOF models, this would entail inhibitive manipulations like knockdown or pharmacologic treatment, which also posit concerns about specificity; for LOF models, reestablishment of the lost function should be attained via either RNA/plasmid injection, preferable with tractable models but prone to mosaicism, or generation of genetically reconstituted lines, cleaner but more time-consuming. Finally, once a model is generated, its usefulness has to be addressed. This apparently trivial consideration is actually of pivotal importance, as phenotypes may not be macroscopic or immediate, but observable only under suitable paradigms, whose adoption or *de novo* design is particularly problematic when "chasing in the dark", i.e. when too little (and sometimes even, on the opposite, too much) corollary information on the gene of interest is available.

In the next sections, the role of LRRK2 in both physiology and PD-related pathology will be introduced and the difficulties with current *LRRK2* models discussed.

1.2 The enigma of *LRRK2*

In 2002, the discovery of the eighth *PARK* locus (*PARK8, 12p11.2–q13.1*) provided the first genetic link for late-onset PD in families characterised by autosomal dominant inheritance pattern[34]. Two years later, two independent studies[34,35] identified mutations segregating with *PARK8*-linked PD and located in a single large gene (51 exons spanning 144 kbp) putatively coding for a cytoplasmic kinase, termed "dardarin" (from the Basque word *dardara*, 'tremor') or, as today more commonly known, "leucine-rich repeat kinase 2" (LRRK2, because of the similarity with a predicted LRRK1 kinase previously reported[36]). Since then, several *LRRK2* gene polymorphisms have been identified, but only five segregate with disease in large families: c.5096A>G (p.Tyr1699Cys), c.4321C>T (p.Arg1441Cys), c.4321C>G (p.Arg1441Gly), c.6059T>C (p.Ile2020Thr), and c.6055G>A (p.Gly2019Ser)[37]. Altogether, they represent the most recurrent genetic cause of familial and sporadic late-onset PD, accounting for 5–13% of familial and 1–5% of sporadic PD cases[38]. For this reason, LRRK2 and its PD-associated variants have been receiving growing attention (Figure 1.1).

In particular, the last pathogenic amino acid substitution to be identified, Gly2019Ser[40], is also the most common (4% of familial and 1% of sporadic PD cases[41]) and thereby the privileged subject of investigation. Studies on Gly2019Ser epidemiology have revealed the complexity of the genotype-phenotype relationship. Symptomatic Gly2019Ser carriers are variably frequent in different ethnic
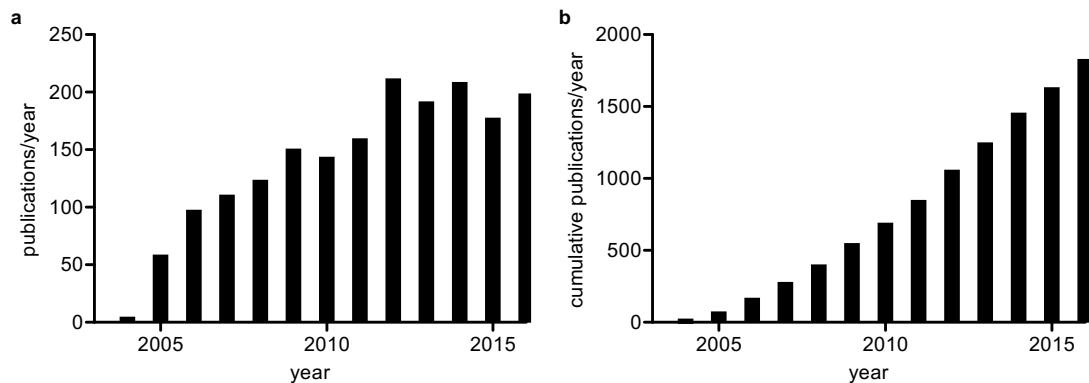
Figure 1.1: Yearly publication trend for `lrrk2` query. Statistics retrieved from Medline[39].

groups (2% of general North American and English population, up to 40% of North African Arabs and Ashkenazi Jews, very rare in Asia[37,42]), more likely to be women[43] and over 60 years of age (PD risk 28% at age 59, 51% at 69, and 74% at 79 years[41]). However, although the penetrance may be higher in homozygotes[44], the phenotype is not worse than in heterozygotes[45,46]. Interestingly, clinically unaffected homozygous individuals have been reported, one of them aged 70 years[46]. It shall also be noted that, despite a consistent overlap with levodopa-sensitive idiopathic PD[8], different mutations may yield different phenotypes. In Gly2019Ser carriers tremor typically appears first; Lewy body pathology is a common finding, but not in non-Gly2019Ser carriers, where a more pleomorphic neuropathology is present, including neurofibrillary tangles, atypical cytosolic fibrils, and motor neuron degeneration[37]. These findings suggest that *LRRK2* mutations may converge on PD via distinct routes. Genetic[47,48] and/or environmental factors may influence phenotypic penetrance, and *LRRK2* itself may be a disease modifier gene[49].

Drawing up the identikit of LRRK2 is further complicated by the elusiveness of its biological role. LRRK2 is a large (2,527 aa) multidomain protein and a bifunctional enzyme, displaying both mitogen-activated protein kinase kinase kinase (MAPKKK), and Ras of complex proteins (ROC) GTPase activities[50]. Several lines of evidence suggest the functional interaction between the two enzymatic domains[51]. In particular, the GTP-bound state is considered the "on" state, as it increases kinase activity[52]. Therefore, the GTPase activity may serve as a molecular switch for the kinase activity. However, the reverse scenario is also plausible[53], as LRRK2 can phosphorylate itself *in vitro*, and most of the autophosphorylation sites lie within the ROC domain[54]. Self-dimerisation of LRRK2 is required for normal functioning[55]. LRRK2 dimers are enriched in membrane fractions and display higher kinase activity than the cytosolic monomeric counterparts[56]. Moreover, the presence of both an ankyrin-like domain (ANK) and a leucine-rich repeat domain (LRR) in the first half of the protein and a tryptophan-aspartic acid repeat (WD40) at the C-terminus suggest that LRRK2 acts as a scaffold for protein-protein interactions[57,58]. Indeed, several interactors have been identified via immunoprecipitation studies[59,60]. These include proteins involved in

cytoskeleton dynamics, like actin isoforms and actin-associated proteins. Notable proposed interactors include PD-associated proteins α-synuclein[61] and parkin[62]. A commendable effort has been the deep-curation of published data to generate an updated visual review of LRRK2 interactome[63]. Despite its relevance for PD, LRRK2 protein is surprisingly scant in the brain, where its expression is scored as "low" according to the Human Protein Atlas[64], compared to other peripheral organs, and prominently lung ("high" score) and kidney ("medium" score). Although only one protein product has been currently characterised, alternative splice forms are possible[65]. In this regard, an interesting study has identified two Lrrk2 splice forms in mice, one resulting from exon 5 skipping, primarily expressed in astrocytes, the other truncated, terminating with an alternative exon 42a, also expressed in neurons[66].

Given the above complexity, it would be easier to mine what biological process LRRK2 *has not* been implicated, than otherwise. It would be beyond the scopes of the present work to review them all; on the other hand, information on LRRK2 functions is still too vague to discern representative ones. Major areas of investigation concern the involvement of LRRK2 in synaptic vesicle functions, cytoskeleton dynamics, mitochondrial biology, and autophagy. For an overview, excellent reviews are referred to[67–69]. It is easy to see that such cellular processes are so general, that dysfunctional LRRK2 may very well partake in a wide gamut of disease states, even unrelated to the brain. Indeed, *LRRK2* polymorphisms have been linked to Crohn's disease (a type of inflammatory bowel disease), cancer, and leprosy[70]. Conceivably, the clarification of non-brain-related signalling pathways is instrumental to predicting the outcome of brain-targeted therapeutic strategies.

In order to characterise and study LRRK2 biology *in vivo*, a flurry of animal models have been developed. These include *C. elegans* and *D. melanogaster*[71]; however, because worm *lrk-1* and fly *lrrk* genes are not true orthologues of the mammalian *LRRK2* gene[72], these models will not be considered. Clearly, the generation of animal models has taken advantage of the discovery of *LRRK2* mutations and will assist the elucidation of their modes of action. Among these, the billion dollar question: what makes LRRK2 toxic?

1.2.1   *LRRK2* gene mutations and PD: GOF or LOF?

The exact involvement of LRRK2 in pathology is incompletely understood. Established or putatively pathogenic variants all fall within or nearby the catalytic core[73]. The ones in the MAPKKK domain (Gly2019Ser, Ile2020Thr) increase kinase activity[74,75] (but for Ile2020Thr the opposite is also claimed[76]), whereas the ones in the ROC domain (Arg1441Cys/Gly, Ile1371Val) increase GTP binding and at least two (Arg1441Cys/Gly) decrease GTPase activity[77] *in vitro*. Pathogenic effects may be also mediated by altered molecular interactions, both within and between LRRK2 monomers. In support of this, the Tyr1699Cys substitution in the COR domain strengthens the ROC:COR intramolecular interaction and weakens LRRK2 dimerisation locally at the ROC-COR tandem domain, akin to Arg1441Cys/Gly/His substitutions, thus leading to decreased GTPase actvity[78].

If the GTPase activity is upstream to the kinase activity, pathogenic variants in the ROC-COR tandem domain might promote the GTP-bound "on" state and hence be analogous to the pathogenic variants in the MAPKKK domain. This reasoning has led to the unifying hypothesis that *LRRK2* mutations confer toxicity via a GOF of the kinase domain. This interpretation receives support from knockin mice carrying human pathogenic *LRRK2* variants and displaying PD-relevant phenotypes, albeit alternately, such as DA neuronal defects[79–82], impaired DA transmission[79,82,83], reduced dopamine levels[80], and behavioural abnormalities[79,81,84].

However, the "GOF hypothesis" is not completely airtight. First of all, different mutations may or may not converge on the same pathways, with some possibly being unrelated to PD[85]. Secondly, the current lack of reliable endogenous substrates or interaction partners makes it impossible to validate *in vitro* findings *in vivo*. More critically, mice overexpressing human wild-type[86] or mutant LRRK2[79–84] do not generally recapitulate DA cell loss, unless transgene levels are artificially enhanced using strong promoters[80,87–90]; Lewy body pathology has never been reported. Paradoxically, enhanced LRRK2 activity in Gly2019Ser knockin mice confers a hyperkinetic phenotype and protects from age-related motor impairment[91]. A further challenge comes from evidence that the Gly2385Arg variant in the WD40 domain, a risk factor for PD in the Chinese ethnicity[92,93], reduces kinase activity[94,95] and enhances LRRK2 degradation[96]. A similar dominant negative effect has been described also for the Ile2020Thr variant[97], usually considered a GOF. This commonality may be the result of both Gly2385Arg and Ile2020Thr increasing GTPase activity[95], possibly favouring the GDP-bound "off" state. Finally, pathogenic variants may disrupt protein-protein interactions that may be essential in cell signalling pathways. Along this line, it has been shown that the substitutions Arg1441Cys/Gly/His, Tyr1699Cys, and Ile2020Thr, but not Gly2019Ser, reduce phosphorylation of LRRK2 residues Ser910/Ser935 in Swiss 3T3 cells, thus disrupting the interaction with 14-3-3 protein and causing non-14-3-3 bound LRRK2 to accumulate in inclusion body-like cytosolic pools[98]. These observations back up an alternative "LOF hypothesis", bolstered by *Lrrk2* knockout in rodents being pathogenic in peripheral organs[99–101]. Remarkably, *Lrrk2* knockout mice develop PD-like pathology in the kidney, most prominently accumulation and aggregation of α-synuclein, but not in the brain[101]. Yet, LRRK2 deficiency in mice induces behavioural alterations similar to BAC human LRRK2 G2019S transgenic mice[102,103]. Conceivably, brain functions other than the DA ones may be implicated.

In a nutshell, both the GOF and the LOF hypotheses present supporting evidence as well as shortcomings. This raises the need of a "look-elsewhere" approach. A possibility to reconcile them would be to consider both mechanisms as two sides of the same coin in the context of PD aetiopathology. If LRRK2 partakes in a tightly regulated system where its activity is optimal within, detrimental outside a certain range, then both hyperactive and hypofunctional LRRK2 could push towards disease. This concept has been suggested since the discovery that Lrrk-mediated phosphorylation of EndophilinA at Ser75 is required for synaptic vesicle endocytosis in drosophila[104]. Dephosphorylated EndophilinA interacts with the

synaptic membrane, induces its deformation, and drives vesicle formation, whereas phosphorylated EndophilinA has lower membrane affinity. Vesicle endocytosis is impaired in both human Gly2019Ser LRRK2 knockin third-instar larvae, where hyperactive LRRK2 prevents membrane association of EndophilinA, and Lrrk LOF mutants, where hypofunctional Lrrk thwarts vesicle recycling because of EndophilinA not efficiently leaving the membrane[104]. Although these results must be taken with caution, as fly Lrrk is no orthologue of mammalian LRRK2[72], the proposed mechanism has the merit to indicate an alternative approach to an over a decade-long conundrum. According to this "homeostasic hypothesis", it is not whether LRRK2 is hyperactive or hypofunctional, but rather whether LRRK2 is "enough" to be patho- and biologically relevant. Pathogenic mutations could render LRRK2 "more than enough" or "not enough", depending on their nature (Figure 1.2).
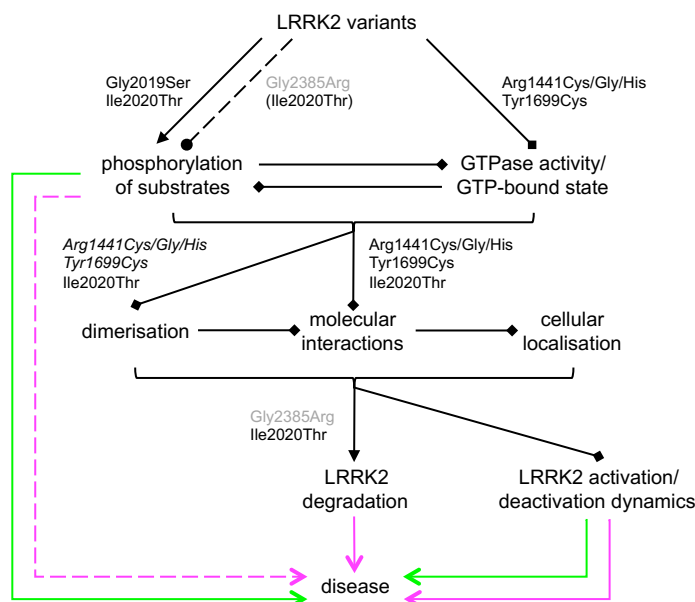
Figure 1.2: Possible aetiopathological mechanisms of LRRK2 variants. Based on *in vitro* evidence, *LRRK2* mutations alter LRRK2 function. This can happen by either promoting (arrow) kinase activity, directly or via reduced GTPase activity/promoted GTP-bound state, or viceversa, by influencing (diamond-headed line) the GTPase activity/GTP-bound state, directly or via kinase activity, depending on weather the output is kinase activity or GTPase activity/GTP-bound state. The former scenario is more widely accepted, with disease being the direct effect of kinase GOF (green arrow). Alternatively (dashed lines), the substitutions Gly2385Arg (risk factor, grey) and Ile2020Thr (within brackets, as more commonly considered to cause GOF) would decrease kinase activity (circle-headed line) and hence cause disease via LOF (magenta). Altered LRRK2 function might also lead to disease via several indirect mechanisms, including impaired local dimerisation of LRRK2 domains (italicized substitutions) or full-length LRRK2 molecules, and disrupted interactions with molecular partners, causing cellular mislocalisation. Dysfunctional LRRK2 would then undergo degradation, causing disease via LOF, or impair LRRK2 activation/deactivation dynamics. The latter mechanism may elicit variable effects in different tissues/cell types and individuals.

Such "quantitative" interpretation could however not explain the discrepancy between existing GOF and LOF models, as a certain degree of equivalence would be expected, instead. Therefore, a more sophisticated "qualitative" interpretation could be envisaged, where LRRK2 toxicity depends not merely on LRRK2 levels, but rather on the balance between LRRK2 activation/deactivation. In turn, this balance may vary depending on tissue or cell type, presence of disease modifier genes, and general health state of the organism. For example, low levels of LRRK2 may be required for normal neuronal function, as suggested by the putative toxicity of GOF mutations, but high levels are found in macrophage and monocytic cells[105] and activated microglia[106]. Conceivably, LRRK2 LOF may have little consequence on neurons directly, yet be detrimental indirectly under immune challenge by impairing the innate inflammatory response. Consequently, the analysis of GOF and LOF models separately would be too reductionist a strategy, as LRRK2 would be either "on" or "off" in all cells, in all tissues, under any circumstance, invariably. Re-thinking LRRK2 in terms of how much is active, rather than present, might be instrumental to elucidating critical aspects of its pathobiology in humans, such as variable penetrance and late clinical onset (see 1.2).

1.3   Is a new *LRRK2* model necessary?

As outlined above, present *LRRK2* models are not robust PD models. This raises the question of how imperfect models can be useful. The emerging complexity of LRRK2 interactions and functions is definitely part of the reason of their shortcomings: the lack of sufficient knowledge of LRRK2 biological context simply makes them compassless. On the other hand, there is also a persistent hermeneutical bias towards, if not yet a dogma of, LRRK2 GOF being the leading cause of pathology. This bias has profoundly influenced the field, not only leading to the sprouting of GOF models and LRRK2 inhibitors, but also limiting the analysis of LOF models to the identification of safety liability in view of LRRK2 inhibition for therapeutics. Hence, double standards are operated when explaining the lack of PD-like features in GOF or LOF models: for the former, the much shorter lifespan of animal models compared to humans would not allow enough time for LRRK2-driven toxic effects to reach threshold; for the latter, observations would simply match expectations. To salvage the "GOF-centric" view, GOF models are generally exalted as the ones capturing the prodromic stages of PD[70]. However, as stressed in the previous section (1.2.1), the GOF hypothesis is based almost exclusively on *in vitro* work, whereas mounting evidence shows that alternative explanations are also plausible. Also, the idea that aspects of LRRK2 biology other than kinase function may lead to disease is gaining ground in the development of alternative, non-kinase-based therapeutic strategies[107].

Arguably, what is truly lacking in the multitude of *LRRK2* models is a real amorphic standard, meaning a purely and unambiguously null model where to study what goes awry when LRRK2 is absent. Such a standard, alone or in combination with a second, hypomorphic model, would help rethinking existing models by fulfilling three objectives:

(*i*) in case LRRK2 GOF is pathogenic, to foresee the side effects of LRRK2 inhibition;

(*ii*) in case LRRK2 LOF is pathogenic, to mimick the human phenotype;

(*iii*) to infer LRRK2 biological role(s) from emerging phenotype(s) and disrupted omic interactions.

Until now, eight mouse and one rat *Lrrk2* knockout models have been generated and variably characterised. The mouse models have all been obtained via homologous recombination targeting different *Lrrk2* gene portions: exon 1[101,108], exon 2[86,109,110], exons 29-30[101], part of exon 39-exon 40[111,112], exons 39-40[113], exon 41[99,102]. The rat model has been generated by the SAGE Laboratories and made commercially available. Zinc-finger nucleases were used to generate an in-del in exon 30 resulting in a premature stop codon. Despite several studies on peripheral organs[100,114–116], no brain characterisation has yet been provided. Therefore, what is known about the effects of LRRK2 LOF on the brain (see 1.2.1) comes exclusively from the mouse models. However, for none of these models has the validation of *Lrrk2* knockout been thoroughly unequivocal. Firstly, all of the strategies adopted cannot rule out the persistence of truncated protein products in knockout animals, though at lower levels than in wild-type controls due to nonsense-mediated RNA decay, but still potentially effective (see 1.1.1). Secondly, absence of LRRK2 in knockout animals has been shown either directly, via western blot[99,101,108–111] and/or immunohistochemistry[102], and/or indirectly, via northern blot[101,111] or *in situ* hybridisation[110]. Each of the above methods have problems, though. LRRK2 is a large protein (>280 kDa), which makes gel transfer difficult. Moreover, expression of *Lrrk2* in the brain is low compared to other peripheral organs (lung, lymphnode, kidney)[117]. Consequently, even rarer, truncated but still large products may go unnoticed simply because below detection threshold. Similar considerations hold true also for the detection of the large (>8 kbp) and rare *Lrrk2* transcripts via northern blot or *in situ* hybridisation. Another aspect is the specificity of anti-LRRK2 antibodies. There have been tremendous efforts to identify suitable antibodies for different applications, and results have been at times contradicting[117–119]. This has been particularly true for immunohistochemistry, for which the problem of antibody specificity adds up to protocol optimisation issues, such as fixation, antigen retrieval, signal-to-noise ratio. Different antibodies give different staining patterns[118] and signal interpreted as "aspecific" in presumably *Lrrk2* knockout tissue[102,119]. Anyway, the smoking gun proving the specificity of any of the above models is missing, as physiological substrates of LRRK2 are yet to be validated and no rescue attempt has been carried out.

Given the above difficulties, a more solid approach would be required to generate a valid LRRK2 amorphic standard. In addition to that, a "suspension of disbelief" towards LRRK2 LOF models might be of value to understand aspects of PD so far ignored or even alternative routes to pathology. Finally, a more tractable animal model than rodents might be more indicated for omic studies and

high-throughput screening aiming at identifying "druggable" targets in a transla-tional perspective. To fulfil these scopes, the present thesis proposes the zebrafish as a vertebrate system wherein to model LRRK2 deficiency. In the next chapter, the advantages and limitations of the zebrafish as a model organism for PD will be summarised and previous attempts to study zebrafish Lrrk2 LOF examined. Finally, the aim of the thesis will be defined.

Aim of the Thesis

Reliable *LRRK2* knockout models may help clarifying the molecular interactions that are disrupted by dysfunctional LRRK2[63] as well as the potential side effects of LRRK2 pharmacological inhibition for therapeutics[120]. Incomplete success in reproducing PD-like pathology in *LRRK2* rodent models raises the need for alternative approaches, including the exploration of different model systems.

2.1 The zebrafish as a model for PD

The zebrafish has long been acknowledged as a powerful model to study basic developmental dynamics. Over the past decades, a wide range of tools and techniques have been assembled. Cheap costs of maintenance, rapid and transparent development, large breeding capacity, and high quality sequenced genome make zebrafish suitable for applications in many disciplines. Being a vertebrate, with stereotypically conserved fundamental brain architecture and neurotransmitter systems, the zebrafish has recently started to be exploited for the study of central nervous system diseases. In particular, emerging data show the value of zebrafish as a new model for movement disorders[121] and neuropsychiatric diseases[122]. Targeting the expression of zebrafish orthologues or driving the expression of human disease-associated genes in zebrafish demonstrated phylogenetically conserved molecular pathways, which lead to comparable defects at the level of specific neuronal populations[123]. These findings, combined with the ease of genetic manipulation and the large offspring numbers, have rendered the zebrafish ideal for functional assessment of putative modifier genes, screening for therapeutics, and direct observation of disease mechanisms *in vivo*. Moreover, the zebrafish displays a complex ethology, whose translational relevance and measurability is granted by the progressive elucidation of underlying neural pathways and refinement of old/establishment of new behavioural paradigms[124]. Another interesting characteristic is the prodigious reparative capacity of damaged tissues, including the brain[125,126]. Restorative neurogenesis decreases along evolution and is almost absent in humans, which may facilitate progression of neurodegeneration. For this reason, the zebrafish ultimately represents a unique possibility to determine which genetic programs might hinder neurodegeneration with a view towards applying these insights in humans.

In the context of PD modelling, the zebrafish proves a feasible model. First of all, the main aminergic systems are conserved, most relevantly the DA system[127]. Secondly, the zebrafish is sensitive to DA neurotoxins 6-OHDA and MPTP[128,129].

Finally, several PD-associated genes in humans have corresponding orthologues in zebrafish, as shown in knockdown or reverse genetics studies: *dj1*[130], *parkin*[131,132], *pink1*[133–135], *lrrk2*[136–138], *atp13a2*[139,140], and *gba*[141,142]. A zebrafish orthologue for *SNCA* (α-synuclein) is not present, but three orthologues for *SNCB* and *SNCG* (β- and γ-synuclein, respectively) exist: *sncb*, *sncg1*, and *sncg2*. Of note, knockdown of either *sncb* or *sncg1* has been reported to cause hypokinesia in zebrafish larvae, whereas knockdown of both would result in a more severe phenotype and reduced dopamine levels[143].

Despite the above similarities, there are important differences between the mammalian and zebrafish DA systems that must be considered in order to define the range of applications, and validity, of the zebrafish as a model for PD. One is the absence of a mesencephalic DA neuronal cluster, meaning the anatomical correlate of mammalian *substantia nigra*[15]. However, the sensitivity to 1-methyl-4-phenylpyridinium (MPP$^+$), the toxic form of MPTP, of the ventral diencephalic DA neuronal cluster suggests this to be the functional homologue[144].

Another peculiarity is the presence of two isoforms of tyrosine hydroxylase (TH), the rate limiting enzyme of dopamine biosynthesis: TH1 and TH2. TH1 is more closely related to mammalian TH; despite one study suggesting TH2 to have tryptophan hydroxylase activity, and therefore be involved in serotonin synthesis[145], there is substantial proof that TH2+ cells are indeed DA neurons[146,147]. TH1+ cells are distributed in clusters throughout the entire brain along the rostro-caudal axis, whereas TH2+ cells are found only in the diencephalon, most numerous in the caudal hypothalamus[148–151]. The respective roles of TH1+ and TH2+ cells are not clear. While *th1* is strongly expressed since early embryonic stages, *th2* expression becomes more prominent at post-embryonic stages[150]. In particular, the high expression of *dat*, coding for the dopamine transporter, in caudal hypo-thalamic TH2+ cells suggests a significant role in synaptic transmission[150]. Of interest, caudal hypothalamic TH2+ cells are continuously generated throughout life and are required for proper initiation of swimming[146]. Therefore, a thorough examination of the DA system, and related (dys)functions, in a putative zebrafish PD model must include the analysis of both TH1+ and TH2+ cell compartments.

The last comparative aspect worth to highlight is DA catabolism. In mammals, biogenic amines, including dopamine, are degraded by two enzymes: monoamine oxidase (MAO), working in tandem with aldehyde dehydrogenase; and catechol-*O*-methyl transferase (COMT). Both MAO and COMT are important pharma-cological targets in the treatment of PD patients[152,153], and both functions are conserved in zebrafish[154,155]. While mammals have two genes for two different MAO enzymes, MAO-A and MAO-B, and only one gene for two COMT forms, one soluble (S-COMT) and the other membrane-bound (MB-COMT)[156], zebrafish have the opposite, i.e. a single *mao* gene[157,158] and two distinct *comt* genes, *comta* and *comtb*[155,159]. Zebrafish Mao has peculiar but also hybrid features compared to mammalian MAO-A and MAO-B: histochemical and biochemical charaterisation suggests it is primarily involved in serotonin degradation[154,160], in this resembling MAO-A, but it can be inhibited by both clorgyline and deprenyl[154], MAO-A and MAO-B inhibitors, respectively. Characterisation of the role of zebrafish Comt is still lacking, but it is thought it may be the main responsible for DA degrada-

tion[160]. MAO levels change with age and are of special relevance for PD[161,162]. In particular, MAO-B converts MPTP to 1-methyl-4-phenyl-2,3-dihydropyridinium ($MPDP^+$) in nigrostriatal astrocytes, from where it flows to the extracellular space and is converted to MPP^+, which is then taken up by neighbouring DA neurons via the dopamine transporter[158]. However, in contrast with mammalian MAO-B, zebrafish Mao has modest affinity for MPTP[154]. Although MPTP does have an effect on zebrafish DA function, direct usage of MPP^+ would be preferred to elicit more specific, PD-mimetic effects[144].

2.1.1 Previous studies on zebrafish *lrrk2*

Attempts to study human PD-associated gene orthologues in zebrafish largely relied on morpholino oligonucleotides (MO)-mediated knockdown[102,130–133,136–138,141]. Only three studies made use of stable lines: two used chemically-induced mutant alles[135,141] and only one the cleaner transcription activator-like effector nuclease (TALEN)-mediated mutagenesis[142]. A major limitation of MO-based studies is the high variability and transiency of induced changes, leaving only a narrow time window for observations, thus making the evaluation of adult or ageing phenotypes difficult. Also, MOs can exhibit off-target effects and have been increasingly questioned about their specificity[27,163–166]. Although the analysis of MO-induced phenotypes may still provide useful information, their validation would inevitably entail the generation of reliable null alleles[167].

So far, three studies investigating zebrafish *lrrk2* gene function have been published, all based on MO-mediated knockdown (MOs), and yielded contradicting results. In one, loss of diencephalic catecholaminergic (CA) neurons and locomotor defects in the larvae were described[136]. However, subsequent work failed to reproduce the reported phenotype, even by using same reagents and MOs[137]. Recently, a third paper rekindled the initial claims, describing a *lrrk2* MO-induced phenotype with macroscopic developmental abnormalities[138]. To solve the quandary, a qualitatively superior approach is therefore warranted.

Previous work in the Brand laboratory conducted by R. Ahrendt (Doctoral Thesis[168]), with the assistance of J. Kaslin, has independently identified and cloned the zebrafish *lrrk2* orthologue and subsequently analysed a mutant zebrafish line, generated by S. Winkler, via *N*-ethyl-*N*-nitrosourea (ENU)-mediated mutagenesis[169] followed by targeting induced local lesions in genomes (TILLING) screening[169], where a point mutation introduces an early stop codon within the *lrrk2* open reading frame (*ORF*; c.3972+2T>C, p.(Ile1252AlafsTer9)) according to the Human Genome Variation Society guidelines[170], henceforth referred to as "*tud112*"; Figure 2.1). The mutation results in a truncated protein product lacking the catalytic core. Characterisation of maternal-zygotic *tud112* mutants (henceforth referred to as "*mzLrrk2^{tud112}*") revealed a phenotype with features reminiscent of human PD, including persistent loss of CA neurons, perturbed CA metabolism and locomotor deficits[168]. Of note, *mzLrrk2^{tud112}* brains also displayed significantly reduced cell proliferation throughout development (Figure 2.1d).
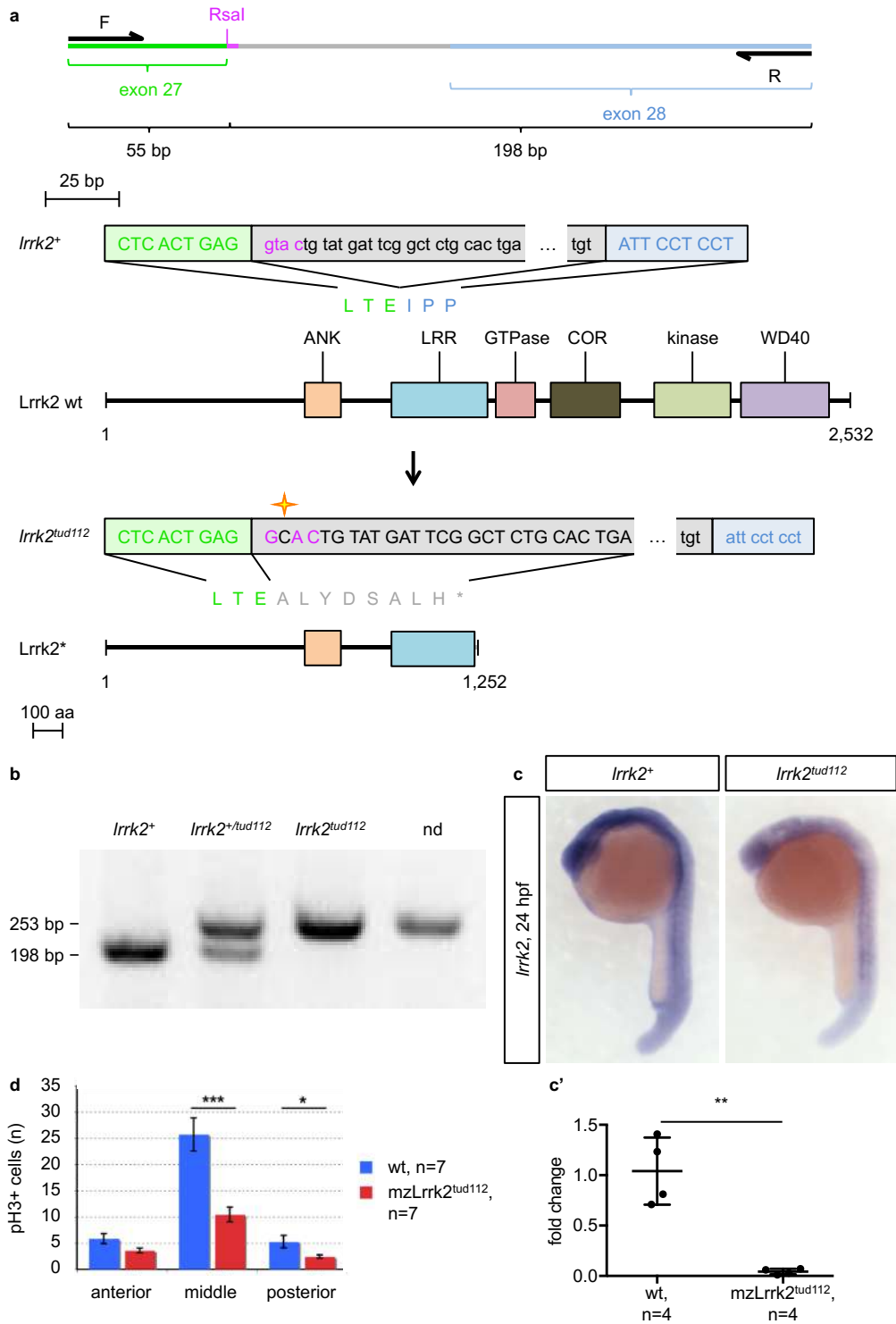
Figure 2.1: Generation and characterisation of the *lrrk2^{tud112}* allele. The *lrrk2^{tud112}* allele was generated by S. Winkler; the *mzLrrk2^{tud112}* line was characterised by R. Ahrendt, J. Kaslin, and S. Suzzi. *N*-ethyl-*N*-nitrosourea-mediated mutagenesis was used to generate a *lrrk2* zebrafish line. The identified allele (*lrrk2^{tud112}*; a) consists in a T>C substitution (c.3972+2T>C) disrupting the splice donor site of *lrrk2* exon 27, causing the retention of the ensuing intron and a premature stop codon (p.(Ile1252AlafsTer9)). (b) The *tud112* mutation also disrupts the RsaI restriction site, allowing identification of mutation

concluded from previous page

carriers via RFLP-PCR. To this aim, PCR primers (F, R in a) were designed to amplify a 253-bp-long product comprising the RsaI site: upon RsaI-mediated digestion, only the wild-type product can be cleaved into two fragments (198 and 55 bp; the shorter is lost during the gel run), allowing identification of wild-type ($lrrk2^{+}$), heterozygous ($lrrk2^{+/tud112}$), and homozygous mutant ($lrrk2^{tud112}$) individuals compared to undigested product (nd). (c, c') Nonsense-mediated $lrrk2$ RNA decay in maternal zygotic $tud112$ mutants ($mzLrrk2^{tud112}$) demonstrated via *in situ* hybridisation on 24-dpf (c) and RT-qPCR (c') on 48-hpf embryos. Plot represents means ± s.d. (d) pH3 immunohistochemistry reveals decreased mitosis in 8-dpf $mzLrrk2^{tud112}$ brains (data from R. Ahrendt[168]). (c') Bar plot represents means ± standard error of the mean. Statistical analyses: (c', d) two-tailed Student's t test.

Given its characteristics, the zebrafish $mzLrrk2^{tud112}$ phenotype appeared as a promising model to study mutant $LRRK2$-mediated pathology in a vertebrate *in vivo*. However, because ENU-mediated mutagenesis is prone to off-target effects, the generation of a second allele using more advanced genomic editing, more protective towards the genetic background, was required to assess the specificity of the $mzLrrk2^{tud112}$ phenotype. The ultimate scope is to achieve an unambiguous characterisation of the brain phenotype upon constitutive Lrrk2 LOF.

With this purpose, the thesis herein presented pursues the following main aims:

(i) generation of an alternative $lrrk2$ knockout line and validation of the main phenotypic findings in the $tud112$ line;

(ii) more comprehensive characterisation of the brain phenotype and adult behaviour;

(iii) evaluation of the impact of Lrrk2 LOF on the brain regenerative potential.

Materials

3.1 Technical equipment

Table 3.1: Technical equipment

equipment	manufacturer
Behavioural setup	ZebraBox, ViewPoint
Confocal microscope	ZEISS LSM 780, upright
Cryostat	Microm HM 560
Digital cameras	Olympus DP71
	Olympus DP80
Excitation light source	X-cite 120Q
Fibre optic light source	Leica KL 1500 LCD
LightCycler 480 System	Roche
PCR machine	Eppendorf Mastercycler epGradientS
Stereo microscopes	Olympus SZX10
	Olympus SZX16
	Olympus MVX10
Syringe Pump AL1000-220	World Precision Instruments
Thermal Cycler	Eppendorf Mastercycler pro PCR Thermal Cycler System
Transilluminator	QUANTUM Modell 1100, Peqlab

3.2 Fish lines

Table 3.2: Fish lines

zebrafish line	reference
$lrrk2^{\mathrm{del11bp}}$	described here
$lrrk2^{\mathrm{tud112}}$	[168]
$lrrk2^{\mathrm{tud113}}$	described here
$Tg(hsp70l{:}mCherry\text{-}T2A\text{-}lrrk2(c.3009\_7130)\text{-}Myc)^{tud114}$	[168]

3.3 Reagents and kits

Table 3.3: Reagents and kits

name	manufacturer
10X DreamTaq Green Buffer	Thermo Scientific
ApopTag Red/Fluorescein In Situ Apoptosis Detection Kit	Chemicon
BM Purple	Roche
DAPI	Invitrogen
dNTP Mix (10 mM)	Thermo Scientific
DreamTaq DNA Polymerase	Thermo Scientific
LightCycler 480 SYBR Green I Master	Roche
mMessage mMachine Kit	Ambion
NBT/BCIP Stock Solution	Roche
Proteinase K, recombinant, PCR grade	Roche
SIGMAFAST 3,3'-diaminobenzidine tablets	Sigma-Aldrich
Transcriptor First Strand cDNA Synthesis Kit	Roche
TRIzol	Ambion
Zymoclean Gel DNA Recovery Kit	Zymo Research

3.4 Buffers and solutions

All chemicals were purchased from Applichem, Merck, Roth, and Sigma-Aldrich. All restriction enzymes were purchased from Fermentas.

Table 3.4: Buffers and solutions

reagent or buffer	composition and preparation
AcOH	Acetic acid 100%
AcOH/EtOH 1 : 2	One part of acetic acid, two parts of ethanol
Agarose 2% Gel Solution	For 200 ml: add 4 g of agarose to 180 ml TAE 1×; microwave at full power until dissolved, add 8 µl of ethidium bromide 200 mg/ml solution and bring the volume to 200 ml with TAE 1x
Bleaching Solution	Immediately before use, add hydrogen peroxide to 3% in potassium hydroxide 1%, Tween 20 0.1%
BrdU/E3	5-bromo-2'-deoxyuridine 10 mM in E3 medium
BrdU/FFW	5-bromo-2'-deoxyuridine 5 mM in FFW
CUBIC-1	Urea 25%, quadrol 25%, Triton X-100 15% in distilled water
CUBIC-2	Sucrose 50%, urea 25%, triethanolamine 10%, Triton X-100 0.1%
CUBIC-2 50%	Dilution of CUBIC-2 with PBS

reagent or buffer	composition and preparation
Deionised formamide	For 1 l: add 10 g of amberlite IRN-150 ion exchange resin to 1 l of formamide 100%, mix for 1 h on a magnetic stirrer, then sterile filter
DEPC-water	For 1 l: add diethylpyrocarbonate to 0.1%, then autoclave
DIG Blocking Solution	Digoxigenin Blocking Reagent 2% in MAB
DMK	dimethyl ketone, or acetone, 100%
DMSO	Dimethyl sulphoxide 100%
E3 medium	Sodium chloride 5 mM, potassium chloride 0.17 mM, calcium chloride dihydrate 0.33 mM, magnesium sulphate heptahydrate 0.33 m, methylene blue 0.0002% in deionised water, $pH = 6.5$
EDAC/NHS	N-Ethyl-N'-(3-dimethylaminopropyl)carbodiimide hydrochloride 4%, N-hydroxysuccinimide 0.4% in PB
EDTA	For 1 l, 0.5 M: add 186.1 g of ethylenedinitrilotetraacetic acid disodium salt dehydrate to 800 ml of distilled water; use sodium hydroxide pellets to clear the solution and adjust the pH to 8.0, then bring the volume to 1 l with distilled water
EtOH 70, 95%	Dilution from ethanol 100%
FFW	Fish Facility Water
Gelatine/Sucrose Buffer	For 100 ml: add 7.5 g of gelatine and 20 g of sucrose to 80 ml of PB; microwave at full power until dissolved, then bring the volume to 100 ml; equilibrate at 37 °C in water bath for at least 1 h before use
Glycerol 50, 80%	Dilution of glycerol 100% with PBS
Hybridisation− (Hyb−) Buffer	For 50 ml: add 25 ml formamide, 12.5 ml SSC 20×, Tween 20 to 0.1%, then bring the volume to 50 ml with DEPC-water
Hybridisation+ (Hyb+) Buffer	For 50 ml: dissolve 25 mg torula yeast RNA, 50 mg of heparin in 25 ml of deionised formamide, 12.5 ml of SSC 20×, Tween 20 to 0.1%, then bring the volume to 50 ml with DEPC-water
i-PrOH	Isopropanol 100%
MAB	100 mM maleic acid, sodium chloride 150 mM in distilled water, $pH = 7.5$
MABT	MAB, 0.1% Tween 20
Mao Staining Solution	To prepare fresh before use: dissolve one 0.7 g tablet of 3,3'-diaminobenzidine in 0.875 ml of a solution containing nickel sulphate 6 mg/ml, tyramine 1 mg/ml, horseradish peroxidase 1 mg/ml, Tris-HCl 50 mM, $pH = 7.5$

reagent or buffer	composition and preparation
MESAB	For 100-ml stock: 0.4 g of ethyl 3-aminobenzoate methanesulfonate, 1 g of disodium phosphate dehydrate in 100 ml of distilled water
MetOH	Methanol
NBT/BCIP Staining Solution	To prepare fresh before use: 20 µl of NBT/BCIP Stock Solution in NTMT Buffer
NGS 2, 4% Blocking Solution	Dilution from normal goat serum in PBSTx
NTMT Buffer	Sodium chloride 100 mM, magnesium chloride 50 mM M, 0.1% Tween 20 in Tris 100 mM M, $pH = 9.5$
PB	For 5 l, 0.1 M: mix 100 ml of disodium phosphate 1 M and 400 ml of monosodium phosphate 1 M, then bring the volume to 5 l with DEPC-water; adjust the pH to 7.4 with either disodium phosphate (basic) or monosodium phosphate (acid) 0.1 M
PBS	Monopotassium phosphate 1.7 mM, disodium phosphate 5.2 mM, sodium chloride 150 mM mM in distilled water
PBST	PBS, 0.1% Tween 20
PBSTx	PBS, 0.3% Triton X-100
PCR Mix	For 20 µl: 2.5 µl of 10X DreamTaq Green Buffer, 0.5 µl of dNTP Mix, 0.5 µl of *for* primer 10 µM, 0.5 µl of *rev* primer 10 µM, 0.2 µl of DreamTaq DNA Polymerase, 5.8 µl of distilled water
PFA 2%	Dilution from PFA 4% with PB
PFA 4%	For 2 l: make 1 l of PB 0.2 M, $pH = 7.4$ (solution A); add 80 g of paraformaldehyde to 800 ml of distilled water on a hot plate at 65 °C, clear with sodium hydroxide 5 M, cool down, adjust the pH to 7.4 with sodium hydroxide 5 M, then bring the volume to 1 l (solution B); finally, mix solutions A and B
RT-qPCR Mix	For 9 µl: 5 µl of LightCycler 480 SYBR Green I Master, 0.5 µl of *for* primer 2.5 µM, 0.5 µl of *rev* primer 2.5 µM, 3 µl of DEPC-water
Sodium Citrate Buffer	For 1 l, 10 mM: dissolve 2.94 g of sodium citrate dehydrate in 950 ml of distilled water; adjust the pH to 6.0 with acetic acid, then bring the volume to 1 l
Sodium Citrate/PBSTx0.1	To prepare fresh before use: sodium citrate 0.1%, Triton X-100 0.1% in PBS
Sodium Tetraborate Buffer	Sodium tetraborate decahydrate 0.1 M in distilled water, $pH = 8.5$

reagent or buffer	composition and preparation
SSC 20×	Sodium chloride 3 M, trisodium citrate dehydrate 0.3 M in DEPC-water; use citric acid 1 M to adjust the *pH* to 6.0
SSCT 0.2, 2×	Dilution from SSC 20× with the addition of Tween 20 to 0.1%
Sucrose/EDTA Buffer	For 2 l: add 400 g of ethylenedinitrilotetraacetic acid disodium salt dehydrate in 1.5 l of PB; adjust the *pH* to 7.4 with sodium hydroxide pellets; dissolve 400 g of sucrose, then bring the volume to 2 l with PB
TAE 1×	Dilution from TAE 50× with deionised water
TAE 50×	For 1 l: add 242 g of Tris base, 57.1 ml of acetic acid, 100 ml of EDTA 0.5 M, *pH* = 8.0 to 700 ml of distilled water; adjust the *pH* to 8.5 with acetic acid if necessary and bring the volume to 1 l with distilled water
TCM	Trichloromethane, or chloroform, 100%
Tissue Lysis Buffer	To prepare fresh before use: sodium chloride 0.2 M, sodium dodecyl sulphate 0.2%, EDTA 5 mM, proteinase K 10 mg/ml in Tris-HCl 100 mM, *pH* = 8
TPA Stock Solution	0.05 mg of 12-*O*-tetradecanoylphorbol 13-acetate in 1 ml of DMSO
TPA Working Solution	1:5,000 dilution from TPA Stock Solution with E3 medium
TPA Control Solution	1:5,000 DMSO
Tris-HCl 7.5, 8.0 Buffer	For 2 l, 50 mM: add 12.1 g of Tris base to 1.9 l of distilled water; adjust the *pH* to 7.5 or 8.0 with concentrated hydrochloric acid

3.5 Antibodies

Table 3.5: Primary antibodies

name	manufacturer	dilution	host	reference
Anti-acetylated Tubulin	Sigma	1:1,000 in NGS 2% Blocking Solution	mouse (IgG2b)	[171]
Anti-BrdU	Serotec	1:500 in NGS 2% Blocking Solution	rat	[172]
Anti-Claudin k	provided by the Reimer lab	1:1,000 in NGS 2% Blocking Solution	rat	[173]
Anti-DIG-AP Fab fragments	Roche	1:4,000 in DIG Blocking Solution	sheep	
Anti-HuC/D	Molecular Probes	1:200 in NGS 2% Blocking Solution	mouse (IgG2b)	[172]
Anti-L-Plastin	expression plasmid provided by MIchael J. Redd	1:5000 in NGS 2% Blocking Solution	rabbit	[174]
Anti-PCNA	Dako	1:500 in NGS 2% Blocking Solution	mouse (IgG2a)	[172]
Anti-pH3	Millipore	1:200 in NGS 2% Blocking Solution	rabbit	[172]
Anti-TH(1)	Immunostar	1:1,000 in NGS 2% Blocking Solution	mouse (IgG1)	[127]
Anti-TH(1/2)	provided by the Panula lab	1:1,000 in NGS 2% Blocking Solution	rabbit	[147]

Table 3.6: Secondary antibodies

name	fluorophore	company	dilution	host
Anti-mouse IgG	Alexa 488, 555	Molecular Probes	1:500 in NGS 2% Blocking Solution	goat
Anti-mouse IgG1	Alexa 488, 555			
Anti-mouse IgG2a	Alexa 555, 633			
Anti-mouse IgG2b	Alexa 488			
Anti-rabbit	Alexa 488, 700			
Anti-rat	Alexa 488, 633			

3.6 Antisense DIG-labelled riboprobes

Table 3.7: Antisense DIG-labelled riboprobes

target gene	reference
lrrk2	"Lrrk2-6", "L2m2" in [168]

3.7 PCR primers

All primers were designed using the Primer3 software[175,176]. Primers for RT-qPCR were tested for displaying amplification efficiency between 1.9–2.1.

Table 3.8: PCR primers

sequence (5'>3')	Ta (°C)	amplified region
for: ATGAAATACTGTTCCCCTGTTCGC *rev*: TGTAGTAATGCCAGTGCTCAACAC	60	422 bp flanking the *lrrk2 ORF*
for: TACACAGGCGCCAACATGACCG *rev*: AGCTACACGCTGGACTTGGGGT *for*: TGCGAGCGCTGTCTGCTGTTAC *rev*: TGTCTTTGCTCCTGACGGGCCA	64	204 bp flanking the ORFdel *lrrk2* variant 289 bp within the *lrrk2 ORF*
for: TACAAGTGGGCCCGACTGGAGAAAC *rev*: ATCCAGAGGCAGATCCCACAGATGC	66	253 bp flanking the tud112 *lrrk2* mutation
for: CCTTCCTGGGTATGGAATCT *rev*: GACAGCACTGTGTTGGCATA	60	106 bp within the *actb1*-001 transcript
for: GTGCCCATCTACGAGGGTTA *rev*: TCTCAGCTGTGGTGGTGAAG	62	130 bp within the *actb2*-001 transcript[177]
for: CTTCAACATGGAGGACTGCG *rev*: CGTGAGGGGAAGTCTGTCAT	62	129 bp within the *lrrk2*-001 transcript
for: GGACCAGTCTAGACCGATGG *rev*: CAAAATGTGTCCCGCTCTCG	62	100 bp within the *lrrk2*-001 transcript
for: CTTCAACATGGAGGACTGCG *rev*: CGTGAGGGGAAGTCTGTCAT	62	129 bp within the *lrrk1*-001 transcript
for: TATGCTCGTGTCCTGGGATC *rev*: CAAGACCCTGCCAAACTGTG	60	141 bp within the *mao*-001 transcript

Methods

Unless otherwise stated, methods were performed according to standard procedures[178], or according to the manufacturer's instructions of the employed kits.

4.1 Fish maintenance and handling

Zebrafish (*Danio rerio*) were raised and maintained as described previously[179]. Embryos were obtained by natural spawning of adult fish, raised in E3 medium and staged according to hours or days post-fertilisation (hpf or dpf) or standard criteria[180]. All efforts were made to minimise animal suffering and the number of animals used.

4.2 *In vivo* treatments

4.2.1 Behavioural analysis

The ZebraBox and ZebraCube apparatus were used in combination with the Viewpoint Application Manager software. All recordings were performed on individually isolated animals between 2–6 PM. Larvae at 4 dpf were transferred into 24-well plates and therein grown until 10 dpf. Each well was internally lined with Parafilm to minimize reflection and filled with 750 μL E3 medium, changed daily. Because larvae are less motile, tracking could be lost for some time: animals lost for over 20% of the total recording time were excluded from the analyses. To quantify spontaneous swimming and thigmotaxis, adult fish were lodged in opaque cylindrical boxes ($\oslash = 80$ mm) filled with SI100 FFW, else in opaque parallelepipedal boxes ($l \times w = 190 \times 80$ mm) filled with 500 mL FFW. Each recording was preceded by 10 min acclimatization inside the apparatus. Spontaneous swimming was assessed for 10 min (integration period: 600 s) in the dark under infrared light. Appropriate speed thresholds were chosen based on developmental stage: 2–10 mm/s for larvae; 2–40 mm/s for adults. Based on the speed thresholds, three swimming phases were defined: inactive phase, below the lower threshold; normal swimming phase, between the lower and upper threshold; bursting phase, above the upper threshold. For each swimming phase, three parameters were considered: entry count, duration (s), and distance swum (mm). Thigmotaxis was assessed using the same recordings of spontaneous swimming activity. To this aim, the recording arena was digitally subdivided into an outer and inner area (for larvae $\oslash = 15.6/10.6$ mm; for adults $\oslash = 80/55$ mm). Scototaxis was assessed for 10 min in half-black, half-white parallelepipedal boxes. Olfactory function was assessed

by delivering a stimulus in either of the shorter sides of parallelepipedal boxes. The stimulus consisted in 0.6 mL of an amino acid mix (Ala, Cys, His, Lys, Met, Val, 0.1 m each) delivered through a syringe pump (1.5). Fish were starved for 24 h before the experiments. Fish behaviour was recorded 5 min before and 5 min after stimulus delivery. For every 1 of recording, a preference index was defined as[181] $\frac{ts-tc}{ts+tc}$, where ts is the time spent in the stimulus side, tc the time spent in the control side.

4.2.2 BrdU labelling

To label cells in the S-phase of the cell cycle, zebrafish larvae were immersed in BrdU/E3 for 4 h prior to killing. For assaying reparative neurogenesis in adult fish, stabbed fish at 2 dpl were immersed in BrdU/FFW for 24 h, then killed at 21 dpl.

4.2.3 Fin clipping

Adult fish were anaesthetised by immersion in a solution of 5 ml of MESAB/100 ml of fish water. A small portion of the tail fin was cut and collected in a tube.

4.2.4 Heat shock treatment

Embryos/larvae were heat shocked every day from 1 dpf until 10 dpf. Heat shocks were administered as follows: E3 medium was replaced with 42 °C-warm E3 medium and incubated for 4 h at 37 °C. On the day of sacrifice, larvae were euthanised 4 h after the heat shock.

4.2.5 Stab lesion

Adult fish were anaesthetised by immersion in a solution of 5 ml of MESAB/100 ml of fish water. A cannula (30 gauge, outer ⌀ 300 µm was inserted through the right nostril and pushed deep along the body axis through the olfactory bulb till the caudal telencephalon. All fish survived the procedure.

4.2.6 TPA treatment

To induce acute inflammation systemically, zebrafish larvae were immersed in TPA Working Solution for 2 h prior to killing. Control larvae were incubated in TPA Control Solution.

4.3 Histology and histochemistry

4.3.1 Sample preparation

Twenty-four-hpf embryos were manually dechorionated, terminally anaesthetised with MESAB, fixed with PFA 4% $1 \times o/n$ at 4 °C, then repeatedly washed with PBS and transferred to pre-cooled MetOH 100% at -20 °C for at least 30 min, otherwise stored until use.

Five- or 10-dpf larvae were terminally anaesthetised with MESAB, fixed with PFA 2%/DMSO 1% for at least $1 \times o/n$ at $4\,^{\circ}\mathrm{C}$, otherwise stored until use. Larvae to be used for Mao histochemistry were fixed with EDAC/NHS/DMSO 1% for $1 \times o/n$ at $4\,^{\circ}\mathrm{C}$, instead. To harvest the brains or tails, larvae were washed with PBS and dissected underneath a stereo microscope. The collected organs were depigmented with Bleaching Solution.

Adult fish were terminally anaesthetised on ice, the skulls opened and the right opercula removed to expose the brain and the heads excised and transferred to PFA 2% $1 \times o/n$ at $4\,^{\circ}\mathrm{C}$. After fixation, the heads were washed twice with PB and decalcified in Sucrose/EDTA Buffer $2 \times o/n$ at $4\,^{\circ}\mathrm{C}$. Finally, the heads were washed twice with PB, placed in $37\,^{\circ}\mathrm{C}$-warm Gelatine/Sucrose Buffer for $30\,\mathrm{min}$, then frozen in fresh Gelatin/Sucrose Buffer in plastic moulds on dry ice and stored at $-20\,^{\circ}\mathrm{C}$. Twelve µm-thick coronal sections were cut, allowed to dry for at least $30\,\mathrm{min}$ at RT, and then stored at $-20\,^{\circ}\mathrm{C}$ until use.

4.3.2 Antibody staining

Depigmented larval brains were washed with PBSTx $3 \times 5\,\mathrm{min}$ and cleared with CUBIC-1 for $1 \times o/n$ at RT[182]. The cleared brains were washed with PBSTx $1 \times 10\,\mathrm{min}$, $3 \times 30\,\mathrm{min}$, subjected to antigen retrieval if required (see 4.3.2.1), otherwise directly blocked in NGS 4% Blocking Solution/DMSO 1% for at least $2\,\mathrm{h}$ at RT, and then incubated with the primary antibodies at the appropriate dilutions (see Table 3.5) $1 \times o/n$. On the second day, the brains were washed with PBSTx $1 \times 10\,\mathrm{min}$, $3 \times 30\,\mathrm{min}$, then incubated with the required secondary antibodies (see Table 3.6) for $2\,\mathrm{h}$ at RT or $1 \times o/n$. Finally, the brains were washed with PBSTx $1 \times 10\,\mathrm{min}$, $3 \times 30\,\mathrm{min}$, impregnated first with CUBIC-2 50% $2 \times 1\,\mathrm{h}$, then CUBIC-2 for $1 \times o/n$ at RT. The stained brains were mounted in CUBIC-2, sandwiched between two silicon grease-sealed coverslips, and stored at $4\,^{\circ}\mathrm{C}$ until imaged. As a remark, 5-dpf brains were more prone to swelling upon clearing than the 10-dpf specimina, resulting in the former appearing larger in size as artefact.

Depigmented larval tails were washed with PBSTx $3 \times 5\,\mathrm{min}$, permeabilised with $-20\,^{\circ}\mathrm{C}$-cold DMK for $8\,\mathrm{min}$ at $-20\,^{\circ}\mathrm{C}$, then washed with PBSTx $3 \times 5\,\mathrm{min}$ at RT. Clearing, blocking, incubation with primary and secondary antibodies, and mounting were performed as for the larval brains.

Adult brain sections were transferred to a humid chamber, allowed to air-dry for $10\,\mathrm{min}$, post-fixed with $-20\,^{\circ}\mathrm{C}$-cold MetOH for $10\,\mathrm{min}$ at RT, and washed with PBSTx $3 \times 5\,\mathrm{min}$ at RT. Incubation with primary and secondary antibodies were performed as for the larval brains, except that the washes in between the steps were done $6 \times 5\,\mathrm{min}$ at RT. The stained sections were counterstained with DAPI $1\,\mathrm{µg/ml}$ for $15\,\mathrm{min}$, then washed with PBSTx $3 \times 5\,\mathrm{min}$ at RT, mounted with glycerol 80%, and stored at $4\,^{\circ}\mathrm{C}$ until imaged.

4.3.2.1 Antigen retrieval

Antigen retrieval protocols for the following stainings were applied:

- BrdU staining: to be performed after staining for other markers: incubate samples with $37\,^{\circ}\mathrm{C}$-warm hydrochloric acid $2\,\mathrm{M}$ for $20\,\mathrm{min}$ at $37\,^{\circ}\mathrm{C}$, wash with

Sodium Tetraborate Buffer 1×5 min at RT, then with PBSTx 3×5 min at RT.

- HuC/D staining: incubate samples with 98 °C-warm Tris-HCl 8.0 Buffer for 5 min at 98 °C, then wash with PBSTx 3×5 min at RT.

- PCNA staining: incubate samples with 85 °C-warm Sodium Citrate Buffer for 15 min at 85 °C, then wash with PBSTx 3×5 min at RT.

- TH(1) staining: for adult sections only, same as for PCNA staining.

4.3.3   TUNEL assay for cell death detection

TUNEL assays were performed using the ApopTag Red/Fluorescein In Situ Apoptosis Detection Kit (see Table 3.3). For larval brains only, the manufacturer's instructions were adjusted as follows. Cleared larval brains were washed with Sodium Citrate/PBSTx0.1 3×10 min at RT, post-fixed with -20-cold AcOH/EtOH 2:1 for 15 min at -20 °C, then washed with PBSTx 3×5 min and incubated in Equilibration Buffer for 1 h at RT. Working Strength TdT Enzyme, Stop/Wash solutions and the anti-DIG antibody were applied as recommended.

4.3.4   Mao histochemistry

Staining was performed as previously described[154], with minor modifications. Briefly, EDAC/NHS/DMSO-fixed brains were washed with PBSTx 3×5 min, incubated with Mao Staining Solution for 90 min in the dark, then washed with Tris-HCl 7.5 Buffer 2×10 min at RT and post-fixed with PFA 4% for 20 min at RT or $1 \times o/n$ at 4 °C. Finally, the stained brains were repeatedly washed with PBS and stored in glycerol 80% until imaged.

4.3.5   *In situ* hybridisation

MetOH-stored embryos were rehydrated with MetOH 50%/PBST 2×5 min followed by PBST 2×5 min, digested with proteinase K 2 µg/ml in PBST for 5 min, and finally post-fixed with PFA 4% for 20 min at RT. The post-fixed embryoswere washed with PBST 2×5 min at RT, blocked in 68 °C-warm Hyb+ Buffer for at least 2 h at 68 °C, and then incubated with the appropriate antisense DIG-labelled riboprobe (see Table 3.7) in Hyb+ buffer for $1 \times o/n$ at 68 degreeCelsius. Stringent washes were performed at 68 °C as follows: with Hyb− Buffer, 1×5 min; with Hyb− Buffer 25%/SSCT 2×, 3×10 min; with SSCT 2×, 1×10 min; with SSCT 0.2×, 3×20 min. After the stringent washes, the embryos were brought at RT and washed with SSCT 0.2×/MABT 50% and MABT only for 10 min each, then incubated with DIG Blocking Solution for at least 1 h at RT, and finally with the anti-DIG-AP antibody for at least 2 h at RT or $1 \times o/n$ at 4 °C. To visualise the alkaline phosphatase activity, the embryos were washed with MABT 4×20 min, incubated with BM Purple in the dark at RT and monitored until the desired signal was obtained. The chromogenic reaction was stopped by rinsing with PBST, the background removed with EtOH 95% for up to 5 min, after which the stained

embryos were washed with PBST $2 \times 5\,\text{min}$, post-fixed with PFA 4% for 20 min at RT, repeatedly washed with PBS and stored in glycerol 80% until imaged.

4.4 Sample preparation for high performance liquid chromatography measurements

Tissue samples consisted each of 10 pooled whole larvae or single adult brain. Larvae were starved 24 h before tissue collection to minimise possible contamination from amines in the gastrointestinal tract. An equal number of male and female adult fish were sacrificed.

4.5 Molecular biology

4.5.1 gDNA extraction and genotyping

Genomic DNA of individual or pooled embryos/larvae was obtained via tissue digestion with Tissue Lysis Buffer for at 55 °C on a shaker, followed by precipitation with i-PrOH for 15 min, $1\times$ wash with EtOH 70% for 5 min at full speed at RT, and resuspension in distilled water.

Genomic DNA of adult fish was extracted from fin clips (see 4.2.3) via tissue lysis with 100–300 µl of sodium hydroxide 50 mM for 20 min at 95 °C, followed by neutralisation with Tris-HCl 8.0 Buffer $0.1\times$ initial sodium hydroxide volume, and centrifugation for 10 min at full speed at RT to pellet debris. A volume of 3 µl of gDNA solution was added to 10 µl of PCR Mix. PCRs were run using the following thermal profile: 3 min of polymerase activation at 94 °C, followed by 30 cycles of 30 s of denaturation at 94 °C/60 s of annealing at variable temperature (see Table 3.8)/20 s of extension at 72 °C, and cooling at 4 °C. For genotyping of the $lrrk2^{\text{del11bp}}$ and the $lrrk2^{\text{tud112}}$ lines, the PCR products were digested with XhoI or RsaI restriction enzymes, respectively. The PCR products were run on agarose gel for 30 min at 120 V.

4.5.2 RNA extraction and purification

Total RNA was obtained from pools of $n = 20$ larvae/sample; each sample was representative of a unique parental pair. Tissue samples were homogenised in 1 ml TRIzol and RNA extracted upon addition of 200 µl of TCM and centrifugation for 15 min at full speed at 4 °C to allow the separation of the RNA-enriched aqueous phase. Collected RNA was added to 500 µl of i-PrOH and precipitated for 30 min, washed with EtOH 70% at 4 °C, and resuspended in 20 µl of distilled water. Residual gDNA was removed via digestion with TURBO DNase and the RNA precipitated with Lithium Chloride Precipitation Solution from the mMessage mMachine Kit (see Table 3.3), according to the manufacturer's instructions. Precipitated RNA was washed with EtOH 70% for 5 min at full speed at 4 °C, resuspended in 20 µl of distilled water and checked for integrity.

4.5.3   Reverse transcriptase-quantitative PCR

Reverse transcription of total RNA to cDNA was obtained using the Transcriptor First Strand cDNA Synthesis Kit (see Table 3.3), according to the manufacturer's instructions. A $1:25$–$1:15$ working dilution from the stock was prepared and a volume of $1\,\mu l$ added to $9\,\mu l$ of RT-qPCR Mix. Reverse transcriptase-qPCR experiments were carried out in the LightCycler 480 System (see Table 3.1) with the following temperature protocol: $10\,min$ of polymerase activation at $95\,°C$, followed by 45 cycles of $15\,s$ seconds of denaturation at $95\,°C/30\,s$ of annealing at 60–$62\,°C/15\,s$ of extension and data collection at $72\,°C$, and finally a 60–$95\,°C$ gradient to allow melting curve analysis. To extract expression data, the second derivative maximum method was applied as provided by the LightCycler 480 quantification software. Data were exported to Microsoft Excel and analysed according to the $2^{-\Delta\Delta C_t}$ method[183]. Target gene expression was calculated relative to *actb1* or *actb2* reference genes.

4.6   RNA-sequencing and transcriptome analysis

RNA samples were prepared as described in 4.5.2. Per each sample, $1\,\mu g$ of total RNA with integrity number > 7.0 was used as input for mRNA library preparation. The sequencing depth was 25 million fragments.

Sequencing data were analysed using QIAGEN's Ingenuity Pathway Analysis (IPA) software (`www.qiagen.com/ingenuity`).

4.7   Sequence alignment analyses

Sequences were retrieved from the latest assemblies of the human and zebrafish genomes (GRCh38p.7 and GRCz10, respectively). Alignment analyses were performed using Clustal Omega[184] and BLAST[185].

4.8   Image acquisition and processing

Confocal images were acquired with a Zeiss LSM 780 upright confocal microscope using C-Apochromat $10\times/0.45$ W and LD LCI Plan-Apochromat $25\times/0.8$ Imm Corr DIC M27 objectives for water immersion. Bright-field images were acquired with an Olympus DP71 or DP80 colour cameras connected to an MVX10 microscope. Images were processed using Fiji[186]. Processing was applied equally across entire images and to controls. Cell quantification was carried out manually through whole stacks. To analyse microglia/leukocyte morphology and complexity, confocal stacks were background-subtracted using the sliding paraboloid method, despeckled, and thresholded using Li's method. Obvious artefacts were manually removed from subsequent processing and analyses. The 3D ImageJ Suite plugin[187] was used to segment objects (minimum size threshold: 1,000; objects on borders excluded) and extract morphological data from 3D masks. The same 3D masks were subsequently skeletonised and subjected to 3D skeleton analysis using the AnalyzeSkeleton plugin on Fiji[188]. Loops were pruned using the shortest branch

method. For each skeleton, the longest shortest path was also calculated. A ramification index was defined as $\frac{2b}{j+e}$, where b is the number of branches, j the number of junctions, e the number of end-points, as previously defined[188].

4.9   Statistical analysis

The data analysis for this thesis was generated using: the Real Statistics Resource Pack software (Release for Mac 3.1.2, copyright 2013–2016) developed by C. Zaiontz (`www.real-statistics.com`); R[189]; and GraphPad Prism version 7.0b for Mac OS X. To compare means, requirements of normal distribution and homoscedasticity were checked using Shapiro-Wilk's test and the F-test, for two groups, or Levene's test, for more than two groups, respectively. To determine the statistical significance of group differences, P values were calculated using: Student's t-test or ANOVA, for normally distributed and homoscedastic data; Student's t-test with Welch's correction, for normally distributed and heteroscedastic data; Mann-Whitney's U-test for non-normally distributed data. Multiple comparisons following ANOVA were performed using Dunnett's or Dunn-Šidák's methods. For multivariate logistic regression analyses, the best fitting models were automatically selected via backward stepwise elimination. The model performance was visualised and assessed using the methods previously described[190]. For each experiment, sample sizes are reported in the Figures. Plot features are described in the Figure legends. Within the Figures, significant comparisons are marked by asterisks: *, $P < 0.05$; **, $P < 0.01$; ***, $P < 0.001$; ****, $P < 0.0001$. P values rounded to three decimal places are reported in the Figure graphs for values comprised between 0.050 and 0.059; P values rounded to four decimal places are reported in the main text.

Results

5.1 Homology between the human *LRRK2* and zebrafish *lrrk2* genes

Confirming previous findings from R. Ahrendt[168], syntenic analysis using the latest assemblies of the human and zebrafish genomes (GRCh38p.7 and GRCz10, respectively) revealed the conservation of the *SLC2A13* locus as the downstream neighbour of *LRRK2* in both species. Moreover, duplication of the zebrafish *lrrk2* locus is not reported. The human LRRK2 and zebrafish Lrrk2 proteins share the same domains, with the kinase domain displaying the highest degree of conservation (Figure 5.1); three of the four LRRK2 amino acid residues implicated in pathogenic substitutions in human PD patients are fully conserved (Supplementary Table 1). Altogether, these data point out that human *LRRK2* and zebrafish *lrrk2* are true orthologues, and not divergent genes.
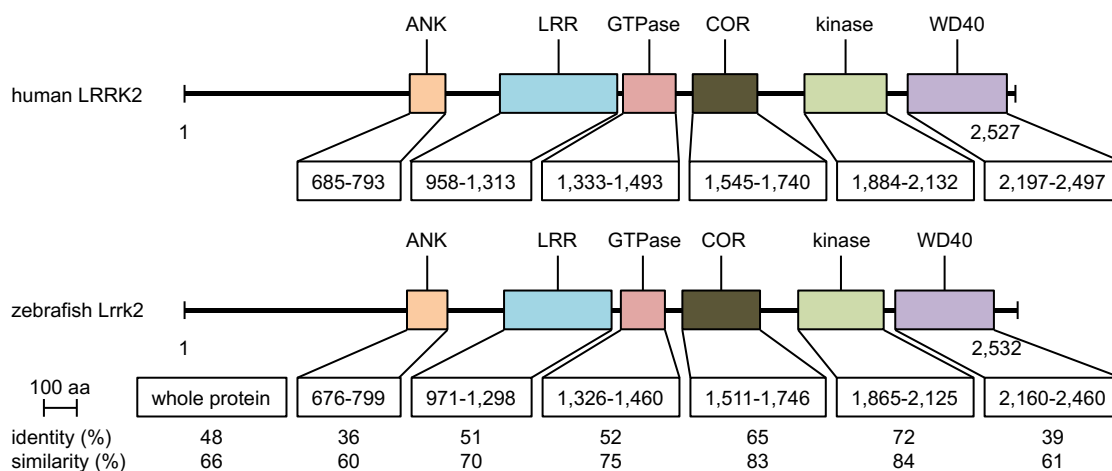
Figure 5.1: Homology between the human LRRK2 and the zebrafish Lrrk2 proteins. Updated data from R. Ahrendt[168] using the latest assemblies of the human and zebrafish genomes (GRCh38p.7 and GRCz10, respectively). Alignment of the whole sequence and the individual domains of human LRRK2 (NP_940980) and zebrafish Lrrk2 (NP_001188385) proteins reveals a high degree of conservation of the catalytic core. The percentages of identity (same residues at the same positions in the alignment) and similarity (identical residues plus conservative substitutions) are indicated. Abbreviations: ANK, ankyrin domain; COR, C-terminal of Ras of complex proteins; LRR, leucine-rich repeat domain.

5.2 Disruption of *lrrk2* via TALEN-mediated mutagenesis

To validate the phenotype previously described in the Lrrk2-deficient *tud112* zebrafish line[168], and to potentially solve the controversy arising from previous MO studies[136–138], Transcription activator-like effector nuclease (TALEN)-mediated mutagenesis was used to generate an additional *lrrk2* null allele. S. Hans planned the mutagenesis strategy; C. Spiegel generated the *lrrk2* allele. Although the *tud112* mutation results in a truncated Lrrk2 protein, the ANK domain and part of the LRR domain are left, thereby making residual biological function possible. Therefore, for the generation of the new allele the *lrrk2* exon 17, corresponding to the beginning of the ankyrin repeat, was targeted. To this aim, two different TALEN constructs were engineered to bind DNA with sufficient reciprocal proximity (Figure 5.2a). TALEN capped RNAs were synthesised and injected in one-cell stage embryos. Surviving embryos were raised and sexually mature fish screened for mutations in the F1 generation. The selected founder bore an 11-bp-long deletion (*c.1980_1990del* according to the Human Genome Variation Society[170]; henceforth referred to as "*tud115*") within *lrrk2* exon 17, causing a frameshift and a premature termination codon (PTC) in exon 18 (p.(Asp660GlufsTer41)). Since the deleted region contained an XhoI restriction site, an RFLP-based genotyping strategy could be devised (Figure 5.2b). F1 heterozygous fish were incrossed to obtain F2 *tud115* homozygous mutants and wild-types (*wt*). Because *lrrk2* is maternally provided[136,168], to exclude potential confounding maternal effects early in development, the F2 fish were further incrossed to establish the maternal-zygotic *tud115* mutant and *wt* control lines.

Unexpectedly, aberrant *lrrk2* transcripts in *11del* mutants did not undergo nonsense-mediated decay (NMD)[31], as revealed via *in situ* hybridisation (ISH; Figure 5.3a) and quantified via reverse transcriptase-quantitative PCR (RT-qPCR; Figure 5.3b); in fact, the *lrrk2^tud115^* allele attenuated NMD driven by the *lrrk2^tud112^* allele in transheterozygous *tud115/tud112* larvae (Figure 5.3b).

One mechanism to regulate transcript abundance in eukaryotes is alternative splicing[191]. Alternative PTC-free transcripts may still lead to functional products, thereby attenuating or even circumventing the desired knockout[192,193]. Indeed, region or cell-specific *LRRK2* splicing variants have been observed in both healthy humans[194] and mice[66]. Although the splicing profile of zebrafish *lrrk2* has never been studied, three transcripts are deposited in the Ensembl library according to the latest genome release (Figure A.2): all share the TALEN-targeted region, thus making the existence of functional *tud115* mutation-free transcripts unlikely. Another way to escape NMD is the re-initiation of protein translation at a downstream, alternative in-frame translation initiation site (aTIS), thus yielding an N-terminally truncated product[195]. The phenomenon may typically occur when an aTIS is in proximity of the canonical TIS (cTIS)[196–198], but occurrences at further downstream sites have also been reported[199,200]. Using the ATGpr_sim program (`http://www.hri.co.jp/atgpr/ATGpr_sim.html`)[201], it was estimated that the first in-frame aTIS downstream to the *tud115* mutation (position *c.2089*)
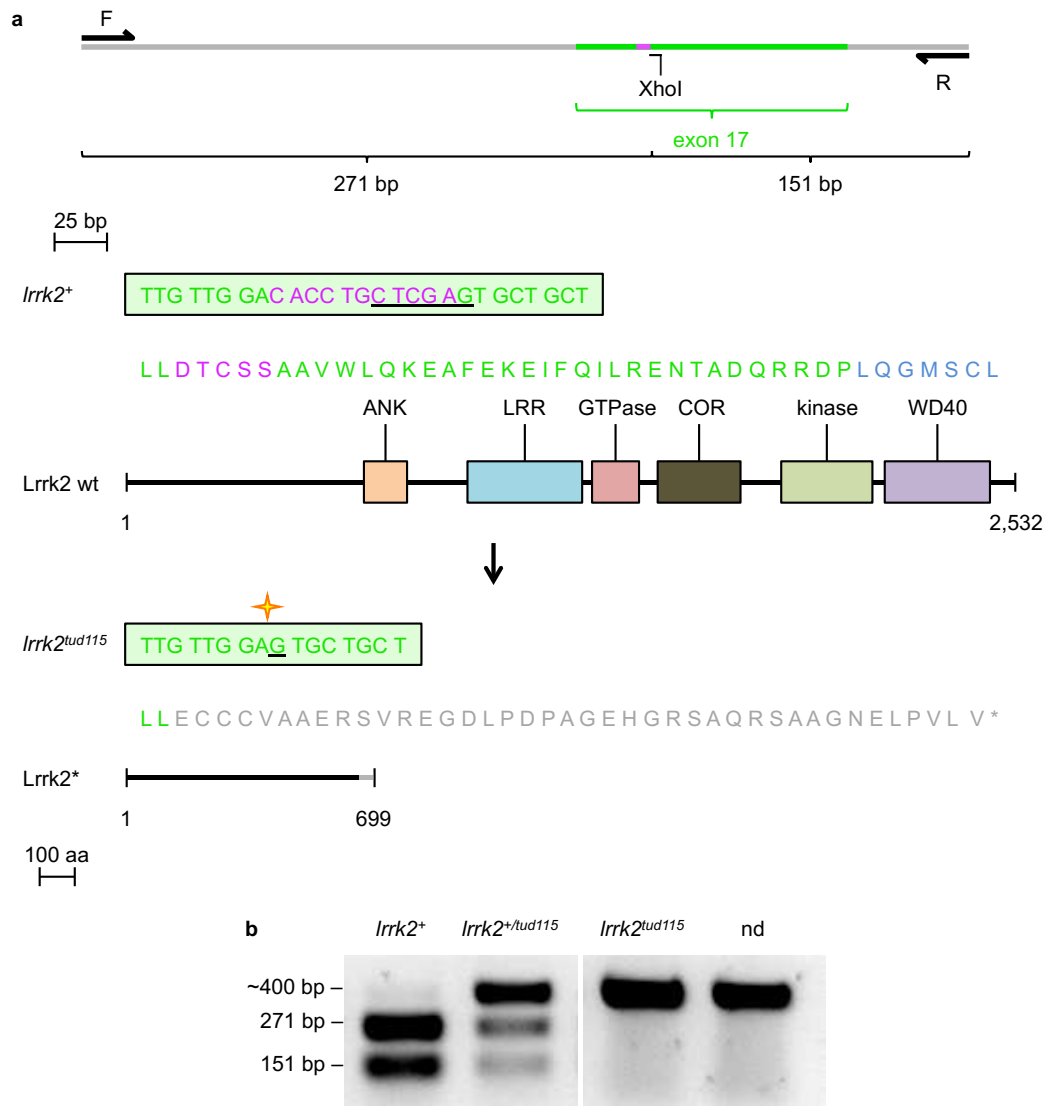
Figure 5.2: Generation of the *lrrk2^{tud115}* allele. The mutagenesis strategy was designed by S. Hans; the *lrrk2^{tud115}* allele was generated by C. Spiegel; characterisation was carried out by S. Suzzi. (a) TALEN-mediated mutagenesis was used to generate a *lrrk2* null allele. The identified allele (*tud115*) consists in an 11-bp-long deletion (*c. 1980_1990del*) within *lrrk2* exon 17, causing a frameshift and a premature termination codon in exon 18 (turquoise; p.(Asp660GlufsTer41)). (b) The *tud115* mutation also disrupts a XhoI restriction site, allowing identification via RFLP-PCR. To this aim, PCR primers (F, R in a) were designed to amplify a 422-bp-long product comprising the XhoI site: upon XhoI-mediated digestion, only the wild-type amplicon is cleaved into two fragments (271 and 151 bp), allowing identification of wild-type *lrrk2^+*), heterozygous (*lrrk2^{+/tud115}*), and homozygous mutant (*lrrk2^{tud115}*) individuals compared to undigested product (nd).
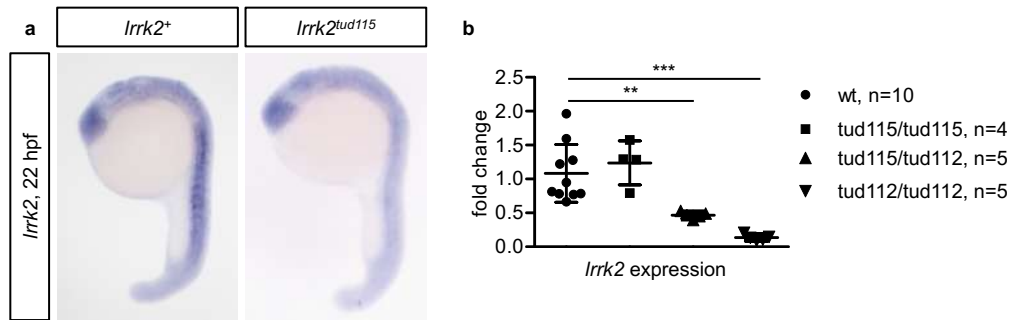
Figure 5.3: The *tud115* allele does not cause NMD of *lrrk2* RNA. (a) *lrrk2* ISH on 22-hpf embryos showing unaltered levels of *lrrk2* expression. (b) RT-qPCR analysis of *lrrk2* expression on *wt*, homozygous *tud115*, transheterozygous *tud115/tud112*, ad homozygous *tud112* mutants at 8 dpf confirms the absence of *lrrk2* NMD in homozygous *del11*bp mutants. Note the intermediate level of *lrrk2* expression in transheterozygous *tud115/tud112* mutants.(b) Plots represents means ± standard error of the mean. Statistical analyses: one-way ANOVA followed by Dunnett's *post hoc* test.

has a reliability score of 0.15 in the *wt* transcript, but 0.36 in the *tud115* transcript, the highest after the cTIS (0.59). The resulting product would consist in a C-terminal Lrrk2 moiety comprising portion of the ankyrin repeat and all the functionally relevant domains, including the catalytic core. Intriguingly, LRRK2 constructs lacking the N-terminus until the LRR domain (1328–2527 aa) result in an approximately threefold increase of autophosphorylation when expressed in human embryonic kidney 293FT cells[55]. Conceivably, the *tud115* mutation, originally selected to study *lrrk2* LOF, might in fact determine a GOF of the Lrrk2 kinase domain via loss of the N-termius. Finally, the presence of functional N-terminal fragments cannot be excluded. It has been shown that the N-terminal portion of LRRK2 is aggregation-prone and that aggregates of N-terminal LRRK2 constructs (1–938 aa) are able to protect transfected human neuroblastoma SH-SY5Y cells from 6-OHDA-induced cell death[202]. In a similar scenario, the *tud115* allele might even act as a neomorph.

Because of the numerous sources of potential setbacks as outlined above, it was crucial to gain proof of the gene knockout on a protein level. To this aim, commercially available rabbit monoclonal anti-LRRK2 antibodies (*ab133474*, *ab133475*) were tested on zebrafish embryo lysates via western blot, but unsuccessfully. In particular, *ab133475* was recently reported to detect the zebrafish Lrrk2 protein in whole-mount embryos[138]. Therefore, the same antibody was also tested on fixed tissue of different origin (whole-mount larvae, adult brain sections), but no specific staining could be recognised. Attempts to produce proprietary antibodies failed. For want of alternative assays to validate *lrrk2* knockout, the *tud115* line was not considered further.

5.3 Deletion of the entire *lrrk2* locus using the CRISPR/Cas9 system

To overcome the undesired side effects of frameshift mutations, including cellular stress due to aberrant transcripts and truncated protein products with residual or new function, the clustered regularly interspaced short palindromic repeats (CRISPR)/CRISPR-associated protein-9 nuclease (Cas9) system was used to delete the ~60-kb-long *lrrk2* locus containing the entire *ORF*. One caveat is that, along with the *lrrk2* ORF, as yet unidentified non-coding RNA genes might be disrupted. However, their existence is not supported by the latest genome assembly. S. Hans designed the mutagenesis strategy; S. Spieß generated the *lrrk2* allele.

To achieve full deletion of the *lrrk2* locus, two CRISPR/Cas9 target sites flanking one 75 bp upstream, the other 33 bp downstream the 60,140-bp-long *ORF* were selected (Figure 5.4a). To identify deletion alleles, a gap-PCR strategy was devised, with primers amplifying a 289-bp-long amplicon inside the target region were duplexed with flanking primers, unable to direct amplification unless a deletion brings them in sufficient reciprocal proximity (Figure 5.4a, b). The selected founder produced offspring where the flanking primers amplified a 204-bp-long product; targeted deletion (*c.−61_*42del*; henceforth simply referred as *tud113*) was confirmed by sequencing. The complete absence of *lrrk2* expression in *tud113* homozygous mutants was verified via ISH (Figure 5.4c). F1 heterozygous fish were incrossed to obtain F2 homozygous *tud113* mutants and wild types. F2 homozygotes were further incrossed to establish the maternal-zygotic mutant (*mzLrrk2*) and wild-type control *wt* lines. In striking contrast with published MO-induced phenotypes[136,138], *mzLrrk2* individuals develop normally, are viable, and reach sexual maturity at the same age as the *wt* controls, with both females and males being fertile.

It has been proposed that the paralogue *LRRK1* may offset the loss of *LRRK2* in mice[101]. To exclude possible compensation from the paralogous *lrrk1* gene, *lrrk1* expression was analysed via RT-qPCR in *mzLrrk2* larvae at both 5 and 10 dpf, but no difference was observed compared to *wt* controls (Figure 5.5).

5.4 Pleomorphic but transient neurodevelopmental phenotype in *mzLrrk2* zebrafish

Because the link between *LRRK2* and PD implies a critical role in brain function[203], *mzLrrk2* zebrafish were characterised with regard to the brain phenotype at both larval (5 and 10 dpf) and adult (6 and 11 mo) stages. For cell quantification in the larval brain, the brain was subdivided into anterior (telencephalon), middle (diencephalon, mesencephalon), and posterior (rhombencephalon) portions (Figure 5.6a').
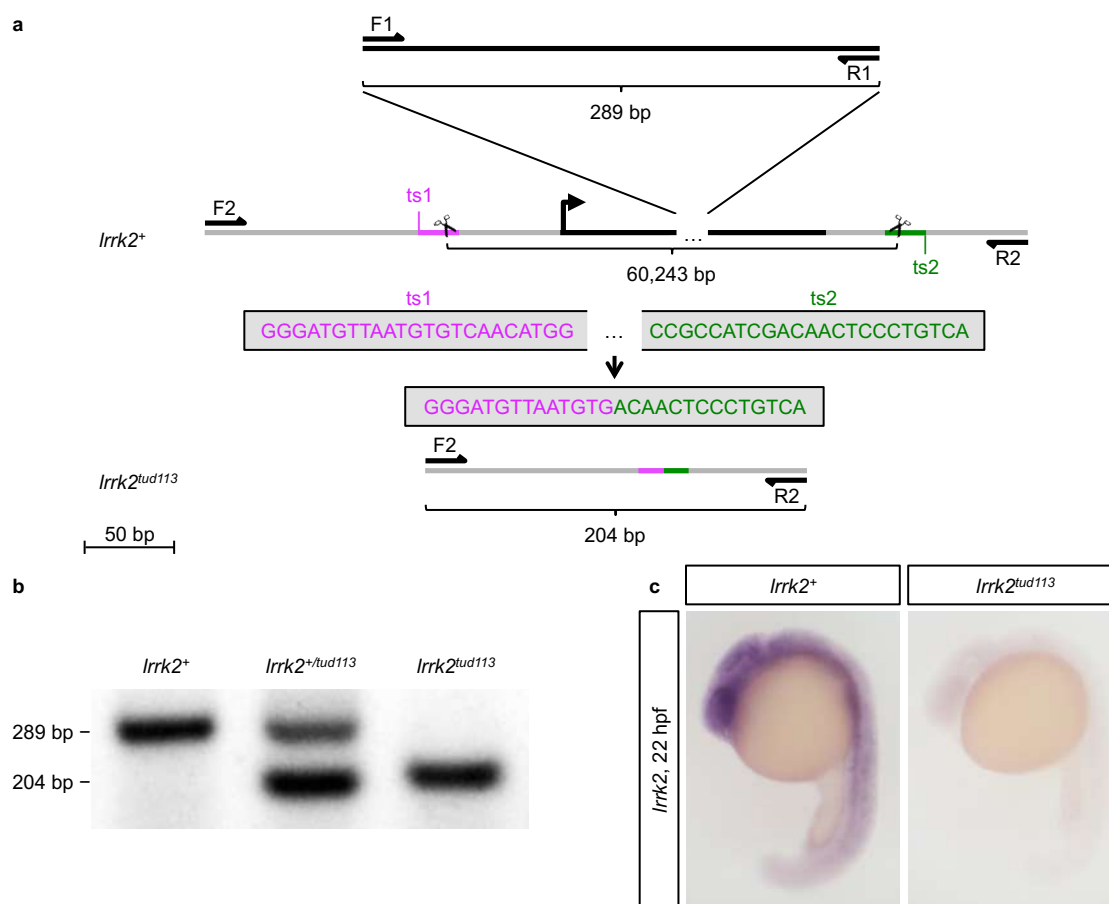
Figure 5.4: Generation of the zebrafish *lrrk2*[tud113] allele. The mutagenesis strategy was designed by S. Hans; the *lrrk2^{tud113}* was generated by Sandra Spieß; characterisation was carried out by S. Suzzi. (a) Scheme reproducing the targeting and screening strategy. The *lrrk2 ORF* is highlighted in black; F1, R1: *lrrk2 ORF*-specific primers; F2, R2: *lrrk2 ORF*-flanking primers; ts1 (magenta), ts2 (green): gRNA target sites (ts). (b) gap-PCR analysis of genomic DNA from wild-type (*lrrk2^+*), heterozygous (*lrrk2^{+/tud113}*), and homozygous mutant (*lrrk2^{tud113}*) individuals. F1 and R1 amplify a 289-bp-long product, F2 and R2 a 204-bp-long product. (c) *lrrk2* ISH confirming the complete absence of *lrrk2* expression in 22-hpf *lrrk2^{tud113}* embryos.
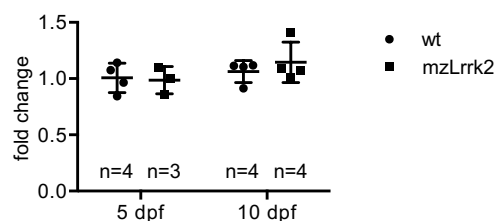
Figure 5.5: Expression of *lrrk1* in *mzLrrk2* larvae. Reverse Transcriptase-quantitative PCR was used to measure *lrrk1* expression at both 5 and 10 dpf. no difference was observed between *mzLrrk2* and *wt* controls.

40

5.4.1 No overt signs of neurodegeneration

Enhanced apoptosis in the brain was found both in MO-injected larvae at 6 dpf [136] and in *mzLrrk2^tud112* larvae at 8 dpf [168], but not in *mzLrrk2^tud112* juveniles at 1.5 mo, were cell death matched control levels. Consistently with the findings in *mzLrrk2^tud112* fish, the apoptosis rate in *mzLrrk2* larvae was transient, being increased threefold at 5 dpf (anterior: $P = 0.0061$; middle: $P < 0.0001$; Figure 5.6a, a'), but comparable to controls at 10 dpf (Figure 5.6b, b').
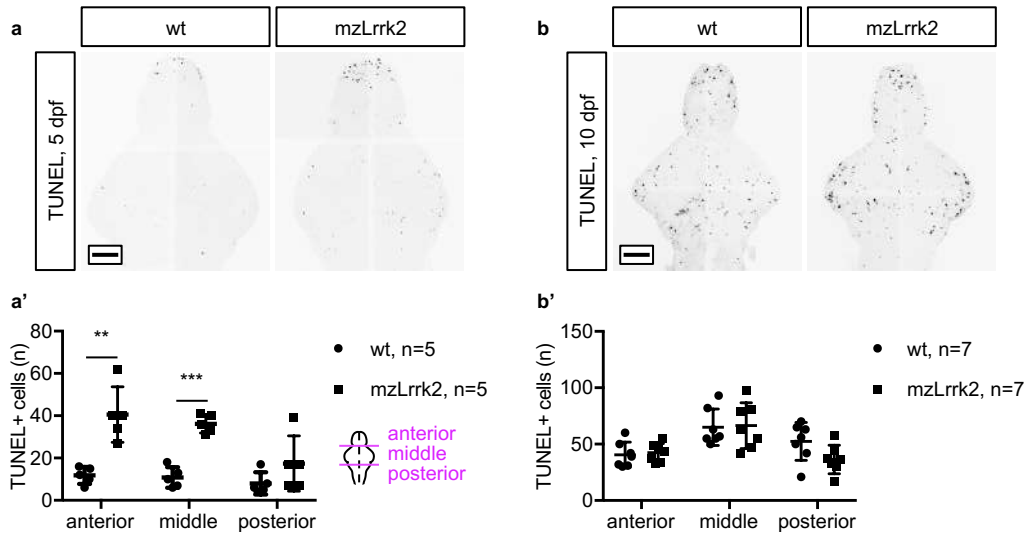
Figure 5.6: Quantification of cell death rate in the brain. TUNEL assay was used to visualise cell death in the brain. Quantification was carried out over the whole brain, subdivided into anterior (telencephalon), middle (diencephalon, mesencephalon), and posterior (rhombencephalon) portions. The number of apoptotic cells in *mzLrrk2* brains is increased at 5 dpf (a, a'), but matched wt levels at 10 dpf (b, b'). (a', b') Plots represent means $\pm$ s.d. Statistical analyses: (a', b') two-tailed Student's *t*-test. Scale bars: (a, b) 100 µm.

In addition, in contrast with MO-injected larvae [136,138], no overt sign of neuronal loss was evident after HuC/D staining at both 5 and 10 dpf (Figure 5.7). Moreover, differently from MO-injected [136] but similarly to *mzLrrk2^tud112* larvae, the axonal network was preserved in *mzLrrk2* brains as revealed by acetylated Tubulin staining (Figure 5.8).
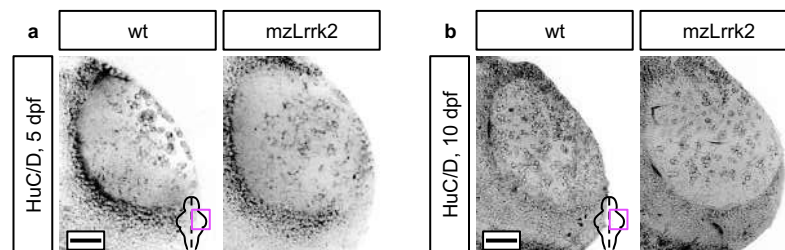
Figure 5.7: Visualisation of mature neurons in the dorsal tectum neuropil. HuC/D IHC was carried out to label mature neurons in the whole brain at 5 dpf (a) and 10 dpf (b). No difference emerges between *mzLrrk2* and controls. Scale bars: (a, b) 50 µm.
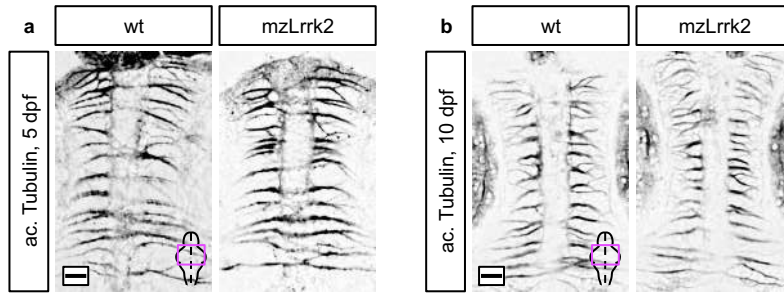
Figure 5.8: Visualisation of the axonal network in the tectal commissure. Acetylated Tubulin IHC was carried out to label axons in the whole brain at 5 dpf (a) and 10 dpf (b). No difference emerges between *mzLrrk2* larvae and controls. Scale bars: (a, b) 20 μm.

To further investigate the consequences of Lrrk2 deficiency on neural development, Claudin k staining was performed to visualise myelination[173]. Claudin k expression was delayed in the ventromedial hindbrain of mzLrrk2 at 5 dpf, but normal at 10 dpf (Figure 5.9). In summary, these data show that loss of *lrrk2* causes early but transient defects, including increased apoptosis and delayed myelination, albeit no obvious signs of neurodegeneration.
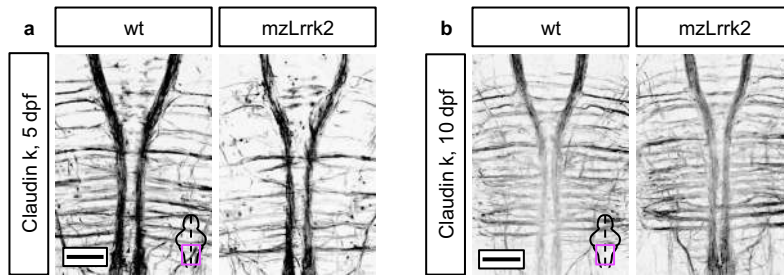
Figure 5.9: Visualisation of myelinated fibres in the ventral hindbrain. Claudin k IHC was carried out to label myelinated fibres in the whole brain. Although *mzLrrk2* larvae show delayed expression at 5 dpf (a), they match control levels at 10 dpf (b). Scale bars: (a, b) 100 μm.

5.4.2 Abnormal leukocyte morphology and response to inflammatory stimulus

Neuroinflammation is an important contributor and a concurring factor in many neurodegenerative conditions, including PD[204,205]. In particular, burgeoning evidence demonstrates a link between *LRRK2* and microglia function[206,207]. Because the shape of microglia may be indicative of their activation state[208], microglia/leukocyte were visualised using L-Plastin as pan-leukocyte marker and processed via a semi-automated procedure to extract relevant morphological features in 3D stacks (see 4.8; Figure A.3a–a''').

The overall number of segmented L-Plastin+ microglia/leukocyte was reduced by about one third in 5-dpf *mzLrrk2* brains (Figure 5.10a); the trend was maintained at 10 dpf, although statistical significance was not reached (Figure 5.10b).
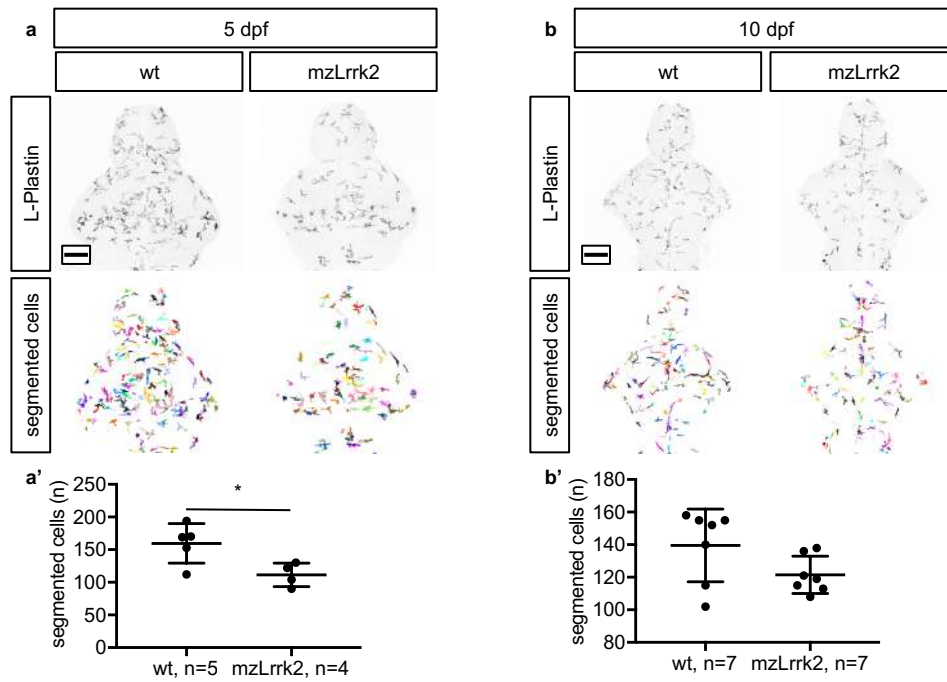
Figure 5.10: Quantification of microglia/leukocyte cell number. L-Plastin IHC was carried out to label microglia/leukocytes in the whole brain. Quantification of segmented L-Plastin+ cells revealed that the number of microglia/leukocytes was reduced in *mzLrrk2* brains at 5 dpf (a, a'), but comparable to controls at 10 dpf (b, b'). (a', b') Plots represent means ± s.d. Statistical analyses: (a', b') two-tailed Student's *t*-test. (a, b) Scale bars: 100 µm.
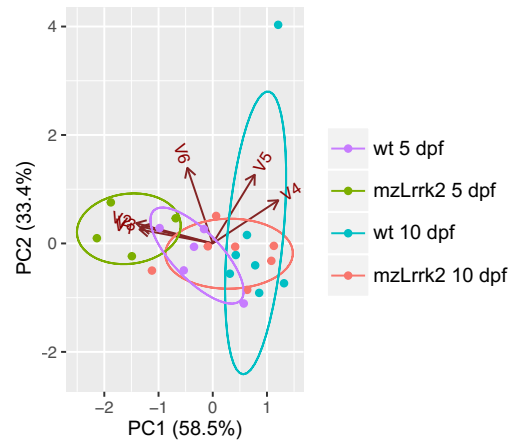
Figure 5.11: PCA of brain microglia/leukocyte morphology. For each animal, the average morphological parameters were considered; standardised data were used. The samples (dots) and the original variables (arrows) are projected on the 2D plane defined by *PC1* and *PC2*: *V1*, volume; *V2*, surface; *V3*, ramification; *V4*, average branch length; *V5*, maximum branch length; *V6*, largest shortest path. *PC1* opposes cell size (*V1*, *V2*) and ramification (*V3*) to branch extension (*V4*, *V5*); *PC2* represents overall cell complexity (*V4*, *V5*, and *V6*). Within brackets, the percentage of total variance explained. Note the poor separation between *mzLrrk2* and *wt* samples at 10 dpf.

43

For each brain, average microglia/leukocyte *volume*, *surface*, *ramification*, *average branch length*, *maximum branch length*, and *longest shortest path* were used to study the variance across samples via principal component analysis (PCA; Figure 5.11). As a result, the first two principal components represented alone over 90% of the total variance: *PC1*, which is the most relevant (58.4% of the total variance), discriminated between small cells with long processes and large cells with short processes; *PC2* (33.4% of the total variance) opposed ramification to cell size and extension (Table 5.1). Of note, while little separation existed between the *wt* samples at the two time points, the *mut* samples were neatly segregated along the PC1 axis, although the 10-dpf *mzLrrk2* samples clustered with the *wt* samples (Figure 5.11). In conclusion, 5-dpf *mut* brains had on average larger and more ramified cells at 5 dpf, smaller and less complex, similar to the *wt*, at 10 dpf. This interpretation is mirrored by the analysis of each morphological parameter separately (Figure A.3b–o).

Table 5.1: PCA loadings of microglia/leukocyte morphology. *V1*: *volume*; *V2*: *surface*; *V3*: *ramification*; *V4*: *average branch length*;*V5*: *maximum branch length*; *longest shortest path*. For each principal component (*PC*), the relative percent of total variance is reported within brackets.

variable	PC1 58.5	PC2 33.4	PC3 6.7	PC4 0.9	PC5 0.4	PC6 0.2
V1	−0.483	0.123	−0.609	0.071	0.062	−0.610
V2	−0.504	0.177	−0.315	0.058	0.142	0.769
V3	−0.472	0.147	0.629	0.571	0.110	−0.148
V4	0.432	0.376	−0.304	0.680	−0.333	0.083
V5	0.276	0.598	0.033	−0.121	0.738	−0.070
V6	−0.167	0.658	0.202	−0.434	−0.555	−0.043

To verify whether even mild morphological alterations correlate with impaired leukocyte function, 10-dpf larvae were treated with 12-*O*-tetradecanoylphorbol 13-acetate (TPA) to induce systemic acute inflammation[209] for 2 h prior to killing. Although treatment was not sufficient to elicit a substantial effect on the brain (not shown), significantly quenched leukocytosis was found in the tail ($P = 0.0368$; Figure 5.12). In conclusion, these data suggest that zebrafish Lrrk2 plays a transient role in leukocyte biology, including a response to proinflammatory stimuli, and additionally hint that the recreation of pathological conditions in animal models, such as inflammation, may be an essential expedient for a thorough understanding of LRRK2 function.
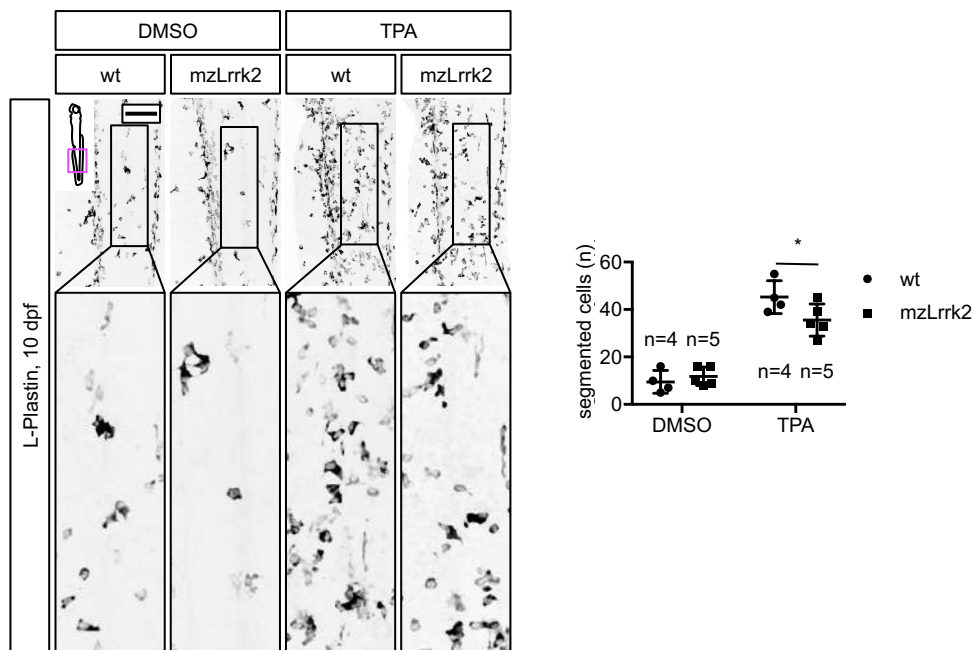
Figure 5.12: Evaluation of the leukocyte response to systemic acute inflammation. Reduced leukocytosis in the tail of 10-dpf *mzLrrk2* larvae after 2 h exposure to TPA to induce systemic acute inflammation. Segmented objects were quantified within a constant 566.79×124.54 µm area caudal to the anus and comprised between the dorsal longitudinal anastomotic vessel and the caudal artery. Sample n are indicated in the graph. Plot represents means $\pm$ s.d. Statistical analyses: one-tailed Student's *t*-test. Scale bar: 100 µm.

5.5 Intact CA system but perturbed aminergic catabolism in older fish

DA neurons are invariably affected by PD in humans. Reduced catecholaminergic (CA) neurons were found in *mzLrrk2*[tud112] throughout development[168]. Therefore, the CA system was thoroughly examined in *mzLrrk2* fish. CA cell populations along the rostro-caudal axis from the olfactory bulb to the locus cœruleus were visualised via tyrosine hydroxylase (TH) IHC and denominated after the nomenclature introduced previously[127,144] (Figure 5.13a). Zebrafish possess two paralogous *th* genes: *th1* and *th2*[148–151]. Because commercially available anti-TH antibodies only recognise TH1, but not TH2 protein (Figure 5.13a'), for an exhaustive scrutiny of the zebrafish CA system, double staining with an anti-TH1 antibody and a recently characterised pan-TH antibody was performed to unequivocally identify TH2+ cells by exclusion[147]. TH2+ cells in larval brains were quantified by S. Bilican. Additionally, the levels of biogenic amines and their catabolites (Figure 5.13b) were measured via electrochemical detection coupled with high performance liquid chromatography. Chromatographic analyses were performed as previously described[144] by S. A. Semenova in the laboratory of P. Panula (Helsinki, Finland).
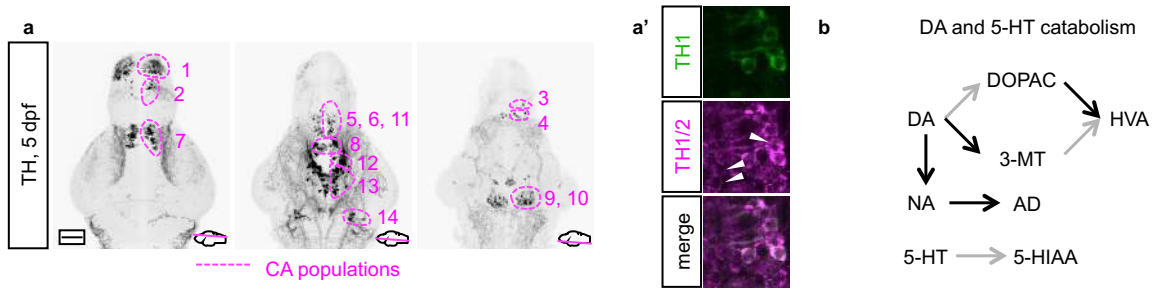
Figure 5.13: Analysis of the CA system and catabolism. (a) The zebrafish catecholaminergic (CA) cell populations in the rostro-caudal axis from the olfactory bulb to the *locus cœruleus* as revealed by tyrosine hydroxylase 1 (TH1) IHC at 5 dpf. Pop. 1: olfactory bulb; pop. 2: telencephalic complex; pop. 3: preoptic area, *pars anterior*; pop. 4: preoptic area, *pars posterior*; pop. 5, 6, 11: diencephalic complex; pop. 7: pretectal area; pop. 8: paraventricular organ, *pars anterior*; pop. 9: paraventricular organ, *pars intermedia*; pop. 10: paraventricular organ, *pars posterior*; pop. 12: posterior tuberal nucleus/posterior tuberculum; pop. 13: hypothalamic complex; pop. 14: *locus cœruleus*. (a') Combination of the anti-TH1 antibody with the pan-TH antibody allows the identification of TH2+ cells (white arrowheads) by exclusion. TH2+ cells are found within the TH1 pop. 8, 9, and 10 in the paraventricular organ, thereby constituting the TH2 pop. 8b, 9b, 10b. (b) Simplified scheme of the catabolism of dopamine and serotonin. Each arrow represents a distinct enzymatically-catalysed step. Grey arrows indicate reactions catalysed by the combined action of monoamine oxidase/aldehyde dehydrogenase. Abbreviations: 3-MT, 3-methoxytyramine; 5-HIAA, 5-hydroxyindoleacetic acid; 5-HT, serotonin; AD, adrenalin; DA, dopamine; DOPA, 3,4-dihydroxyphenylacetic acid; HVA, homovanillic acid; NA, noradrenalin. (a) Scale bar: 100 μm.

No TH+ cell population was missing or overtly altered in *mzLrrk2* fish. Nonetheless, at 5 dpf, *mzLrrk2* brains displayed a lower numbers of TH+ cells in discrete populations: olfactory bulb (pop. 1, $P = 0.0313$); telencephalic complex (pop. 2, $P = 0.0322$); diencephalic complex (pop. 5, 6, 11, $P = 0.0042$); and paraventricular organ, *partes intermedia* and *posterior* (pop. 9, 10 $P = 0.0042$; Figure 5.14a, a'). The net effect was a 20% reduction of the overall number of TH+ cells (not shown). Because *mzLrrk2* brains showed a higher cell death rate at 5 dpf (Figure 5.6), TUNEL assay was combined with TH IHC to investigate whether CA neurons were particularly affected. However, virtually no colocalisation was found (not shown). Consistently, the aminergic catabolism appeared normal (Figure 5.14b). This result is however in contrast with the increased levels of homovanillic acid found in 5-dpf *mzLrrk2*[tud112] larvae[168]; nonetheless, those data are difficult to interpret, as dopamine levels were normal[168].

At 10 dpf, only the hypothalamic complex (pop. 13, $P = 0.0403$) and, mildly, the paraventricular organ, *pars posterior* (pop. 10b, $P = 0.0496$) were significantly affected; in contrast, an increase in the preoptic area, *pars posterior* (pop. 4, $P = 0.0138$) was measured (Figure 5.14c, c'). In general, the overall number of TH+ cells did not differ from the *wt* controls (not shown). Intriguingly, although the DA metabolism was unaffected, a higher concentration of 5-hydroxyindoleacetic acid, catabolite of serotonin, was measured ($P = 0.0190$; Figure 5.14d). Because brain-specific effects could be masked in whole-larvae homogenates, the activity

of monoamine oxidase (Mao), one of the two major catabolising enzymes, was histochemically visualised in 5- and 10-dpf brains (Figure A.4). However, no difference was observed between *mzLrrk2* and controls.
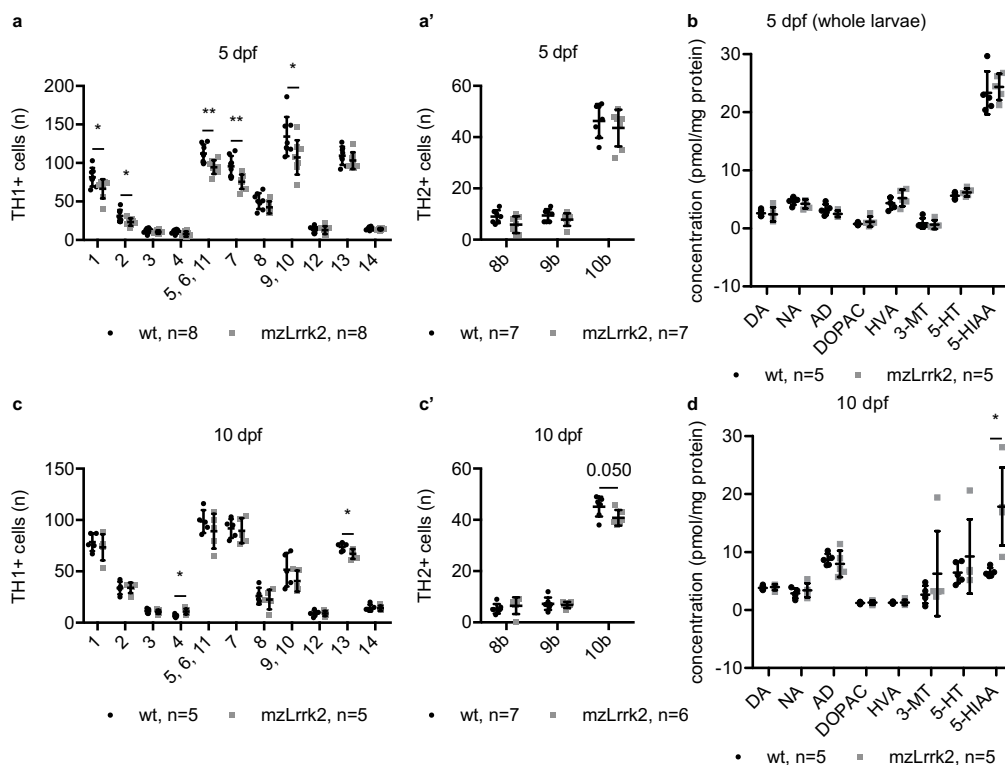
Figure 5.14: Intact CA system at the larval stage. (a–d) Quantification of TH1+ (a, c) and TH2+ cells (a', c') in the brain, quantification of aminergic catabolites in whole larvae (b, d) at 5 dpf (a–b) and 10 dpf (c–d). TH2+ cells were quantified by S. Bilican; chromatographic analysis of amine catabolism was carried out by S. A. Semenova. Early defects in discrete CA cell populations at 5 dpf are resolved by 10 dpf. The DA catabolism is normal at both time points. (a–d) Plots represent means ± s.d. (j) Statistical analyses: (a pop. 2–14, a', d DA–HVA, b 5-HT, b 5-HIAA, c pop. 1, c 3–14, c', d DA–HVA, d 5-HIAA) two-tailed Student's *t*-test; (a pop. 1, b 3-MT, c pop. 2, d 5-HT) two-tailed Mann-Whitney's *U*-test.

In the adult brain, the CA system appeared structurally intact at 6 mo, with a modest increase in cell number in the telencephalic complex (pop. 2, $P = 0.0472$; Figure 5.15a). Furthermore, TH1 protein levels at 11 mo were normal (Figure 5.15b). Altogether, these data indicate that in striking contrast with *mzLrrk2*[tud112] fish[168], the CA phenotype in *mzLrrk2* fish is not persistent, but resolves during early development. However, the aminergic catabolism in the brain was perturbed in 11-mo *mzLrrk2* fish (Figure 5.15c). Specifically, a significant decrease of both dopamine ($P = 0.0216$) and serotonin ($P = 0.0013$) was found and, consistently, a significant increase in their catabolites 3,4-dihydroxyphenylacetic acid ($P = 0.0187$), homovanillic acid ($P = 0.0001$), and 5-hydroxyindoleacetic acid ($P = 0.0004$), all products of Mao activity, was detected. Although Mao levels were unaltered, as determined on both gene expressional (Figure A.5a)

and biochemical level (Figure A.5b), the levels of the dopamine catabolite 3-methoxytyramine, product of catechol-O-methyltransferase activity, were not significantly different ($P = 0.1250$; Figure 5.15c) between *mzLrrk2* and control brains. Because monoamine oxidase and catechol-O-methyltransferase are the major enzymes responsible for catecholamine catabolism in the brain, the neurochemical signatures observed can be ascribed to Mao activity. In conclusion, although the cellular composition of the CA system stays stable, 11-mo *mzLrrk2* fish show increased Mao-mediated aminergic degradation.
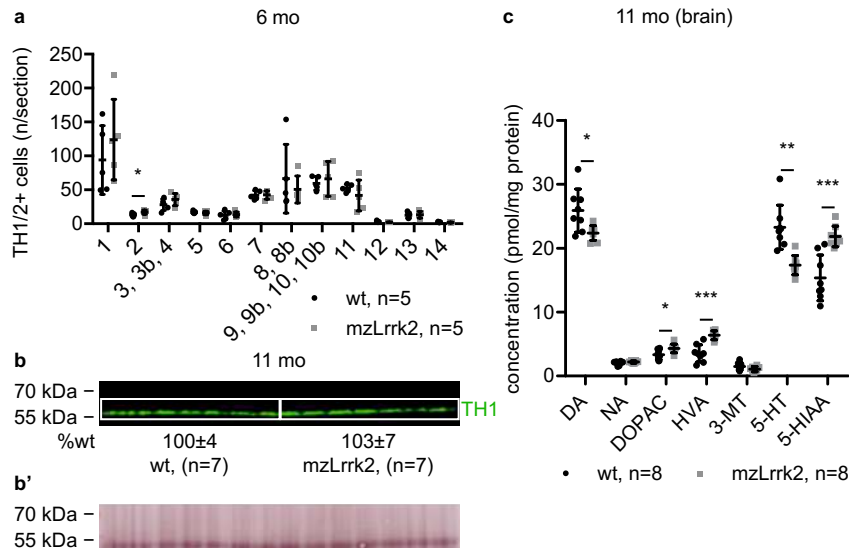
Figure 5.15: Intact CA system but perturbed CA catabolism in 11-mo fish. (a) Quantification of TH1/2+ cells in 6-mo brains and (b) quantification of TH1 protein levels in 11-mo brains show intact CA system in adult fish. (b') Total protein stain as loading control for the immunoblot in (b). (c) Analysis of aminergic catabolism in 11-mo brains reveals increased dopamine and serotonin degradation. Chromatographic analysis of amine catabolism and immunoblotting were carried out by S. A. Semenova. (a, c) Plots represent means ± s.d. (b) Protein levels are reported as means ± s.d. Statistical analyses: (a pop.1, a pop. 3–11, a pop. 13, a pop. 14, b, c DA, c DOPAC–5-HIAA) two-tailed Student's *t*-test; (a pop. 2, a pop. 12) two-tailed Mann-Whitney's *U*-test.

5.6 Decreased mitosis rate in the larval brain

Reduced levels of neurogenesis are found in postmortem specimens of PD patients[210]. Several lines of evidence implicate LRRK2 in cell proliferation and differentiation[211]. However, LOF studies *in vivo* have led to conflicting findings: in mice, the number of DCX+ neuroblasts in the dentate gyrus has been found increased in one study,[110], unaffected in another one[102]; in zebrafish, reduced cell proliferation in the brain was characterised in *mzLrrk2^{tud112}* larvae (Figure 2.1d) and throughout development[168].

To assess cell proliferation in the *mzLrrk2* brain, phospho-histone H3 (pH3) was used as a marker for mitotic cells[172,212]. At 5 dpf, *mzLrrk2* brains displayed moderately, but significantly, less mitotic cells in the forebrain only (Figure 5.16a,

a'), whereas the overall number in the entire organ was unchanged (not shown). However, at 10 dpf the effect was much more pronounced, consisting in a ∼50%-decrease in the anterior ($P = 0.0025$) and middle portions ($P = 0.0062$) (Figure 5.16b, b'). Of note, the phenotype is clearly apparent only in maternal-zygotic individuals (Figure A.6). However, unlike *mzLrrk2*[tud112] larvae, the number of cells in the S phase of the cell cycle did not differ between *mzLrrk2* and controls (anterior: $P = 0.6453$; middle: $P = 0.1455$; posterior: $P = 0.3613$; Figure A.7), suggesting defects either in the progression or in the regulation of the cell cycle length. This is in line with previous evidence showing impaired cell cycle progression, survival and differentiation of human mesencephalic neural progenitor cells upon *LRRK2* knockdown[213]. However, brain size or morphology were unaffected (not shown). Remarkably, the phenotype is merely emerging at 5 dpf and exacerbates by 10 dpf, i.e. during a time window when neural development slows down considerably, judging from the about nine-fold drop in the absolute number of total pH3+ cells in *wt* brains (5 dpf: 281.3 ± 26.7; 10 dpf: 33.9 ± 8.7).
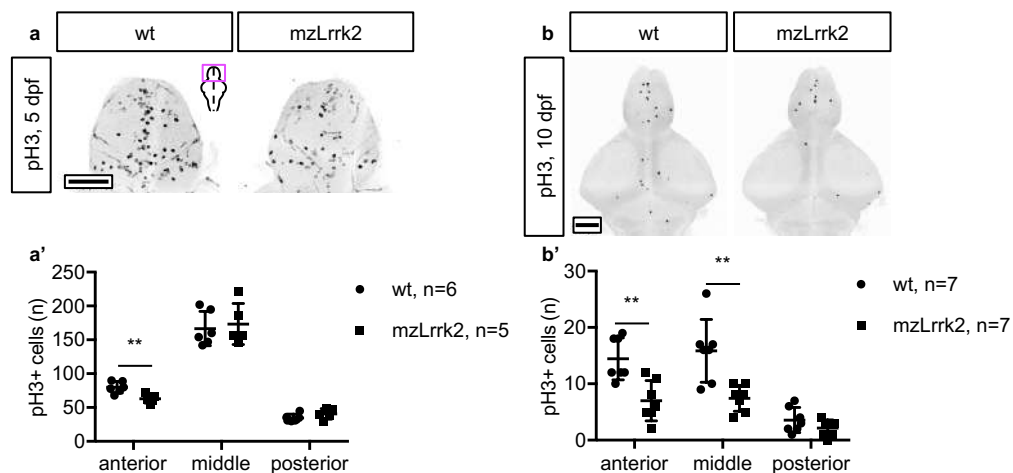
Figure 5.16: Decreased mitosis rate in the larval brain. (a, b) Phospho-histone H3 (pH3) IHC was carried out to label mitotic cells. The mitosis rate is slightly reduced in the anterior portion only at 5 dpf (a, a'), halved over the whole organ at 10 dpf (b, b'). (a', b') Plots represent means ± s.d. Statistical analyses: (a', b') two-tailed Student's *t*-test. Scale bars: (a, b) 100 µm.

To further substantiate the dependence of the hypoproliferative phenotype from Lrrk2 deficiency, the mitosis rate in the brain was evaluated upon combination of the *lrrk2*[tud112] and *lrrk2*[tud113] alleles. To this aim, *mzLrrk2* females were crossed with *mzLrrk2*[tud113] males to obtain transheterozygous larvae, whose brains were harvested at 10 dpf and immunostained for pH3. As a result, the hypoproliferative phenotype was confirmed also in transheterozygotes (compared to wt, anterior: $P = 0.0002$; middle: $P = 0.0007$; Figure 5.17).
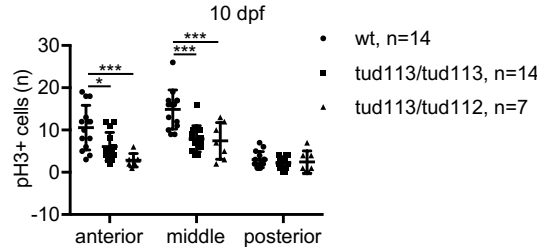
Figure 5.17: Transheterozygous *tud113/tud113* fish recapitulate the hypoproliferative phenotype. Combination of the *lrrk2^{tud113}* and *lrrk2^{tud112}* alleles recapitulates the hypoproliferative phenotype in 10-dpf maternal-zygotic *tud113* brains. Plot represents means ± s.d. Statistical analyses: one-way ANOVA followed by Tukey's *post hoc* test.

Next, a Lrrk2 protein fragment containing the catalytic core was overexpressed in the attempt to restore Lrrk2 function. To this aim, a Tol2 transgenic line was generated, expressing the *lrrk2* rescue construct (c.3009_7130) along with the mCherry reporter under the heat-inducible *hsp70l* promoter (*Tg(hsp70l:mCherry-T2A-lrrk2(c.3009_7130)-Myc)^{tud114}*, henceforth referred to as "rescue"; Figure A.8). The rescue line was combined with the *tud113* line to obtain reconstitution of the maternal-zygotic background. Reconstituted fish were heat-shocked daily for 4 h from 1 to 10 dpf and analysed for mitosis in the brain. Compared to *wt* controls, the overall number of pH3+ cells in the *mzLrrk2+rescue* recovered ($P = 0.1051$), as opposed to 2 controls ($P = 0.0034$; Figure 5.18). This finding indicates that overexpression of a functional Lrrk2 moiety could rescue the phenotype. Altogether, these data reveal an implication of Lrrk2 in the control of cell proliferation in the developing brain.
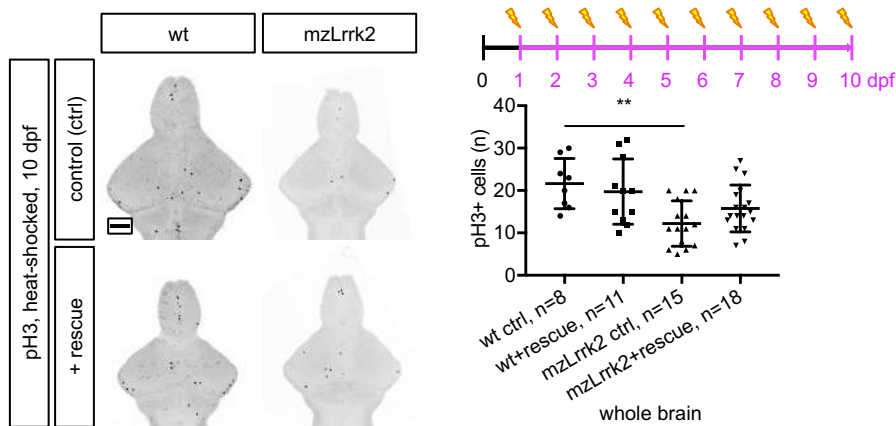
Figure 5.18: Genetic reconstitution of Lrrk2 function rescues the hypoproliferative phenotype in *mzLrrk2* brains. Conditional expression of a Lrrk2 fragment (*wt+rescue*, *mzLrrk2+rescue*) containing the catalytic core rescues the hypoproliferative phenotype in 10-dpf *mzLrrk2* brains (*mzLrrk2+rescue* versus *mzLrrk2* controls, *ctrl*). Plot represents means ± s.d. Statistical analyses: one-way ANOVA followed by Dunn-Dunn-Šidák's correction for multiple comparisons. Multiple comparisons: *wt ctrl* vs. *wt+rescue*; *wt ctrl* vs. *mzLrrk2 ctrl*; *wt ctrl* vs. *mzLrrk2+rescue*; *mzLrrk2 ctrl* vs. *mzLrrk2+rescue*. Scale bar: 100 µm.

5.7 Impaired neuronal regeneration in the adult telencephalon

Zebrafish have a remarkable capacity to regenerate lost appendages and damaged tissues, including the telencephalon[126] and cerebellum[214]. Since regeneration recapitulates several aspects of embryonic development, it is possible that loss of *lrrk2*, responsible for decreased cell proliferation in the larval brain, also affects reactive neurogenesis and regeneration in the adult brain. In the intact 6-mo brain, PCNA+ proliferating cells are mildly reduced in the dorsal telencephalic niche, but significantly in the dorso-posterior (Dp) area ($P = 0.0272$; Figure A.9). To address reactive proliferation and neurogenesis, 6-mo fish were injured using a stab lesion paradigm as previously described[126] (Figure 5.19a) and analysed using a BrdU pulse-chase assay. Reactive proliferation at 3 days post-lesion (dpl) did not differ between *mzLrrk2* and controls (Figure 5.19b). However, *mzLrrk2* brains displayed on average 30% less HuC/D+/BrdU+ neurons at 21 dpl ($P = 0.0262$; Figure 5.19c, c'). In contrast, neurogenesis in the unlesioned hemisphere was normal ($P = 0.284$). Taken together, these results demonstrate a role for Lrrk2 in neuronal regeneration of the lesioned adult telencephalon.

5.8 Association between loss of *lrrk2* and hypokinesia in larvae

To investigate motor ability after loss of *lrrk2*, spontaneous swimming activity of 5- and 10-dpf larvae and 6-mo adult fish was automatically recorded and analysed. Similar work on 8-dpf *mzLrrk2tud112* larvae has pointed out a reduced tendency to initiate swimming and an increased persistence in the *inactive phase*, implying a motor phenotype reminiscent of bradykinesia in human PD patients[168]. However, the differences observed were often very mild. Moreover, the analysis strategy consisted in comparing the means between *mzLrrk2*[tud112] and controls using Student's *t*-test for each behavioural parameter separately. A similar approach is problematic for two reasons: first, the distribution of behavioural data is typically skewed, thus invalidating the use of Student's *t*-test; secondly, the analysis of isolated parameters may be little informative, as complex set of changes may go unnoticed. To overcome such difficulties, multivariate logistic regression was performed to evaluate the relationship between the genotype, a categorical variable with only two possible outcomes ("*mzLrrk2*" or "*wt*"), from a combination of the motor parameters. This is the same as using overall swimming performance as indicator of loss of *lrrk2*. Behavioural data were generated by S. Bilican and S. Sayed. The results are summarised in Table 5.2; the statistics for the individual parameters are reported in Figure A.10; each model's goodness of fit is provided in Figure A.11.

At 5 dpf, the estimated odds ratios revealed that larvae were more likely to be *mzLrrk2* if swimming more frequently at the normal speed range (*normal phase entry count*, $OR = 1.242$) while spending less time in bursting mode (*bursting phase duration*, $OR = 1.242$). At 10 dpf, *mzLrrk2* larvae tended to alternate
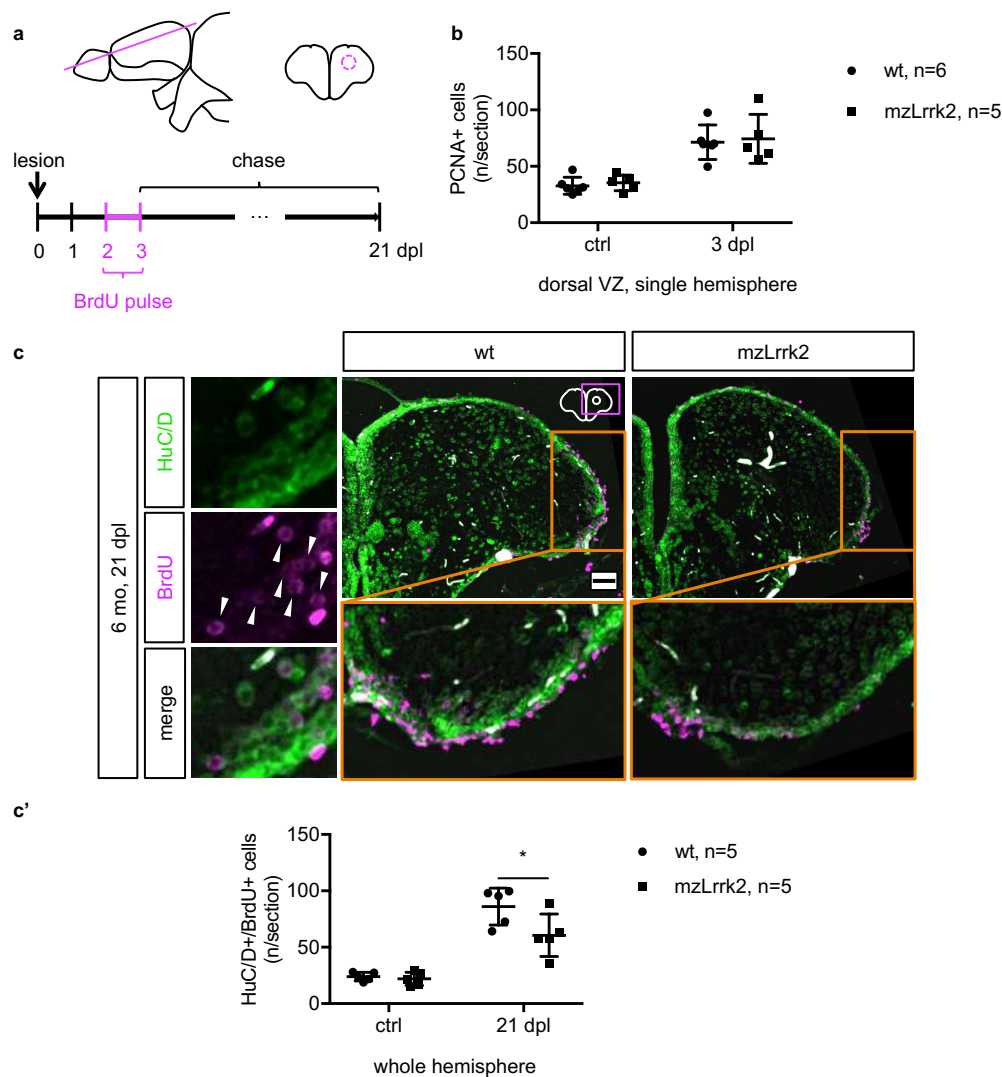
Figure 5.19: Loss of *lrrk2* impairs neuronal regeneration upon stab injury of adult telencephalon. (a) A unilateral stab injury was inflicted to the 6-mo adult telencephalon. To identify newborn neurons, a BrdU pulse was delivered from 2 to 3 days post-lesion (dpl) and incorporating cells analysed at 21 dpl. (b) PCNA IHC to examine reactive proliferation in radial glia stem cells of the ventricular zone (VZ) at 3 dpl. The lesioned hemisphere (3 dpl) was compared to the unlesioned hemisphere as control (*ctrl*) but no difference was observed (c, c'). HuC/D/BrdU double labelling to assess neurogenesis at 21 dpl. Double-positive cells are indicated by white arrowheads in the insets. Quantification was carried out through the entire parenchyma of the lesioned (21 dpl) and *ctrl* hemispheres. Neurogenesis is reduced in the *mzLrrk2* brains. Orange-boxed insets are rotated by 90°. (b, c') Plots represent means ± s.d. Statistical analyses: one-tailed Student's *t*-test. (c) Scale bar: 50 μm.

inactive to bursting phases (*inactive phase distance, $OR = 1.684$; bursting phase distance, $OR = 1.194$*), rather than swimming at the normal speed range (*normal phase distance, $OR = 0.860$*), with lower *bursting phase duration* ($P = 0.847$). This "stop-and-go" swimming pattern might reflect an impaired ability to initiate or sustain movements, similar to bradykinesia in PD patients. However, at 6 mo, although the distance swum in either normal or bursting mode was a very strong predictor ($P < 0.0001$ for both), the estimated odds ratios were very close to 1 ($OR = 1.008$ and $OR = 1.003$, respectively), indicating that the difference between adult *mzLrrk2* fish and controls was very subtle.

Several non-motor symptoms often precede motor disease and aggravate disability in later stages of PD pathology[5]. Anxiety and olfactory dysfunction are amongst the most prevalent in PD patients both after and prior to diagnosis[215]. Therefore, anxiety levels and response to olfactory stimuli were analysed in fish. To test anxiety levels, two paradigms were used: (*i*) wall-hugging behaviour, or thigmotaxis[216], for both larvae and adults (Figure A.12a–d), and (*ii*) dark-to-light preference, or scototaxis[217], for adults only (Figure A.12e). To evaluate the overall olfactory function in adult fish, the response to an amino acid mixture odorant stimulus was measured[181] (Figure A.12f). None of the assays revealed any significant difference between *mzLrrk2* fish and controls.

5.9 Transcriptome analysis of 5- and 10-dpf larvae

To gain an insight into the signalling and metabolic pathways affected by Lrrk2 deficiency during larval development, the transcriptome from *mzLrrk2* and *wt* whole larvae at 5 and 10 dpf was sequenced. The larvae were derived from two independent parental pairs/genotype and collected at the two different time points. Sequencing data were generated by the Deep Sequencing Group (CRTD); primary processing of sequencing data was performed by M. Lesche.

The samples overall displayed a very high amount of uniquely-aligned fragments and good complexity (not shown). The data set features and the biological significance of resulting differentially expressed genes (DEGs) are discussed below. As the validation of the most interesting data is still warranted, it must be cautioned that the *in silico* data henceforth presented are only indicative.

5.9.1 Exploratory differential expression analysis

Spearman's correlation analysis revealed a better separation between the mzLrrk2 and *wt* samples at 5 dpf than at 10 dpf (Figure A.13a). This was also confirmed by the heatmap of the sample-to-sample Euclidean distance (Figure A.13b). Principal component analysis showed no overlap between the sample groups and a clear segregation between the 5-dpf and the 10-dpf groups along the *PC1* axis Figure 5.20). However, within the 10-dpf group the distance along the *PC2* axis between one *wt* sample and the *mzLrrk2* group was much more reduced than within the *mzLrrk2* group.

Table 5.2: Multiple logistic regression analysis of the association of the swimming performance with the loss of *lrrk2*. Behavioural data were generated by S. Bilican and S. Sayed. The original motor variables (*inactive/normal/bursting phase entry count/duration/distance* for 5- and 10-dpf larvae; *normal/bursting phase entry count/duration/distance* for 6-mo adults) were subjected to backward stepwise elimination to identify the best fitting model at each time point. The selected variables and relative statistics are shown. For each variable, the odds ratio (*OR*) represents the change in the relative probability (*p*) of a recorded animal to be *mzLrrk2* ($p = 1$) over *wt* ($p = 0$) for an x-unit change, the other variables held constant. Unit changes of $x = 10$ for phase entry count and phase distance, $x = 1$ for all other variables were deemed opportune. The estimated 95% confidence interval for each *OR* is reported. The intercept, i.e. the estimated *OR* when all covariates equal 0, is omitted.

time point	independent variable	β	*OR* (e^{β})	95% *CI*	P
5 dpf	*inactive phase distance*	−0.841	0.432	0.258 –0.721	0.0014
	inactive phase entry count	0.216	1.242	1.071–1.439	0.0041
	normal phase duration	−0.050	0.951	0.916–0.988	0.0091
	bursting phase duration	−0.269	0.764	0.628–0.929	0.0071
10 dpf	*inactive phase entry count*	−0.071	0.932	0.873–0.994	0.0316
	inactive phase duration	−0.033	0.968	0.948–0.988	0.0018
	inactive phase distance	0.521	1.684	1.149–2.468	0.0076
	normal phase duration	0.064	1.066	1.014–1.121	0.0126
	normal phase distance	−0.151	0.860	0.792–0.933	0.0003
	bursting phase duration	−0.166	0.847	0.735–1.976	0.0219
	bursting phase distance	0.177	1.194	1.079–1.321	0.0006
6 mo	*normal phase distance*	0.008	1.008	1.004–1.011	< 0.0001
	bursting phase distance	0.003	1.003	1.002–1.004	< 0.0001

Table 5.3: Overview of total DEGs at different FDR. The direction of change (up: upregulation; down: downregulation) is indicated.

time point	FDR (%)	DEGs	up	down
5 dpf	10	4,782	2,966	1,816
	5	3,783	2,380	1,403
	1	2,390	1,498	892
10 dpf	10	252	37	215
	5	185	27	158
	1	131	21	110
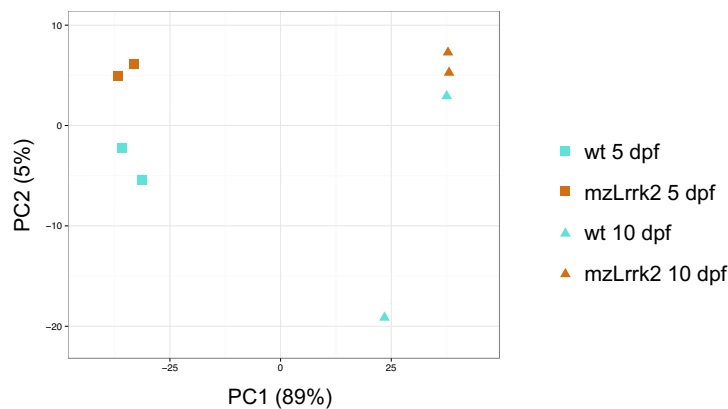
Figure 5.20: PCA of top 500 most variable genes. Principal component analysis plot showing the sample projections on the 2D plane defined by the two directions explaining most of the variance. The percent of total variance associated with each principal component is reported. Figure generated by M. Lesche.

The number of DEGs in *mzLrrk2* versus *wt* at 5 dpf was more than eighteen times higher than at 10 dpf, irrespective of which false discovery rate (FDR) was applied (see Table 5.3 and Figure 5.21). Part of the reason may lie in the relatively large inner variance of the 10-dpf *wt* group. Nonetheless, it shall be noted that *PC2* accounts for only 5% of the total variance (Figure 5.20).

To visualise persistent expressional changes from 5 to 10 dpf, the DEGs at both time points were considered (see Table 5.4 and Figure 5.22). More than half underwent a directional switch, but for only 1 of them the expression change was relevant at both time points ($|log_2(\text{fold change})| > 1$, FDR 10%).
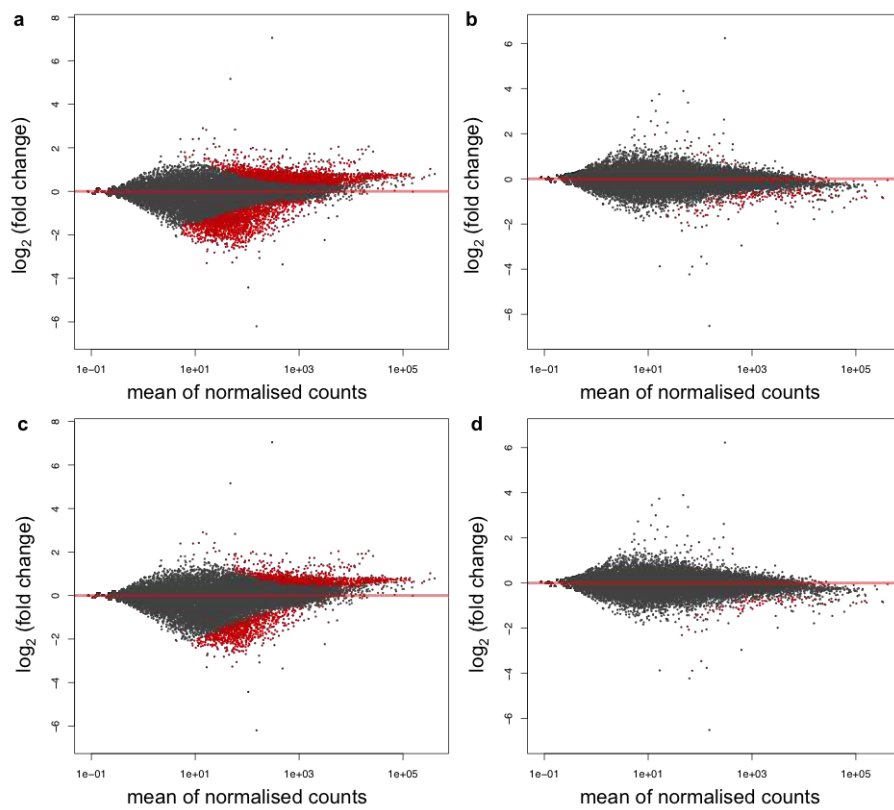
Figure 5.21: MA plots. DEGs at (a, c) 5 dpf and (b, d) 10 dpf when a FDR of (a, b) 10% and (c, d) 1% was applied. Panels generated by M. Lesche.
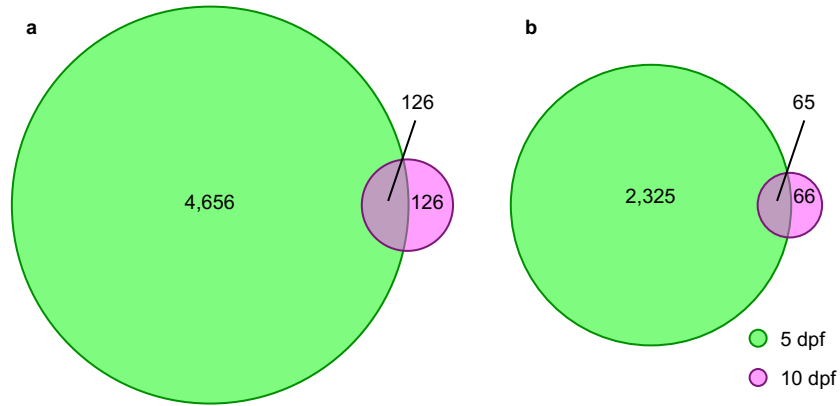
Figure 5.22: DEGs overlapping between 5 and 10 dpf. (a, b) Absolute number and relative proportion of DEGs overlapping between 5 and 10 dpf at (a) FDR 10% and (b) FDR 1%.

Table 5.4: Overview of DEGs overlapping between 5 and 10 dpf at different FDR. The direction of change (up: upregulation; down: downregulation) at 5/10 dpf is indicated.

FDR (%)	DEGs	up/up	up/down	down/up	down/down
10	126	24	79	1	22
1	65	16	37	0	12

The heatmap of the variance across samples highlighted the most variable DEGs in the data set (Figure 5.23). The expression of *lrrk2* was, of course, suppressed in all *mzLrrk2*. In contrast, one gene was virtually not expressed in the *wt* (average 0.11 versus 52.72 transcripts per kilobase million in the *mzLrrk2*): *si:ch211-121a2.2*, orthologous to *DUSP27* in humans, coding for a dual specific phosphatase (UniProtKB accession numbers: A8E7M1 to Q68J44; 78% query cover, 46% identity, 61% similarity). The HCX_2GX_2R consensus sequence, containing the nucleophilic cysteine of the catalytic core, is conserved in both species. In mice, the *Dusp27* gene is expressed in tissues characterised by high energy metabolism, prominently in the skeletal muscle, liver, and adipose tissue, and to a lesser extent in other tissues, including the brain[218]. The DUSP27 phosphatase has been shown to mediate the effects of prolactin via the short isoform of the prolactin receptor by deactivating the ERK1/2 and p38 MAP kinases in the ovary and decidua[219,220]. Several studies support a role for LRRK2 to activate the ERK1/2 pathway via phosphorylation[68,221,222]. This can be achieved via LRRK2 MAPKKK activity[223]. Therefore, loss of Lrrk2 might work synergistically with *si:ch211-121a2.2* upregulation to inhibit the ERK1/2-dependent cascade. Validation of *si:ch211-121a2.2* upregulation and further studies on the interplay between *lrrk2* and *si:ch211-121a2.2* to modulate the Erk1/2 signalling pathways are definitely worth pursuing.
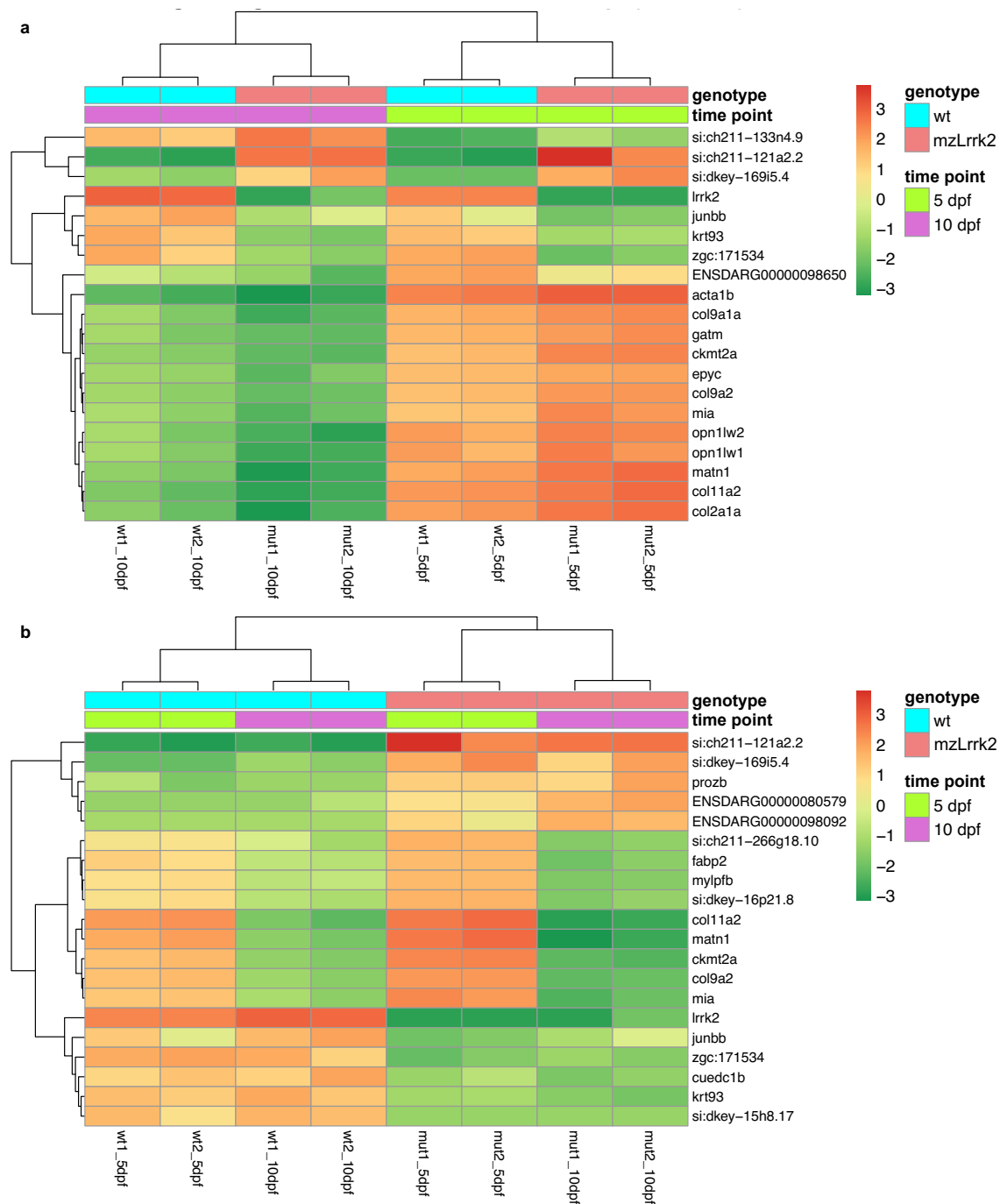
Figure 5.23: Most variable overlapping DEGs. (a, b) Top twenty overlapping DEGs showing the highest variance across samples at (a) FDR 10% and (b) FDR 1%. Note the almost specular heat pattern of *lrrk2* and *si:ch211-121a2.2*. Samples: wt1/2_5/10dpf, *wt* replicates; mut1/2_5/10dpf, *mzLrrk2* replicates. Panels generated by M. Lesche.

5.9.2   Gene set enrichment analysis

To identify enriched canonical pathways and predicted upstream regulators, sequencing data were mined using the IPA software (see 4.6). Because the species supported are human, mouse, and rat, different species are supported through orthologue information. This means that one gene in the zebrafish data set could map to multiple genes in the IPA data set, or vice versa, or none. In order to extract the most out of the data set, DEGs with an FDR 10%-stringency level were considered.

A summary of the most enriched canonical pathways is provided in Table 5.5. At 5 dpf, the most enriched gene ontology (GO) terms included "mitochondrial dysfunction" and "oxidative phosphorylation". These *in silico* data are consistent with previous reports implicating LRRK2 in mitochondrial dynamics[224]. At 10 dpf, "calcium signalling" and "glycolysis I" were among the most significant. "Calcium signalling" was highly enriched also when considering the DEGs at both time points. The "calcium signalling" GO term includes several molecules that play a role in muscle contraction. It is known that *LRRK2* is expressed in the muscular tissue in both mouse[117] and zebrafish[136]. However, no direct involvement of LRRK2 in muscle biology has yet been proposed. Intriguingly, the most significant predicted upstream regulators of DEGs overlapping between 5 and 10 dpf (see Table 5.6) included the protein SMTLN1, involved in muscle contraction[225], the transcription factors MYOD1 and MEF2C, and the transcription activator SMARCA4, all implicated in myogenesis[226–229]. The IPA software predicted a mechanistic network (Figure 5.24) wherein the upstream regulator MYOD1 directly affects *MEF2C* activation, which in turn controls *GATA4*, a transcription factor required for correct cardiogenesis[230]. The downstream effect would be a an impact on body size. Strikingly, the directional effect at the two time points is the opposite: "activating/increasing" at 5 dpf (Figure 5.24a), "inhibiting/decreasing" at 10 dpf (Figure 5.24b). Notwithstanding, the algorithmically generated model hints that some developmental programs may go awry in the absence of Lrrk2. The muscular system stands out as a potential target, plausibly because muscle genes were relatively abundant due to sample source. Nonetheless, the expressional changes were modest ($|log_2(\text{fold change})| < 1$). This might explain the lack of macroscopically appreciable growth retardation in the *mut* larvae and adults. On the other hand, the cell proliferative defect described in the brain is itself evidence of developmental impairment. In the light of the enrichment data hitherto discussed, a thorough investigation of the muscular system might be revealing.

Table 5.5: Top canonical pathways (FDR 10%-filtered DEGs)

time point	canonical pathways	$log_{10}p$	overlap
5 dpf	EIF2 signalling	37.83	103/194
	mitochondrial dysfunction	34.46	92/171
	oxidative phosphorylation	34.19	71/109
	regulation of eIF4 and p70S6K signalling	18.13	67/157
	mTOR signalling	12.09	67/199
10 dpf	calcium signalling	10.58	13/178
	hepatic fibrosis/ hepatic stellate cell activation	9.25	12/183
	atherosclerosis signalling	5.10	7/127
	cellular effects of Sildenafil (Viagra)	5.03	7/130
	glycolysis I	4.95	4/25
5 and 10 dpf	calcium signalling	9.97	10/178
	cellular effects of Sildenafil (Viagra)	5.64	6/130
	regulation of actin-based motility by Rho	5.14	5/91
	formaldehyde oxidation II (glutatione-dependent)	5.07	2/2
	tight junction signalling	5.01	6/167

Table 5.6: Top upstream regulators (FDR 10%-filtered DEGs). A positive z-score reflects predicted activation; negative, inhibition. An absolute z-score value higher than 2 is considered significant. Note the directional switch from 5 to 10 dpf of the predicted regulators of overlapping DEGs.

time point	upstream regulators	$log_{10}p$	z-score	
5 dpf	RICTOR	61.33	−11.08	
	HNF4A	44.36	2.89	
	MYCN	35.21	6.43	
	KDM5A	34.62	−6.57	
	MAPT	32.98	−2.00	
10 dpf	SMTLN1	18.02	2.85	
	MEF2C	11.58	−1.92	
	KDM5A	11.40	2.89	
	MYC	10.84	−2.11	
	MYOD1	10.77	−3.41	
5 to 10 dpf	SMTNL1	14.32	−2.83	2.83
	MYOD1	11.64	3.11	−3.11
	MEF2C	9.79	2.80	−2.80
	SMARCA4	9.52	3.15	−3.15
	3,5-diiodothyronine	7.82	2.00	−2.00
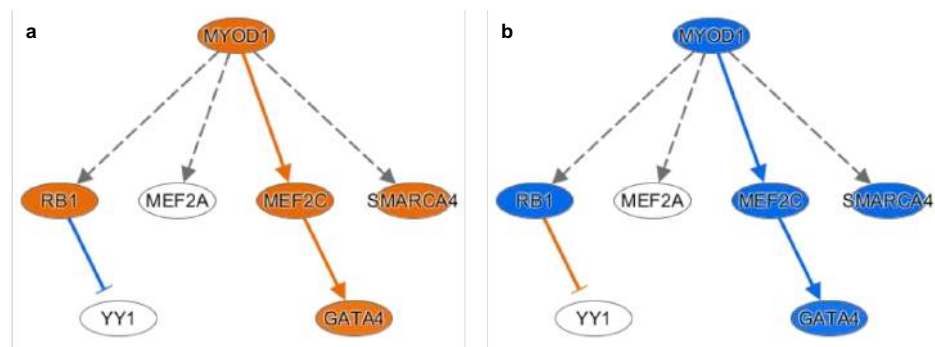
Figure 5.24: Top predicted upstream regulators of overlapping DEGs and mechanistic network at (a) 5 and (b) 10 dpf. The continuous lines represent direct relationships, the dashed lines indirect relationships. Pointed arrowheads indicate activating effects, blunt arrowheads inhibiting effects. Orange denotes activation, blue inhibition; grey means that the findings underlying the path segment support no causal role.

Discussion

6.1 Strength of the *mzLrrk2* zebrafish model

In the present work, the brain phenotype of the first zebrafish *lrrk2* knockout model is characterised. Compared to the published MO-induced phenotypes[136–138] and the unpublished ENU-induced *mzLrrk2^{tud112}* phenotype[168], the superior reliability of the *mzLrrk2* model lies in the complete removal of the ∼60-kbp-long *lrrk2* locus. In contrast with previous studies[136,138,168], the present results demonstrate that zebrafish *lrrk2* is a resilient locus (see 5.4 and below 6.1.1). In particular, *mzLrrk2* larvae initially display reduced CA neurons and a combination of distinct motor signatures interpretable as hypokinesia that resolve spontaneously during development. Recent work has suggested that buffering mechanisms may be triggered by deleterious mutations, but not knockdown[167]. Hence, MO-induced phenotypes might indeed provide useful information, which could be masked in constitutive mutants. However, the same study cautions that the MO dose should be carefully titrated in a reliable null mutant background in order to exclude off-target effects[167]. Moreover, the transiency of MO-induced effects is a limitation for phenotypic analyses in the long term. Consequently, MOs should rather be the exception, and not the rule, for the assessment of gene function[163].

However, genome editing strategies are not exempt from setbacks, as exemplified by the *tud115* allele herein described (see 5.2). The most worrisome caveat are off-target effects, a lurking risk even when appropriate precautions are taken. The ideal solution would be cross-validation using different alleles for the same gene. If the suspected phenotype is recessive, a more stringent assay would be testing whether different mutant alleles can complement each other. Upon comparing *mzLrrk2^{tud112}*[168] and *mzLrrk2* phenotypes, it was verified that only reduced mitosis in the larval brain is consistent (Figure 5.16, Figure 2.1d) and persistent in transheterozygous *tud113/tud112* fish (Figure 5.17). Furthermore, the hypoproliferative phenotype could be rescued by conditional overexpression of a Lrrk2 fragment in genetically reconstituted *mzLrrk2* mutants (Figures 5.18 and A.8).

Altogether, these results suggest the *mzLrrk2* hypoproliferative phenotype to exclusively depend on Lrrk2 LOF. Moreover, the phenotype is manifest only when both the maternal and zygotic Lrrk2 function is abolished (Figure A.6). Therefore, the *mzLrrk2* zebrafish represents the first complete *LRRK2* knockout in a vertebrate *in vivo* model.

6.1.1 Robustness against *lrrk2* locus deletion

One limitation of the *mzLrrk2* model is the extent and duration of most phenotypic manifestations. This finding is particularly striking in the light of the more stable *mzLrrk2^{tud112}* phenotype, including persistently reduced CA neurons. Given the better specificity of CRISPR/Cas9-mediated genome editing over ENU-mediated mutagenesis, one explanation could be confounding off-target effects in the *tud112* line. However, it cannot be excluded that aberrant *lrrk2^{tud112}* transcripts determine cellular stress and this be directly responsible for the defects observed in *mzLrrk2^{tud112}* fish. If so, *mzLrrk2^{tud112}* fish would more closely mimic the situation in humans, where *LRRK2* transcripts carrying deleterious mutations are produced. This event appears little likely, though, as *lrrk2^{tud112}* transcripts undergo NMD (Figure 2.1c, c').

Analysis of transcriptome from whole *mzLrrk2* larvae reveal a dramatic, eighteen-fold drop in the number of DEGs, from several thousands at 5 dpf to few hundreds at 10 dpf (Table 5.3). The progressive narrowing of the gap between *mzLrrk2* and control larvae may be an indication of functional compensation for Lrrk2 LOF. Two possible mechanisms may come into play: (*i*) gene duplication, and (*ii*) functional redundancy[216]. No evidence for *lrrk2* duplication is found in the latest genome assembly (see 5.1). A possible source of redundant zebrafish Lrrk2 function may come from the paralogous *lrrk1* gene, as proposed for mice[101,117]. However, the zebrafish *lrrk2* and *lrrk1* genes have almost non-overlapping expression patterns and domains in the developing embryos[168], as do the respective orthologues in the mouse brain[66]. Furthermore, it was verified that *lrrk1* expression is unaltered in *mzLrrk2* larvae at both 5 and 10 dpf (Figure 5.5). Therefore, if a functional analogue replaced Lrrk2, this would not be the most obvious candidate, i.e. the paralogue Lrrk1. In fact, knockout studies in mice[113] and interactome data from SH-SY5Y neuroblastoma cell lines[231] rather suggest that LRRK2 and LRRK1 are divergent proteins with distinct functions.

Another possibility is that Lrrk2 deficiency can be functionally compensated on a metabolic or network level. Transcriptome analysis might be revealing in this sense. However, it shall be noted that the effects of Lrrk2 deficiency may be regional and therefore masked in whole-body total-RNA samples. In fact, an average of as low as 0.57 and 0.47 *lrrk2* transcripts per kilobase million was sequenced in 5- and 10-dpf *wt* samples, respectively. Nonetheless, these transcriptome data may still provide useful information, particularly if coupled with data from adult brains at different stages of development. Upon validation, they would provide the starting point for subsequent analyses aiming at elucidating what mechanisms are disrupted/triggered by the *lrrk2* locus deletion and possibly explain the observed, or even new, *mzLrrk2* phenotypes.

6.2 Model relevance in the context of PD research

A good model of PD should recapitulate at least two fundamental aspects: (*i*) selective DA cell loss; (*ii*) levodopa-sensitive syndrome, including motor and non-motor symptoms. In addition, an ideal model of PD should display a progressive

and chronic phenotype. In the *mzLrrk2* model, despite an early developmental delay, the CA system appears intact until 11 mo (see 5.5).

A possible reason for the lack of an overt PD-like phenotype may be the lack of a zebrafish α-synuclein orthologue. Although α-synucleinopathy is not pathognomonic of PD, not even in LRRK2 mutation carriers, progression of Lewy body pathology correlates with non-motor symptoms[8], including psychiatric disturbances and olfactory dysfunctions[232]. On these grounds, the normal anxiety levels and olfactory responsiveness in *mzLrrk2* fish seem reasonable (Figure A.12). Yet, no PD-like brain pathology manifests in either transgenic[79–81,83,84,86] or knockout[102] *LRRK2* mouse models, where α-synuclein is present.

It cannot be excluded that the DA system is affected on a more subtle level, for example connectivity or synaptic transmission. On the other hand, PD is a multisystem disorder, and the CA system is not the exclusive target of pathology[9]. In this regard, the hypokinetic phenotype observed in 10-dpf larvae (see 5.8), where no obvious CA defect was found, may indicate that Lrrk2 deficiency elicits dopamine-independent behavioural abnormalities, as also reported in *LRRK2* knockout mice[102]. Conceivably, neurotransmitter systems other than the CA system may also be affected. An interesting candidate would be the serotonergic system. Serotonergic dysfunction has been extensively studied in relation to non-motor features and treatment-related complications in PD[233,234], but the serotonergic system has only recently started to be considered also in relation to *LRRK2*[235]. Intriguingly, increased 5-hydroxyindoleacetic acid, catabolite of serotonin, was found in 10-dpf *mzLrrk2* larve (Figure 5.14d) and increased serotonin degradation in 11-mo fish (Figure 5.15c). Furthermore, the zebrafish Mao enzyme has higher affinity for serotonin than dopamine and the highest levels of Mao activity in the adult brain are found at the serotonergic cell clusters[154]. For these reasons, the serotonergic system and function in *mzLrrk2* fish is worth detailed investigation via quantitative IHC and behavioural analyses, including approach-avoidance and social paradigms[236].

6.2.1 A role for MAO in LRRK2-driven pathology?

Strikingly, perturbed amine catabolism, most prominently increased dopamine degradation, appears in 11-mo *mzLrrk2* fish (Figure 5.15c). This result is particularly meaningful considering that brain dopamine and/or catabolite levels are normal in mice lacking endogenous[101,102] or overexpressing human wild-type LRRK2[80], but reduced in mice expressing pathogenic LRRK2 variants, although the effect may be only regional[80,81] or transgene-dependent[80]. In any case, the neurochemical signatures in those mouse models have been difficult to interpret, because they are not clearly linked to problems in either dopamine synthesis[81] or turnover[80,81]. In contrast, *mzLrrk2* fish specifically display enhanced monoamine oxidase (Mao)-dependent amine degradation. Of note, increased expression of *mao* gene was found in the dorsal telencephalon and cerebellum or 10.5-*mzLrrk2*[tud112] brains via ISH[168]; unfortunately, catabolism was not addressed in age-matched individuals, thus making direct comparison with *mzLrrk2* fish not possible. Although Mao levels in *mzLrrk2* brains appeared unaffected as measured via RT-

qPCR and enzymatic assay (Figure A.5), local enrichment of *mao* transcripts/Mao protein in distinct brain regions cannot be excluded. For want of an anti-MAO antibody working in zebrafish, ISH analysis of *mao* expression in 11-mo *mzLrrk2* brains is warranted.

Previous observations have shown that both expression of the pathogenic LRRK2 R1441C variant[101] and LRRK2 knockdown[237] impair synaptic transmission. If this is the case also for *mzLrrk2* fish, increased Mao activity may be a protective mechanism against dopamine accumulation either at the presynaptic terminal, due to impaired neurotransmitter release, or at the synaptic cleft, due to impaired reuptake, as excess dopamine represents an oxidative threat due to radical formation[238]. However, while removing excess dopamine, Mao would also generate toxic hydrogen peroxide[238], being potentially deleterious in the long term. Given the clinical relevance of MAO inhibitors as a treatment for PD[152], the present findings highlight the importance of clarifying the role of MAO given a predisposing genetic background.

Alternatively, increased Mao activity may be an age-related phenomenon in zebrafish, as is in mammals[161,162], but exaggerated in absence of Lrrk2. The interplay between physiological modifications of MAO levels and sensitising genetic factors in humans and animal models, including *LRRK2* mutations, awaits further investigation. To this aim, models tweaked to accelerate ageing or mimic age-related features could offer valuable insights. Of interest, mice where the isoform B of the human MAO orthologue can be conditionally overexpressed develop PD-like features, including selective DA cell loss and decreased locomotor activity[239]. A similar approach in the *mzLrrk2* fish background might then be revealing.

6.3 Insights made possible by a zebrafish *lrrk2* model

An interesting question is whether *mzLrrk2* fish may be protected, to some extent, from neurodegeneration by their potential to regenerate the brain after lesion[126,214]. However, evidence that loss of *lrrk2* reduces the mitosis rate in the *mzLrrk2* brain is compelling (see 5.6). Although the exact impact of the hypoproliferative phenotype is yet to be elucidated, *ad hoc* formation of cells to replace hypothetically lost neurons is unlikely. However, this does not rule out that pro-regenerative cues may be present. Conceivably, the suppression of pro-regenerative mechanisms should aggravate the phenotype. One such mechanism may be protective autoimmunity[240]. Treatment with dexamethasone, a steroid anti-inflammatory drug, has been shown to dampen the regenerative ability of the zebrafish central nervous system[177,241]. It was verified that chronic exposure to dexamethasone has no influence on cell proliferation in 10-dpf *mzLrrk2* brains (Figure A.14). Therefore, if a regenerative response were underway, this would be independent of neuroinflammation. Other forms of plasticity might as well come into play, including transdifferentiation[242]. Consequently, longitudinal studies will be needed to search for cell loss in aging fish.

Finally, perturbing assays may reveal aspects of Lrrk2 pathobiology otherwise

unnoticeable in unchallenged *mzLrrk2* fish. In particular, the zebrafish as a regenerating organism was exploited and the brain reparative potential tested[126]. As a result, neuronal regeneration is impaired upon stabbing the adult telencephalon (Figure 5.19). It cannot be ruled out whether this conditional phenotype is an indirect consequence of the hypoproliferative phenotype observed in the larval brain. It is possible that the two are merely distinct. Alternatively, the role of Lrrk2 in the control of cell proliferation may be more general during development and more specialised later on in adult brains. Such changing role could be reflected by *lrrk2* expression in the brain, which switches from being ubiquitous during development, to being more confined to specific areas in the adult brain, notably including the telencephalic neurogenic niche[168]. In either case, priming or supporting mechanisms might be required for Lrrk2 to partake in neuronal regeneration. Neuroinflammation appears as a promising candidate[207]. Of note, cultured rat microglia exhibit increased *Lrrk2* expression upon acute inflammation and impaired inflammatory response upon *Lrrk2* knockdown[106]. Furthermore, microglia in BAC human LRRK2 G2019S transgenic mice subjected to stab-wound or laser-injury display impaired ability to isolate the lesion site[243]. The zebrafish Lrrk2 may have a similar pro-inflammatory role, as suggested by reduced leukocytosis in larvae after TPA-induced systemic acute inflammation (Figure 5.12). Because acute inflammation is required for neuronal regeneration[177], a plausible scenario would then be that impaired production of neural precursor cells combined with defective microglia in *mzLrrk2* fish impede brain repair. Transferred to humans, impaired *LRRK2* function may lead to neurodegeneration through the accumulation of unresolved damages such the ones following traumatic brain injury. Albeit recognised alone as a risk factor for PD[244], traumatic brain injuries are yet to be examined in conjunction with known genetic factors, including *LRRK2* mutations. Targeted analyses on animal models and epidemiological studies are therefore warranted.

6.4   Concluding remarks

As highlighted in the Introduction, modelling PD is likely a Sisyphean task (see 1.1): strictly speaking, no matter the strategies and efforts, no animal model, be it mouse or fish or else, will likely ever contract PD. This of course does not imply good models being impossible to obtain. Albeit necessarily approximate and incomplete, a good model shall capture key aspects of the complex picture and be informative enough to be worth exploiting. The kernel here is then how to describe and interpret findings in the light of the bigger context, and therewith pave the way for future work.

The results herein presented show that loss of *lrrk2* can compromise specific zebrafish brain functions, including Mao-dependent amine catabolism and regenerative capacity upon lesion. Conceivably, similar defects in humans may play a contributing role in the prodromal stages of PD, thus supporting the pathogenicity of LRRK2 LOF. At the moment, it is not known how loss of *lrrk2* may cause the above defects. In particular, it is unclear whether the defects in amine catabol-

ism and mitosis are connected, and to what extent they impact on regeneration. Future work shall specifically address these issues, with special attention on the underlying molecular mechanisms.

Admittedly, having no Lrrk2 at all is not the same as having hypofunctional Lrrk2, as it may (or may not) be in humans. This is not a limitation, though, but rather an enriching contribution, as the availability of a completely amorphic standard would serve as a *tabula rasa* for novel information to stem out of existing models. Further investigation in this direction is therefore necessary. Along the same line, the comparison between the complete LOF *mzLrrk2* model and a GOF fish model, for example a Lrrk2 mutant or a humanised knockin, would be valuable and is worth pursuing. Finally, a reliable *LRRK2* knockout model would provide a valuable tool to titrate LRRK2 inhibitors and test toxicity for therapeutic application.

To conclude, the zebrafish *mzLrrk2* model offers a unique possibility to study *in vivo* the consequences of LRRK2 LOF in a regenerating vertebrate system and, coupled with the well-established high-throughput screening amenability of zebrafish, provides an outlook for identifying targets of interest in a fish-to-mammal translational perspective.

Appendix

Table A.1: Sites of pathogenic aa substitutions in human LRRK2 and corresponding residues in zebrafish Lrrk2. Data retrieved from the Parkinson Disease Mutation Database (PDmutDB, http://www.molgen.vib-ua.be/PDmutDB)[245,246]

substitution in humans	corresponding site in zebrafish	domain
p.Arg1441Cys		
p.Arg1441Gly		
p.Arg1441His		
p.Tyr1699Cys	Tyr1685	COR
p.Gly2019Ser	Gly2009	kinase
p.Ile2020Thr	Ile2010	kinase
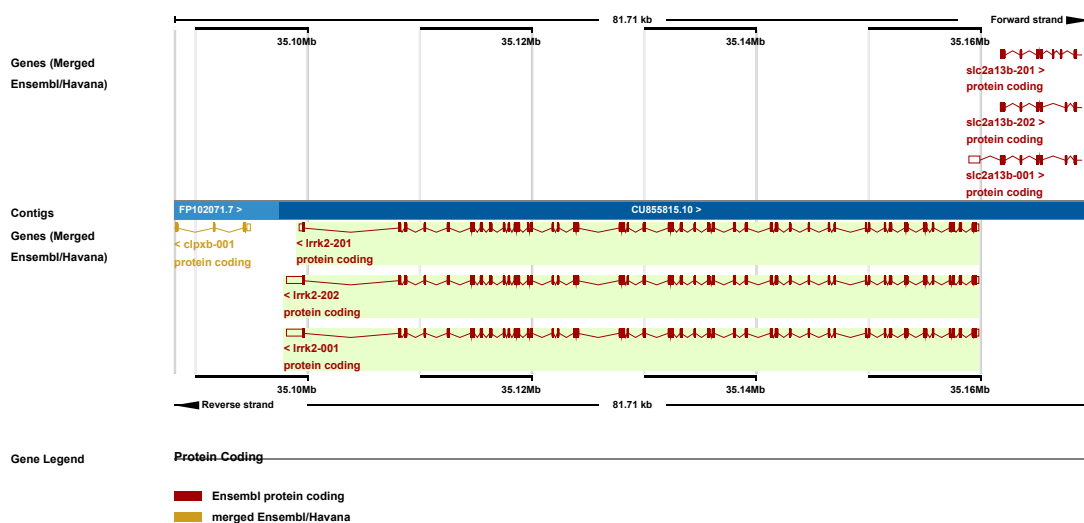
Figure A.2: Zebrafish *lrrk2* transcripts deposited in Ensembl (GRCz10 genome assembly)
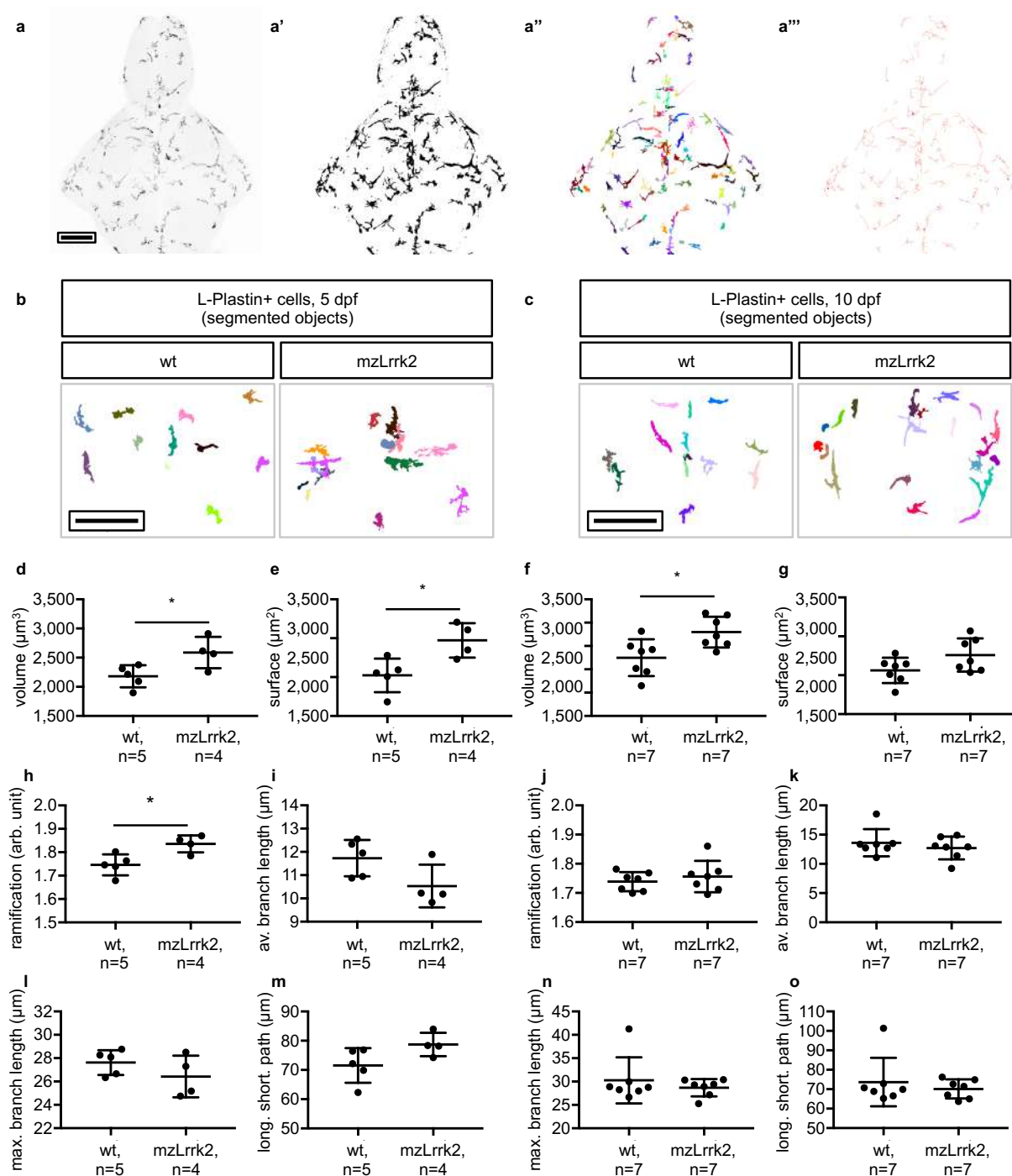
Figure A.3: Analysis of microglia/leukocyte morphology. (a–a''') Maximum intensity projection of: (a) the original, unprocessed stack of a whole 10-rain showing L-Plastin+ microglia/leukocytes; (a') the background-subtracted, despeckled and thresholded stack; (a'') the segmented objects, coloured with Glasbey's lookup table to render them maximally distinguishable from one another; (a''') the skeletons of the segmented objects. (b–o) Microglia/leukocytes are larger in size and more ramified at 5 dpf (b, d, e, h, i, l, m) and display a similar trend, though less pronounced, at 10 dpf (c, f, g, j, k, n, o). Considered morphological parameters are: (d, f) *volume*; (e, g) *surface*; (h, j) *ramification*; (i, k) *average branch length*; (l, n) *maximum branch length*; (m, o) *longest shortest path*. (d–o) Plots represent means ± s.d. Statistical analyses: (a–j, l, m) two-tailed Student's *t*-test; (k, n, o) two-tailed Mann-Whitney's *U* test. (a–c) Scale bars: 100 µm.
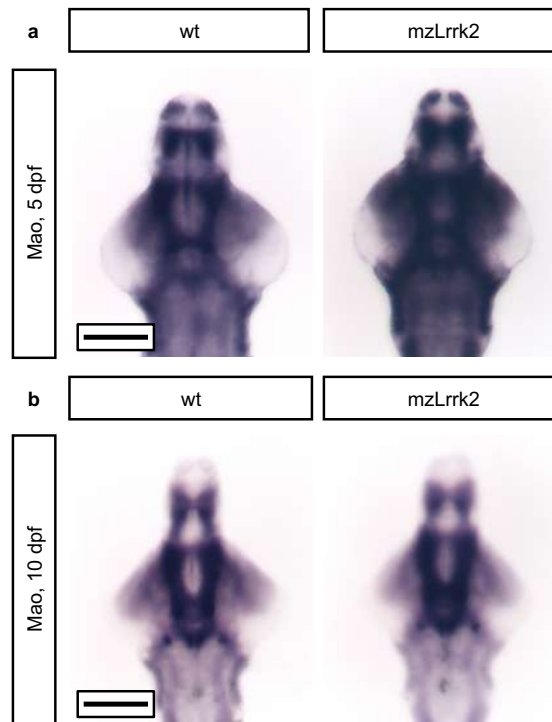
Figure A.4: Unaltered Mao enzymatic activity in the larval brain.
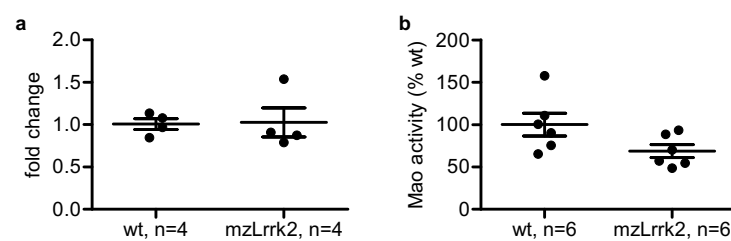
Figure A.5: Mao expression is unaffected in 11-mo brains. Mao expression was evaluated in 11-mo brains by quantifying *mao* transcripts via RT-qPCR (a) and Mao enzymatic activity via peroxidase-linked colorimetric assay (b). No statistically significant difference between *mzLrrk2* and controls was detected. Mao activity assay was performed as previously described[154] by S. A. Semenova in the laboratory of P. Panula (Helsinki, Finland). Plots represent means ± s.d. Statistical analyses: two-tailed Student's *t*-test.
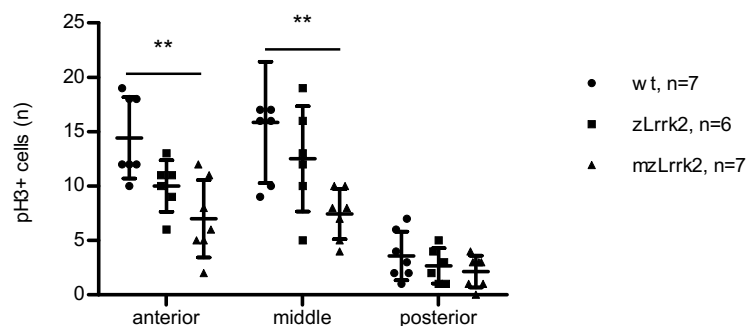
Figure A.6: The hypoproliferative phenotype is worse in maternal-zygotic individuals. The mitosis rate was checked in the brains of 10-dpf zygotic Lrrk2 mutants (*zLrrk2*) derived from heterozygote incross. Although they also display lower pH3+ cell number, the tendency is milder than in *mzLrrk2* individuals and is not statistically significant. Plot represents means ± s.d. Statistical analyses: one-way ANOVA followed by Tukey's *post hoc* test.
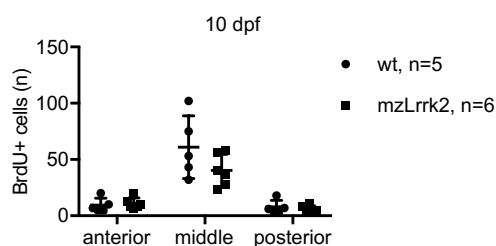
Figure A.7: Intact S phase of the cell cycle in *mzLrrk2 brains*. BrdU IHC was carried out to label cells in the S phase of the cell cycle. To this aim, a 30 min BrdU pulse was delivered prior to killing. No significant difference between *mzLrrk2* and controls was apparent. Plot represents means ± s.d. Statistical analyses: (anterior, middle) two-tailed Student's *t*-test; (posterior) two-tailed Mann-Whitney's *U*-test.
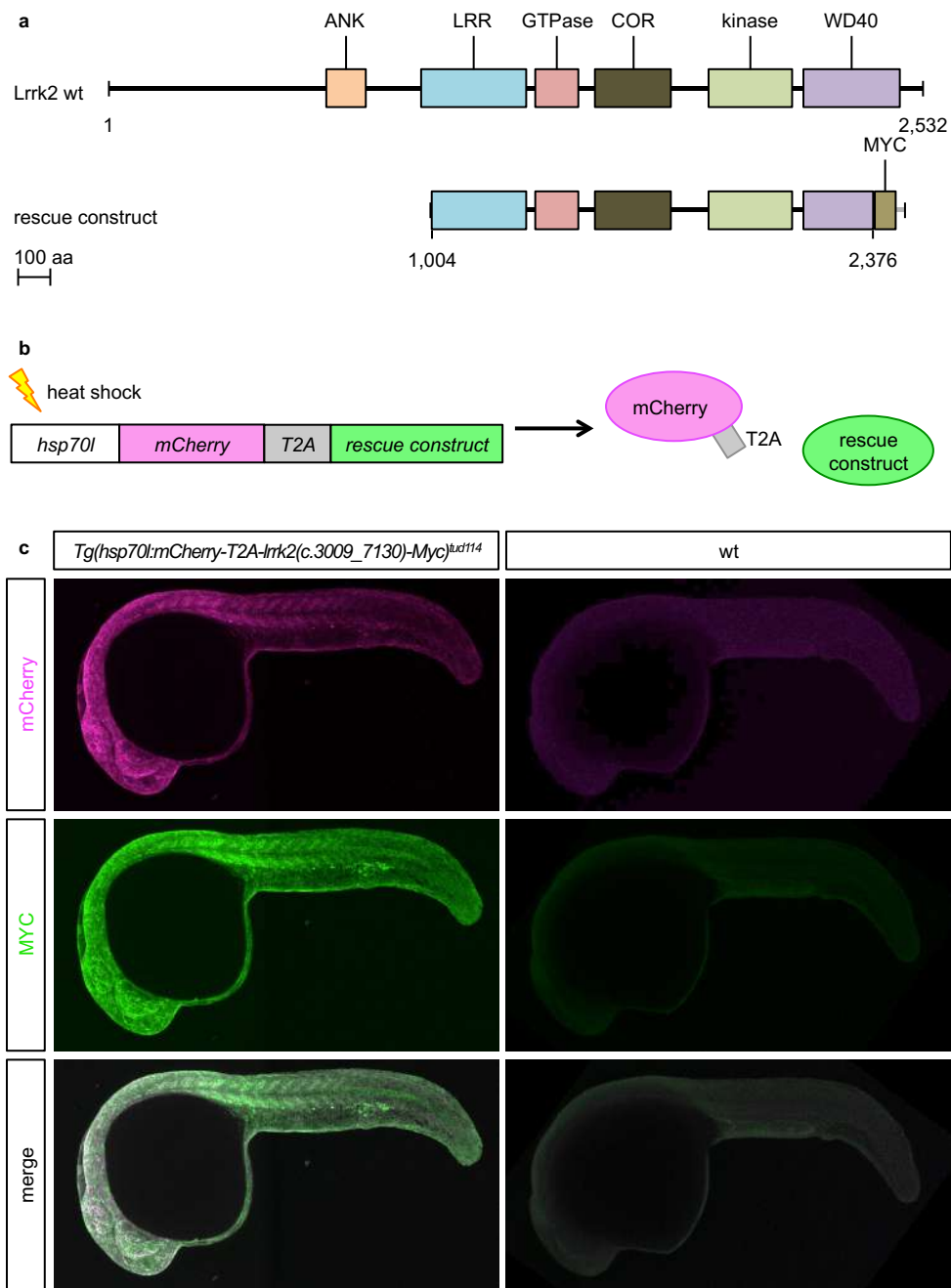
Figure A.8: Generation of the conditional *lrrk2* rescue line. (a) A rescue construct encoding a C-terminally MYC-tagged Lrrk2 fragment (*lrrk2* c.3009_7130) containing the catalytic core. (b) The rescue construct was fused via a *T2A* signal sequence with the *mCherry* reporter and placed under the heat-inducible promoter *hsp70l* (*Tg(hsp70l:mCherry-T2A-lrrk2(c.3009_7130)-Myc)*^{*tud114*}) to enable conditional expression. (c) Correlation between mCherry and MYC IHC demonstrates the ubiquitous expression of the rescue construct in 24-hpf embryos after 4 heat shock.
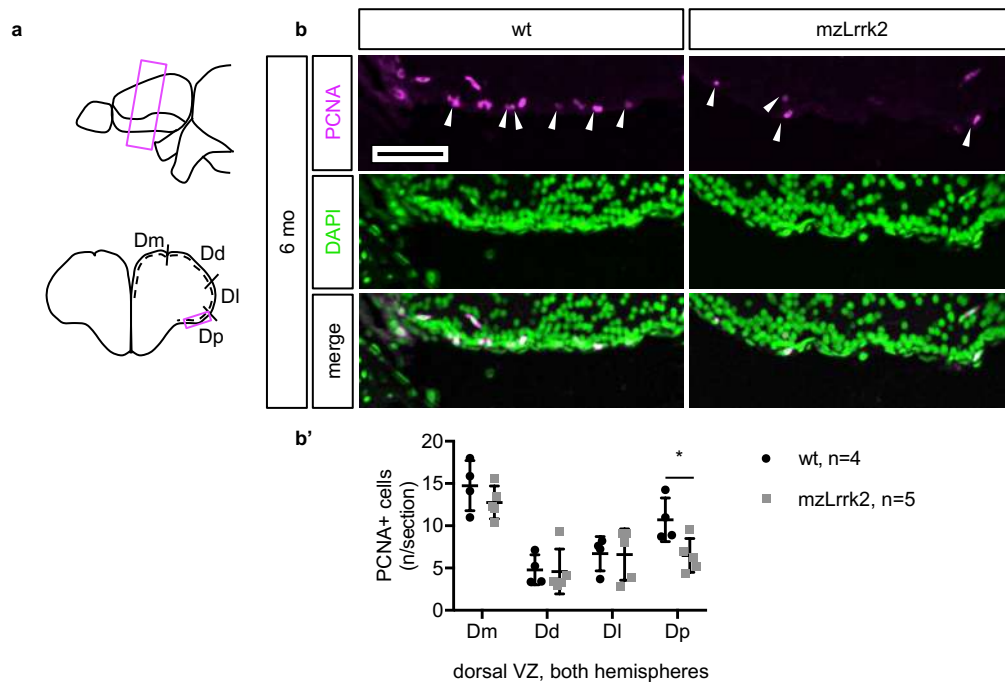
Figure A.9: Reduced proliferation in the adult dorsal telencephalic neurogenic niche. (a) Sections of 6-mo adult telencephalon comprising the *sulcus ypsiloniformis* were stained for PCNA to label proliferating cells in the ventricular zone (VZ) niche. (b, b') Quantification of PCNA+ cells in the individual subdomains of the VZ reveals a significant reduction in the posterior part of the dorsal telencephalon (Dp) of *mzLrrk2* brains. (b') Plot represents means ± s.d. (b') Statistical analyses: two-tailed Student's *t*-test. (b) Scale bar: 50 μm.
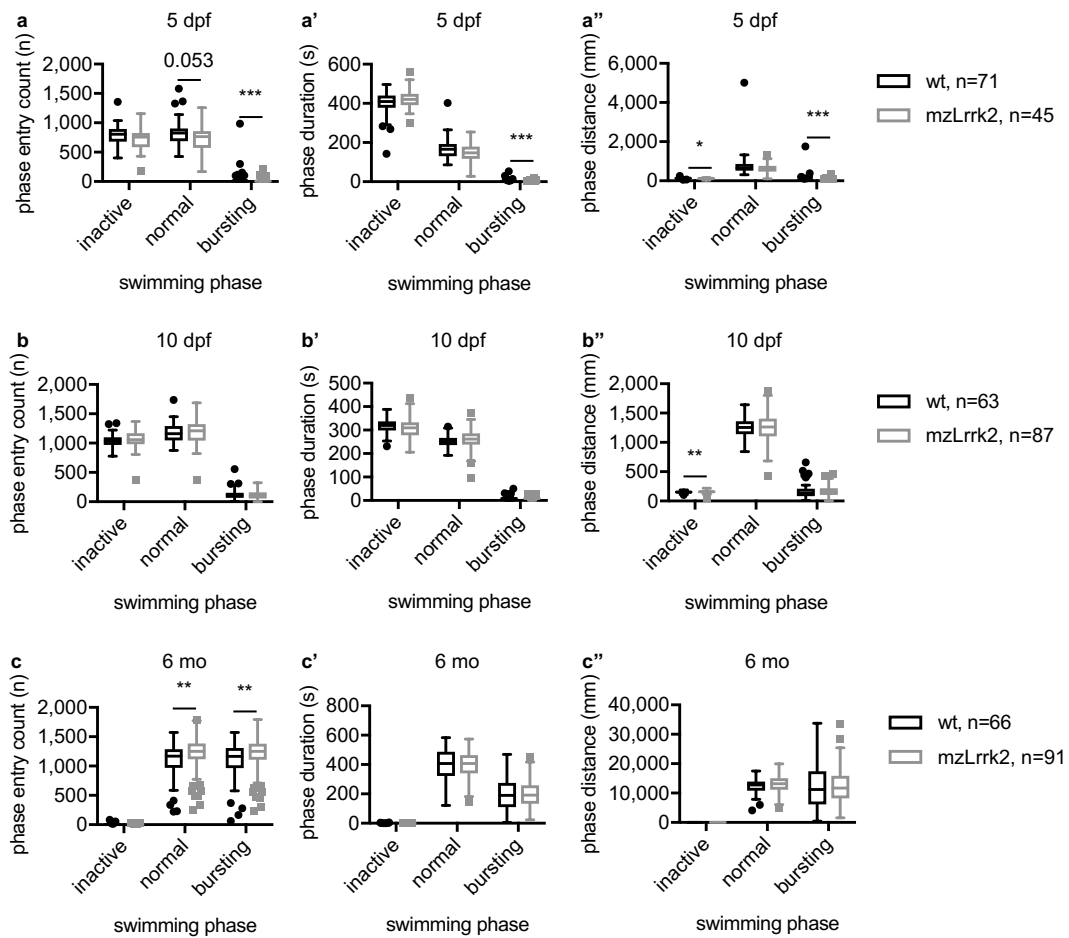
Figure A.10: Analysis of spontaneous motor activity. Swimming performance at 5 dpf (a, a', a"), 10 dpf (b, b', b"), and 6 mo (c, c', c"). Considered motor parameters are: *phase entry count* (a, b, c), *duration of swimming* (a', b', c'), and *distance swum* (a", b", c") in each swimming phase. Tukey's box plots summarise data distributions. Statistical analyses: two-tailed Mann-Whitney's U test.
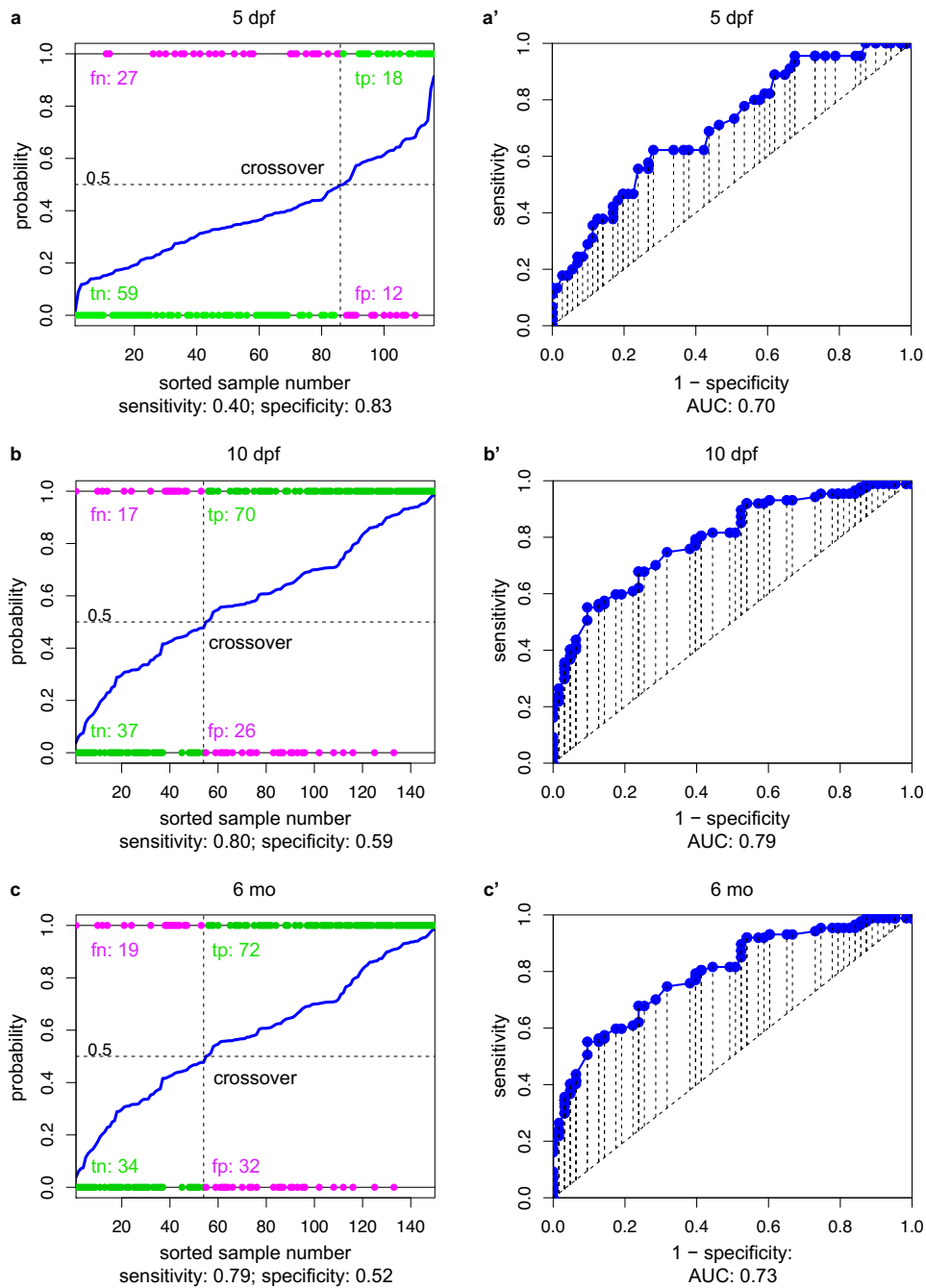
Figure A.11: Performance of the logistic regression models for spontaneous motor activity. Diagnostic plots for the best-fitting logistic regression models for recorded animals at 5 dpf (a, a'), 10 dpf (b, b'), and 6 mo (c, c'). (a, b, c) For a probability threshold of 0.5 (horizontal dashed line), each model's crossover (highest fitted sample below threshold, vertical dashed line), fitted probability curve (continuous blue line), correct (green; *tp*, true positives; *tn*, true negatives) and false predictions (magenta; *fp*, false positives; textslfn, false negatives), sensitivity (*tp* rate), and specificity (*tn* rate) are reported. (a', b', c') Receiver operating characteristic (ROC) curves evaluating the model performance. Each ROC curve plots each model's sensitivity against the complement of its specificity (i.e., the *fp* rate) at the probability threshold of 0.5. The diagonal represents the random case: the closer the curve to the left-hand and top borders, the better the model. The measure of model fit is given by the area under curve (AUC).
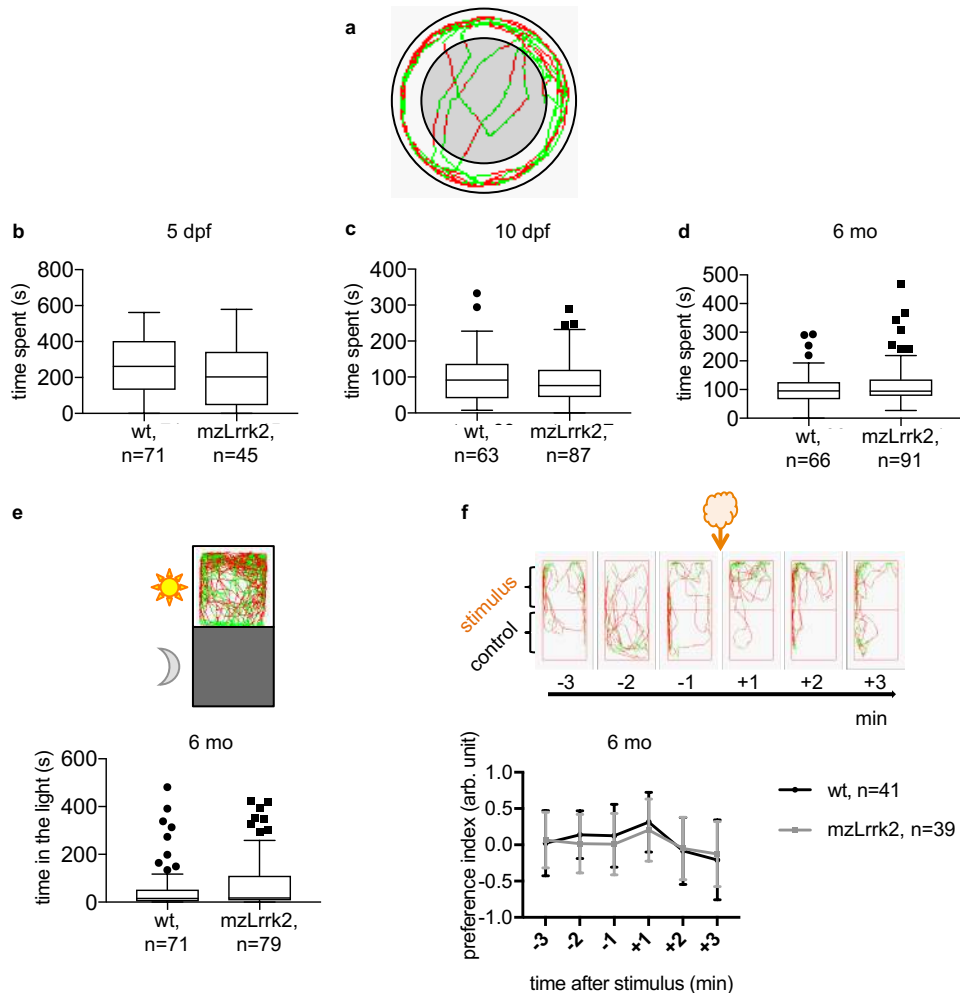
Figure A.12: Analysis of anxiety levels and odour response. (a–d) Analysis of thigmo-taxis at 5 dpf (b), 10 dpf (c), and 6 mo (d). (a) Sample 1-min tracking showing normal swimming (green) and bursting (red) activities. For analysis of thigmotaxis, the same recordings for spontaneous swimming activity were used, with the tracking arena divided into an inner and outer zone, and the time spent in the inner zone was quantified. (e) Analysis of scototaxis at 6 mo. (b–e) Tukey's box plots summarise data distributions. (f) Analysis of the response to an odourant stimulus (amino acid mixture) at 6 mo. The preference index was defined as $\frac{ts-tc}{ts+tc}$, where ts is the time spent in the stimulus side, tc the time spent in the control side. The plot represents means $\pm$ s.d. Statistical analyses: (b–f) two-tailed Mann-Whitney's U test.
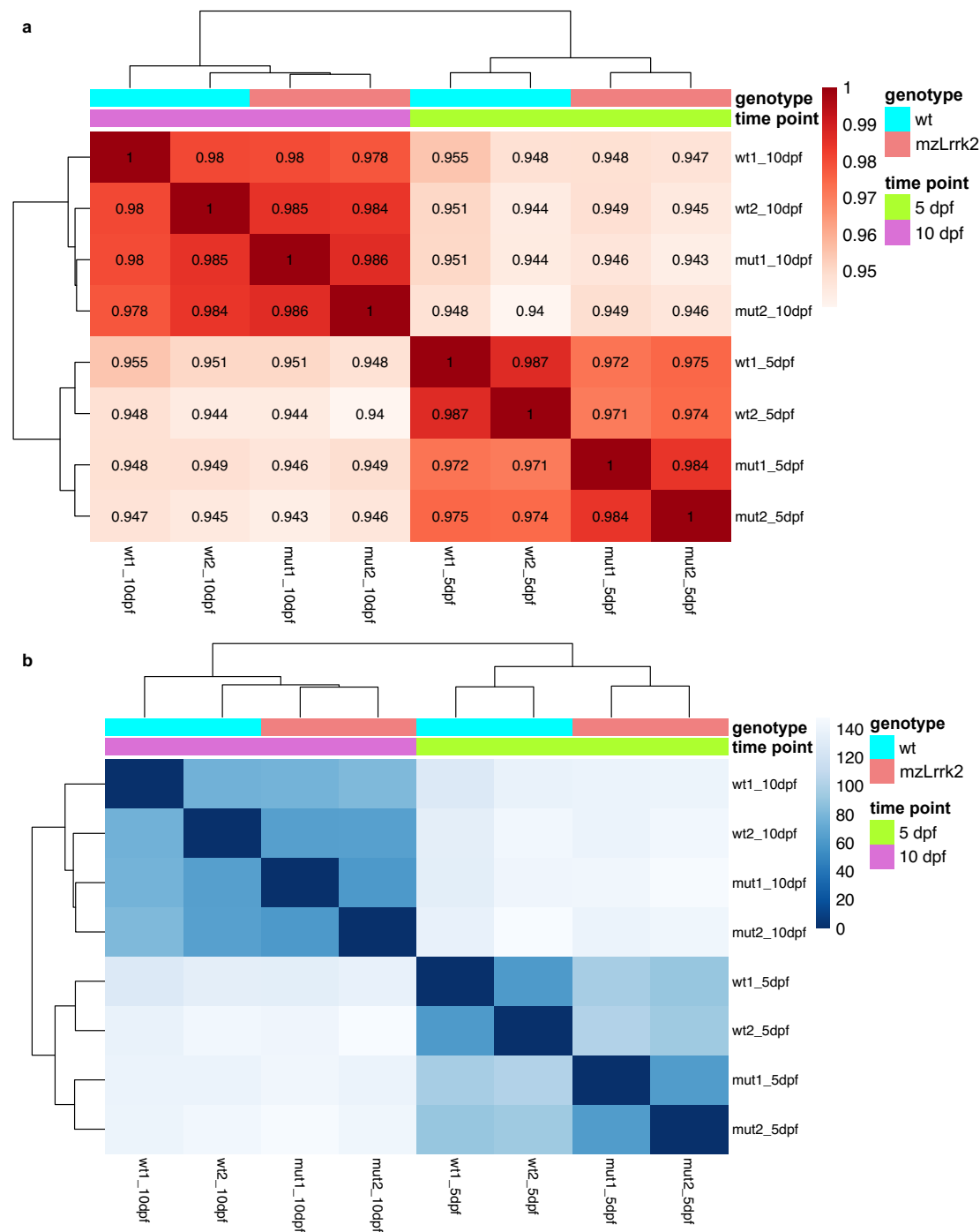
Figure A.13: Assessment of overall similarity between samples. (a) Spearman correlation plot based on normalised, ranked gene counts: the higher the correlation, the darker the cell colour. (b) Heatmap of the sample-to-sample euclidean distance: the closer the samples, the darker the cell colour. Samples: `wt1/2_5/10dpf`, *wt* replicates; `mut1/2_5/10dpf`, *mzLrrk2* replicates.
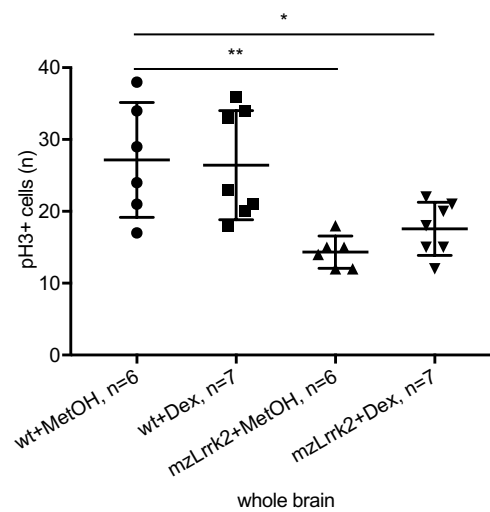
Figure A.14: Chronic immunosuppression does not affect brain cell proliferation in 10-dpf *mzLrrk2*. Dexamethasone (Dex) treatment from 1 to 10 dpf has no influence on the mitosis rate in *mzLrrk2* or *wt* brains compared to methanol (MetOH)-treated controls. Note the persistent reduction of pH3+ cells in *mzLrrk2* brains. Plot represents means ± s.d. Statistical analyses: one-way ANOVA followed by Dunn-Šidák's correction for multiple comparisons. Multiple comparisons: *wt+MetOH* vs. *wt+Dex*; *wt+MetOH* vs. *mzLrrk2+MetOH*; *wt+MetOH* vs. *mzLrrk2+Dex*; *mzLrrk2+MetOH* vs. *mzLrrk2+Dex*.

Bibliography

[1] Goetz, C. G. The History of Parkinson's Disease: Early Clinical Descriptions and Neurological Therapies. *Cold Spring Harbor Perspectives in Medicine:*, 1(1): a008862, 09 2011. doi: 10.1101/cshperspect.a008862. URL `http://www.ncbi.nlm.nih.gov/pmc/articles/PMC3234454/`.

[2] de Lau, L. M. and Breteler, M. M. Epidemiology of Parkinson's disease. *The Lancet Neurology*, 5(6):525–535, 04/22 2017. doi: 10.1016/S1474-4422(06)70471-9. URL `http://dx.doi.org/10.1016/S1474-4422(06)70471-9`.

[3] Inzelberg, R., Schecthman, E., Paleacu, D., Zach, L., Bonwitt, R., Carasso, R., and Nisipeanu, P. Onset and progression of disease in familial and sporadic Parkinson's disease. *American Journal of Medical Genetics Part A*, 124A(3):255–258, 2004. ISSN 1552-4833. doi: 10.1002/ajmg.a.20405. URL `http://dx.doi.org/10.1002/ajmg.a.20405`.

[4] Haaxma, C. A., Bloem, B. R., Borm, G. F., Oyen, W. J. G., Leenders, K. L., Eshuis, S., Booij, J., Dluzen, D. E., and Horstink, M. W. I. M. Gender differences in Parkinson's disease. *Journal of Neurology, Neurosurgery, and Psychiatry*, 78(8): 819–824, 08 2007. doi: 10.1136/jnnp.2006.103788. URL `http://www.ncbi.nlm.nih.gov/pmc/articles/PMC2117736/`.

[5] Chaudhuri, K. R., Healy, D. G., and Schapira, A. H. V. Non-motor symptoms of Parkinson's disease: diagnosis and management. *The Lancet Neurology*, 5 (3):235–245, 2006. ISSN 1474-4422. doi: http://dx.doi.org/10.1016/S1474-4422(06)70373-8. URL `http://www.sciencedirect.com/science/article/pii/S1474442206703738`.

[6] Cheng, H. C., Ulane, C. M., and Burke, R. E. Clinical Progression in Parkinson's Disease and the Neurobiology of Axons. *Annals of neurology*, 67(6):715–725, 06 2010. doi: 10.1002/ana.21995. URL `http://www.ncbi.nlm.nih.gov/pmc/articles/PMC2918373/`.

[7] Spillantini, M. G. and Goedert, M. The α-Synucleinopathies: Parkinson's Disease, Dementia with Lewy Bodies, and Multiple System Atrophy. *Annals of the New York Academy of Sciences*, 920(1):16–27, 2000. ISSN 1749-6632. doi: 10.1111/j.1749-6632.2000.tb06900.x. URL `http://dx.doi.org/10.1111/j.1749-6632.2000.tb06900.x`.

[8] Kalia, L. V., Lang, A. E., Hazrati, L., and et al. Clinical correlations with Lewy body pathology in LRRK2-related Parkinson disease. *JAMA Neurology*, 72(1): 100–105, 2015. ISSN 2168-6149. doi: 10.1001/jamaneurol.2014.2704. URL `http://dx.doi.org/10.1001/jamaneurol.2014.2704`.

[9] Alexander, G. E. Biology of Parkinson's disease: pathogenesis and pathophysiology of a multisystem neurodegenerative disorder. *Dialogues in Clinical Neuroscience*, 6(3):259–280, 09 2004. URL `http://www.ncbi.nlm.nih.gov/pmc/articles/PMC3181806/`.

[10] Jankovic, J. and Aguilar, L. G. Current approaches to the treatment of Parkinson's disease. *Neuropsychiatric Disease and Treatment*, 4(4):743–757, 08 2008. URL `http://www.ncbi.nlm.nih.gov/pmc/articles/PMC2536542/`.

[11] Ben-Shlomo, Y. and Sieradzan, K. Idiopathic Parkinson's disease: epidemiology, diagnosis and management. *The British Journal of General Practice*, 45(394):261–268, 05 1995. URL `http://www.ncbi.nlm.nih.gov/pmc/articles/PMC1239233/`.

[12] Jucker, M. The benefits and limitations of animal models for translational research in neurodegenerative diseases. *Nat Med*, 16(11):1210–1214, 11 2010. URL `http://dx.doi.org/10.1038/nm.2224`.

[13] Alberio, T., Lopiano, L., and Fasano, M. Cellular models to investigate biochemical pathways in Parkinson's disease. *FEBS Journal*, 279(7):1146–1155, 2012. ISSN 1742-4658. doi: 10.1111/j.1742-4658.2012.08516.x. URL `http://dx.doi.org/10.1111/j.1742-4658.2012.08516.x`.

[14] Martínez-Morales, P. L. and Liste, I. Stem Cells as In Vitro Model of Parkinson's Disease. *Stem Cells International*, 2012:980941, 2012. doi: 10.1155/2012/980941. URL `http://www.ncbi.nlm.nih.gov/pmc/articles/PMC3350852/`.

[15] Yamamoto, K. and Vernier, P. The Evolution of Dopamine Systems in Chordates. *Frontiers in Neuroanatomy*, 5:21, 2011. doi: 10.3389/fnana.2011.00021. URL `http://www.ncbi.nlm.nih.gov/pmc/articles/PMC3070214/`.

[16] Bové, J., Prou, D., Perier, C., and Przedborski, S. Toxin-Induced Models of Parkinson's Disease. *NeuroRx*, 2(3):484–494, 07 2005. URL `http://www.ncbi.nlm.nih.gov/pmc/articles/PMC1144492/`.

[17] Duty, S. and Jenner, P. Animal models of Parkinson's disease: a source of novel treatments and clues to the cause of the disease. *British Journal of Pharmacology*, 164(4):1357–1391, 10 2011. doi: 10.1111/j.1476-5381.2011.01426.x. URL `http://www.ncbi.nlm.nih.gov/pmc/articles/PMC3229766/`.

[18] Gasser, T. Molecular pathogenesis of Parkinson disease: insights from genetic studies. *Expert Reviews in Molecular Medicine*, 11, 2009. doi: DOI: 10.1017/S1462399409001148. URL `https://www.cambridge.org/core/article/molecular-pathogenesis-of-parkinson-disease-insights-from-genetic-studies/D51BB2661D06D3F113A7918BAD63B4B5`.

[19] Klein, C. and Westenberger, A. Genetics of Parkinson's Disease. *Cold Spring Harbor Perspectives in Medicine*, 2(1):a008888, 01 2012. doi: 10.1101/cshperspect.a008888. URL `http://www.ncbi.nlm.nih.gov/pmc/articles/PMC3253033/`.

[20] Dick, F. D., De Palma, G., Ahmadi, A., Osborne, A., Scott, N. W., Prescott, G. J., Bennett, J., Semple, S., Dick, S., Mozzoni, P., Haites, N., Wettinger, S. B., Mutti,

A., Otelea, M., Seaton, A., Soderkvist, P., and Felice, A. Gene-environment interactions in parkinsonism and Parkinson's disease: the Geoparkinson study. *Occupational and Environmental Medicine*, 64(10):673–680, 10 2007. doi: 10.1136/oem. 2006.032078. URL `http://www.ncbi.nlm.nih.gov/pmc/articles/PMC2078383/`.

[21] Hill-Burns, E. M., Ross, O. A., Wissemann, W. T., Soto-Ortolaza, A. I., Zareparsi, S., Siuda, J., Lynch, T., Wszolek, Z. K., Silburn, P. A., Mellick, G. D., Ritz, B., Scherzer, C. R., Zabetian, C. P., Factor, S. A., Breheny, P. J., and Payami, H. Identification of genetic modifiers of age-at-onset for familial Parkinson's disease. *Human Molecular Genetics*, 25(17):3849–3862, 09 2016. doi: 10.1093/hmg/ddw206. URL `http://www.ncbi.nlm.nih.gov/pmc/articles/PMC5216611/`.

[22] Dick, F. D., De Palma, G., Ahmadi, A., Scott, N. W., Prescott, G. J., Bennett, J., Semple, S., Dick, S., Counsell, C., Mozzoni, P., Haites, N., Wettinger, S. B., Mutti, A., Otelea, M., Seaton, A., Söderkvist, P., and Felice, A. Environmental risk factors for Parkinson's disease and parkinsonism: the Geoparkinson study. *Occupational and Environmental Medicine*, 64(10):666–672, 10 2007. doi: 10.1136/oem.2006. 027003. URL `http://www.ncbi.nlm.nih.gov/pmc/articles/PMC2078401/`.

[23] Low, K. and Aebischer, P. Use of viral vectors to create animal models for Parkinson's disease. *Neurobiol Dis*, 48(2):189–201, Nov 2012. ISSN 1095-953X (Electronic); 0969-9961 (Linking). doi: 10.1016/j.nbd.2011.12.038.

[24] Dawson, T. M., Ko, H. S., and Dawson, V. L. Genetic Animal Models of Parkinson's Disease. *Neuron*, 66(5):646–661, 6 2010. doi: http://doi.org/10.1016/j. neuron.2010.04.034. URL `http://www.sciencedirect.com/science/article/pii/S0896627310003272`.

[25] Jagmag, S. A., Tripathi, N., Shukla, S. D., Maiti, S., and Khurana, S. Evaluation of Models of Parkinson's Disease. *Frontiers in Neuroscience*, 9:503, 2015. doi: 10.3389/fnins.2015.00503. URL `http://www.ncbi.nlm.nih.gov/pmc/articles/PMC4718050/`.

[26] Boettcher, M. and McManus, M. T. Choosing the Right Tool for the Job: RNAi, TALEN, or CRISPR. *Molecular Cell*, 58(4):575–585, 5 2015. doi: http://doi.org/10.1016/j.molcel.2015.04.028. URL `http://www.sciencedirect.com/science/article/pii/S109727651500310X`.

[27] Schulte-Merker, S. and Stainier, D. Y. Out with the old, in with the new: reassessing morpholino knockdowns in light of genome editing technology. *Development*, 141(16):3103–4, 2014. ISSN 0950-1991. doi: 10.1242/dev.112003.

[28] Gaj, T., Gersbach, C. A., and Barbas, C. F. ZFN, TALEN and CRISPR/Cas-based methods for genome engineering. *Trends in biotechnology*, 31(7):397–405, 07 2013. doi: 10.1016/j.tibtech.2013.04.004. URL `http://www.ncbi.nlm.nih.gov/pmc/articles/PMC3694601/`.

[29] Kim, H.-J. and Jeon, B. S. Hypothesis: Somatic Mosaicism and Parkinson Disease. *Experimental Neurobiology*, 23(4):271–276, 12 2014. doi: 10.5607/en.2014.23.4.271. URL `http://www.ncbi.nlm.nih.gov/pmc/articles/PMC4276799/`.

[30] Lettice, L. A., Daniels, S., Sweeney, E., Venkataraman, S., Devenney, P. S., Gautier, P., Morrison, H., Fantes, J., Hill, R. E., and FitzPatrick, D. R. Enhancer-adoption as a mechanism of human developmental disease. *Human Mutation*, 32(12):1492–1499, 2011. ISSN 1098-1004. doi: 10.1002/humu.21615. URL `http://dx.doi.org/10.1002/humu.21615`.

[31] Chang, Y. F., Imam, J. S., and Wilkinson, M. F. The nonsense-mediated decay RNA surveillance pathway. *Annu Rev Biochem*, 76:51–74, 2007. ISSN 0066-4154 (Print); 0066-4154 (Linking). doi: 10.1146/annurev.biochem.76.050106.093909.

[32] Doma, M. K. and Parker, R. RNA Quality Control in Eukaryotes. *Cell*, 131(4): 660–668, 04/24 2017. doi: 10.1016/j.cell.2007.10.041. URL `http://dx.doi.org/10.1016/j.cell.2007.10.041`.

[33] Abrams, E. W. and Mullins, M. C. Early zebrafish development: It's in the maternal genes. *Current opinion in genetics & development*, 19(4):396–403, 08 2009. doi: 10.1016/j.gde.2009.06.002. URL `http://www.ncbi.nlm.nih.gov/pmc/articles/PMC2752143/`.

[34] Funayama, M., Hasegawa, K., Kowa, H., Saito, M., Tsuji, S., and Obata, F. A new locus for Parkinson's disease (PARK8) maps to chromosome 12p11.2-q13.1. *Ann Neurol*, 51(3):296–301, Mar 2002. ISSN 0364-5134 (Print); 0364-5134 (Linking).

[35] Paisan-Ruiz, C., Jain, S., Evans, E. W., Gilks, W. P., Simon, J., van der Brug, M., Lopez de Munain, A., Aparicio, S., Gil, A. M., Khan, N., Johnson, J., Martinez, J. R., Nicholl, D., Carrera, I. M., Pena, A. S., de Silva, R., Lees, A., Marti-Masso, J. F., Perez-Tur, J., Wood, N. W., and Singleton, A. B. Cloning of the gene containing mutations that cause PARK8-linked Parkinson's disease. *Neuron*, 44 (4):595–600, Nov 2004. ISSN 0896-6273 (Print); 0896-6273 (Linking). doi: 10.1016/j.neuron.2004.10.023.

[36] Manning, G., Whyte, D. B., Martinez, R., Hunter, T., and Sudarsanam, S. The Protein Kinase Complement of the Human Genome. *Science*, 298(5600):1912–1934, 2002. ISSN 0036-8075. doi: 10.1126/science.1075762. URL `http://science.sciencemag.org/content/298/5600/1912`.

[37] Kett, L. R. and Dauer, W. T. Leucine-Rich Repeat Kinase 2 for Beginners: Six Key Questions. *Cold Spring Harbor Perspectives in Medicine*, 2(3):a009407, 03 2012. doi: 10.1101/cshperspect.a009407. URL `http://www.ncbi.nlm.nih.gov/pmc/articles/PMC3282500/`.

[38] Kumari, U. and Tan, E. K. LRRK2 in Parkinson's disease: genetic and clinical studies from patients. *FEBS J*, 276(22):6455–6463, Nov 2009. ISSN 1742-4658 (Electronic); 1742-464X (Linking). doi: 10.1111/j.1742-4658.2009.07344.x.

[39] Alexandru, D. C. Medline trend: automated yearly statistics of PubMed results for any query, 2004. URL `http://dan.corlan.net/medline-trend.html`.

[40] Kachergus, J., Mata, I. F., Hulihan, M., Taylor, J. P., Lincoln, S., Aasly, J., Gibson, J. M., Ross, O. A., Lynch, T., Wiley, J., Payami, H., Nutt, J., Maraganore, D. M., Czyzewski, K., Styczynska, M., Wszolek, Z. K., Farrer, M. J., and Toft, M. Identification of a Novel *LRRK2* Mutation Linked to Autosomal Dominant

Parkinsonism: Evidence of a Common Founder across European Populations. *The American Journal of Human Genetics*, 76(4):672–680, 05/02 2017. doi: 10.1086/429256. URL `http://dx.doi.org/10.1086/429256`.

[41] Healy, D. G., Falchi, M., O'Sullivan, S. S., Bonifati, V., Durr, A., Bressman, S., Brice, A., Aasly, J., Zabetian, C. P., Goldwurm, S., Ferreira, J. J., Tolosa, E., Kay, D. M., Klein, C., Williams, D. R., Marras, C., Lang, A. E., Wszolek, Z. K., Berciano, J., Schapira, A. H., Lynch, T., Bhatia, K. P., Gasser, T., Lees, A. J., Wood, N. W., and on behalf of the International LRRK2 Consortium. Phenotype, genotype, and worldwide genetic penetrance of LRRK2-associated Parkinson's disease: a case-control study. *Lancet Neurology*, 7(7):583–590, 07 2008. doi: 10.1016/S1474-4422(08)70117-0. URL `http://www.ncbi.nlm.nih.gov/pmc/articles/PMC2832754/`.

[42] Bonifati, V. Parkinson's disease: the LRRK2-G2019S mutation: opening a novel era in Parkinson's disease genetics. *Eur J Hum Genet*, 14(10):1061–1062, Oct 2006. ISSN 1018-4813 (Print); 1018-4813 (Linking). doi: 10.1038/sj.ejhg.5201695.

[43] Cilia, R., Siri, C., Rusconi, D., Allegra, R., Ghiglietti, A., Sacilotto, G., Zini, M., Zecchinelli, A. L., Asselta, R., Duga, S., Paganoni, A. M., Pezzoli, G., Seia, M., and Goldwurm, S. LRRK2 mutations in Parkinson's disease: Confirmation of a gender effect in the Italian population. *Parkinsonism & Related Disorders*, 20(8): 911–914, 08 2014. doi: 10.1016/j.parkreldis.2014.04.016. URL `http://www.ncbi.nlm.nih.gov/pmc/articles/PMC4144811/`.

[44] Ishihara, L., Gibson, R. A., Warren, L., Amouri, R., Lyons, K., Wielinski, C., Hunter, C., Swartz, J. E., Elango, R., Akkari, P. A., Leppert, D., Surh, L., Reeves, K. H., Thomas, S., Ragone, L., Hattori, N., Pahwa, R., Jankovic, J., Nance, M., Freeman, A., Gouider-Khouja, N., Kefi, M., Zouari, M., Ben Sassi, S., Ben Yahmed, S., El Euch-Fayeche, G., Middleton, L., Burn, D. J., Watts, R. L., and Hentati, F. Screening for Lrrk2 G2019S and clinical comparison of Tunisian and North American Caucasian Parkinson's disease families. *Mov Disord*, 22(1):55–61, Jan 2007. ISSN 0885-3185 (Print); 0885-3185 (Linking). doi: 10.1002/mds.21180.

[45] Nichols, W. C., Pankratz, N., Hernandez, D., Paisan-Ruiz, C., Jain, S., Halter, C. A., Michaels, V. E., Reed, T., Rudolph, A., Shults, C. W., Singleton, A., and Foroud, T. Genetic screening for a single common LRRK2 mutation in familial Parkinson's disease. *Lancet*, 365(9457):410–412, Jan 2005. ISSN 1474-547X (Electronic); 0140-6736 (Linking). doi: 10.1016/S0140-6736(05)17828-3.

[46] Ishihara, L., Warren, L., Gibson, R., Amouri, R., Lesage, S., Durr, A., Tazir, M., Wszolek, Z. K., Uitti, R. J., Nichols, W. C., Griffith, A., Hattori, N., Leppert, D., Watts, R., Zabetian, C. P., Foroud, T. M., Farrer, M. J., Brice, A., Middleton, L., and Hentati, F. Clinical features of Parkinson disease patients with homozygous leucine-rich repeat kinase 2 G2019S mutations. *Arch Neurol*, 63(9):1250–1254, Sep 2006. ISSN 0003-9942 (Print); 0003-9942 (Linking). doi: 10.1001/archneur.63.9.1250.

[47] Wang, C., Cai, Y., Zheng, Z., Tang, B.-S., Xu, Y., Wang, T., Ma, J., Chen, S.-D., Langston, J. W., Tanner, C. M., and Chan, P. Penetrance of LRRK2 G2385R

and R1628P is modified by common PD-associated genetic variants. *Parkinsonism Relat Disord*, 18(8):958–963, Sep 2012. ISSN 1873-5126 (Electronic); 1353-8020 (Linking). doi: 10.1016/j.parkreldis.2012.05.003.

[48] Trinh, J., Gustavsson, E. K., Vilariño-Güell, C., Bortnick, S., Latourelle, J., McKenzie, M. B., Tu, C. S., Nosova, E., Khinda, J., Milnerwood, A., Lesage, S., Brice, A., Tazir, M., Aasly, J. O., Parkkinen, L., Haytural, H., Foroud, T., Myers, R. H., Sassi, S. B., Hentati, E., Nabli, F., Farhat, E., Amouri, R., Hentati, F., and Farrer, M. J. *DNM3* and genetic modifiers of age of onset in LRRK2 Gly2019Ser parkinsonism: a genome-wide linkage and association study. *The Lancet Neurology*, 15(12):1248–1256, November 2016. ISSN 1474-4422. doi: 10.1016/S1474-4422(16)30203-4. URL `http://dx.doi.org/10.1016/S1474-4422(16)30203-4`.

[49] Hyun, C. H., Yoon, C. Y., Lee, H. J., and Lee, S. J. LRRK2 as a Potential Genetic Modifier of Synucleinopathies: Interlacing the Two Major Genetic Factors of Parkinson's Disease. *Experimental Neurobiology*, 22(4):249–257, 2013. ISSN 1226-2560 2093-8144. doi: 10.5607/en.2013.22.4.249. URL `http://www.ncbi.nlm.nih.gov/pmc/articles/PMC3897686/`.

[50] Guo, L., Gandhi, P. N., Wang, W., Petersen, R. B., Wilson-Delfosse, A. L., and Chen, S. G. The Parkinson's disease-associated protein, leucine-rich repeat kinase 2 (LRRK2), is an authentic GTPase that stimulates kinase activity. *Exp Cell Res*, 313(16):3658–70, 2007. ISSN 0014-4827 (Print) 0014-4827. doi: 10.1016/j.yexcr.2007.07.007.

[51] Weiss, B. ROCO kinase activity is controlled by internal GTPase function. *Sci Signal*, 1(23):pe27, 2008. ISSN 1945-0877. doi: 10.1126/scisignal.123pe27.

[52] Taymans, J. M., Vancraenenbroeck, R., Ollikainen, P., Beilina, A., Lobbestael, E., De Maeyer, M., Baekelandt, V., and Cookson, M. R. LRRK2 kinase activity is dependent on LRRK2 GTP binding capacity but independent of LRRK2 GTP binding. *PLoS One*, 6(8):e23207, 2011. ISSN 1932-6203. doi: 10.1371/journal.pone.0023207.

[53] Taymans, J. M. and Cookson, M. R. Mechanisms in dominant parkinsonism; The toxic triangle of LRRK2, α-synuclein and tau. *BioEssays : news and reviews in molecular, cellular and developmental biology*, 32(3):227–235, 03 2010. doi: 10.1002/bies.200900163. URL `http://www.ncbi.nlm.nih.gov/pmc/articles/PMC4662284/`.

[54] Greggio, E., Taymans, J. M., Zhen, E. Y., Ryder, J., Vancraenenbroeck, R., Beilina, A., Sun, P., Deng, J., Jaffe, H., Baekelandt, V., Merchant, K., and Cookson, M. R. The Parkinson's disease kinase LRRK2 autophosphorylates its GTPase domain at multiple sites. *Biochemical and biophysical research communications*, 389(3):449–454, 11 2009. doi: 10.1016/j.bbrc.2009.08.163. URL `http://www.ncbi.nlm.nih.gov/pmc/articles/PMC2759846/`.

[55] Greggio, E., Zambrano, I., Kaganovich, A., Beilina, A., Taymans, J. M., Daniëls, V., Lewis, P., Jain, S., Ding, J., Syed, A., Thomas, K. J., Baekelandt, V., and Cookson, M. R. The Parkinson disease-associated leucine-rich repeat kinase 2 (LRRK2) is a dimer that undergoes intramolecular autophosphorylation. *The*

Journal of Biological Chemistry, 283(24):16906–16914, 2008. ISSN 0021-9258 1083-351X. doi: 10.1074/jbc.M708718200. URL `http://www.ncbi.nlm.nih.gov/pmc/articles/PMC2423262/`.

[56] Berger, Z., Smith, K. A., and Lavoie, M. J. Membrane localization of LRRK2 is associated with increased formation of the highly active LRRK2 dimer and changes in its phosphorylation. *Biochemistry*, 49(26):5511–5523, Jul 2010. ISSN 1520-4995 (Electronic); 0006-2960 (Linking). doi: 10.1021/bi100157u.

[57] Li, J. Q., Tan, L., and Yu, J. T. The role of the LRRK2 gene in Parkinsonism. *Molecular Neurodegeneration*, 9:47, 2014. ISSN 1750-1326. doi: 10.1186/1750-1326-9-47. URL `http://www.ncbi.nlm.nih.gov/pmc/articles/PMC4246469/`.

[58] Mills, R. D., Mulhern, T. D., Cheng, H. C., and Culvenor, J. G. Analysis of LRRK2 accessory repeat domains: prediction of repeat length, number and sites of Parkinson's disease mutations. *Biochem Soc Trans*, 40(5):1086–9, 2012. ISSN 0300-5127. doi: 10.1042/bst20120088.

[59] Dächsel, J. C., Taylor, J. P., Mok, S. S., Ross, O. A., Hinkle, K. M., Bailey, R. M., Hines, J. H., Szutu, J., Madden, B., Petrucelli, L., and Farrer, M. J. Identification of potential protein interactors of Lrrk2. *Parkinsonism & related disorders*, 13(7):382–385, 10 2007. doi: 10.1016/j.parkreldis.2007.01.008. URL `http://www.ncbi.nlm.nih.gov/pmc/articles/PMC2970619/`.

[60] Meixner, A., Boldt, K., Van Troys, M., Askenazi, M., Gloeckner, C. J., Bauer, M., Marto, J. A., Ampe, C., Kinkl, N., and Ueffing, M. A QUICK screen for Lrrk2 interaction partners–leucine-rich repeat kinase 2 is involved in actin cytoskeleton dynamics. *Mol Cell Proteomics*, 10(1):M110.001172, 2011. ISSN 1535-9476. doi: 10.1074/mcp.M110.001172.

[61] Guerreiro, P. S., Huang, Y., Gysbers, A., Cheng, D., Gai, W. P., Outeiro, T. F., and Halliday, G. M. LRRK2 interactions with α-synuclein in Parkinson's disease brains and in cell models. *J Mol Med (Berl)*, 91(4):513–522, Apr 2013. ISSN 1432-1440 (Electronic); 0946-2716 (Linking). doi: 10.1007/s00109-012-0984-y.

[62] Smith, W. W., Pei, Z., Jiang, H., Moore, D. J., Liang, Y., West, A. B., Dawson, V. L., Dawson, T. M., and Ross, C. A. Leucine-rich repeat kinase 2 (LRRK2) interacts with parkin, and mutant LRRK2 induces neuronal degeneration. *Proc Natl Acad Sci U S A*, 102(51):18676–18681, Dec 2005. ISSN 0027-8424 (Print); 0027-8424 (Linking). doi: 10.1073/pnas.0508052102.

[63] Porras, P., Duesbury, M., Fabregat, A., Ueffing, M., Orchard, S., Gloeckner, C. J., and Hermjakob, H. A visual review of the interactome of LRRK2: Using deep-curated molecular interaction data to represent biology. *Proteomics*, 15(8):1390–1404, 2015. ISSN 1615-9853 1615-9861. doi: 10.1002/pmic.201400390. URL `http://www.ncbi.nlm.nih.gov/pmc/articles/PMC4415485/`.

[64] Uhlen, M., Fagerberg, L., Hallstrom, B. M., Lindskog, C., Oksvold, P., Mardinoglu, A., Sivertsson, A., Kampf, C., Sjostedt, E., Asplund, A., Olsson, I., Edlund, K., Lundberg, E., Navani, S., Szigyarto, C. A., Odeberg, J., Djureinovic, D., Takanen, J. O., Hober, S., Alm, T., Edqvist, P.-H., Berling, H., Tegel, H., Mulder, J., Rockberg, J., Nilsson, P., Schwenk, J. M., Hamsten, M., von Feilitzen, K., Forsberg,

M., Persson, L., Johansson, F., Zwahlen, M., von Heijne, G., Nielsen, J., and Ponten, F. Proteomics. Tissue-based map of the human proteome. *Science*, 347 (6220):1260419, Jan 2015. ISSN 1095-9203 (Electronic); 0036-8075 (Linking). doi: 10.1126/science.1260419.

[65] La Cognata, V., D'Agata, V., Cavalcanti, F., and Cavallaro, S. Splicing: is there an alternative contribution to Parkinson's disease? *Neurogenetics*, 16:245–263, 2015. doi: 10.1007/s10048-015-0449-x. URL http://www.ncbi.nlm.nih.gov/pmc/articles/PMC4573652/.

[66] Giesert, F., Hofmann, A., Bürger, A., Zerle, J., Kloos, K., Hafen, U., Ernst, L., Zhang, J., Vogt-Weisenhorn, D. M., and Wurst, W. Expression Analysis of *Lrrk1*, *Lrrk2* and *Lrrk2* Splice Variants in Mice. *PLoS ONE*, 8(5):e63778, 2013. ISSN 1932-6203. doi: 10.1371/journal.pone.0063778. URL http://www.ncbi.nlm.nih.gov/pmc/articles/PMC3651128/.

[67] Wallings, R., Manzoni, C., and Bandopadhyay, R. Cellular processes associated with LRRK2 function and dysfunction. *The Febs Journal*, 282(15):2806–2826, 2015. ISSN 1742-464X 1742-4658. doi: 10.1111/febs.13305. URL http://www.ncbi.nlm.nih.gov/pmc/articles/PMC4522467/.

[68] Berwick, D. C. and Harvey, K. LRRK2 signaling pathways: the key to unlocking neurodegeneration? *Trends in Cell Biology*, 21(5):257–265, 05/04 2017. doi: 10.1016/j.tcb.2011.01.001. URL http://dx.doi.org/10.1016/j.tcb.2011.01.001.

[69] Bae, J. R. and Lee, B. D. Function and dysfunction of leucine-rich repeat kinase 2 (LRRK2): Parkinson's disease and beyond. *BMB Rep*, 48(5):243–248, May 2015. ISSN 1976-670X (Electronic); 1976-6696 (Linking).

[70] Yue, Z. and Lachenmayer, M. L. Genetic LRRK2 Models of Parkinson's Disease: Dissecting Pathogenic pathway and Exploring Clinical Application. *Movement disorders : official journal of the Movement Disorder Society*, 26(8):1386–1397, 07 2011. doi: 10.1002/mds.23737. URL http://www.ncbi.nlm.nih.gov/pmc/articles/PMC3150637/.

[71] Langston, R. G., Rudenko, I. N., and Cookson, M. R. The function of orthologues of the human Parkinson's disease gene LRRK2 across species: implications for disease modeling in preclinical research. *The Biochemical journal*, 473(3):221–232, 02 2016. doi: 10.1042/BJ20150985. URL http://www.ncbi.nlm.nih.gov/pmc/articles/PMC5165698/.

[72] Marín, I. Ancient Origin of the Parkinson Disease Gene LRRK2. *Journal of Molecular Evolution*, 67(1):41–50, 2008. doi: 10.1007/s00239-008-9122-4. URL http://dx.doi.org/10.1007/s00239-008-9122-4.

[73] Lesage, S. and Brice, A. Parkinson's disease: from monogenic forms to genetic susceptibility factors. *Human Molecular Genetics*, 18(R1):R48–R59, 2009. ISSN 0964-6906. doi: 10.1093/hmg/ddp012. URL http://dx.doi.org/10.1093/hmg/ddp012.

[74] West, A. B., Moore, D. J., Biskup, S., Bugayenko, A., Smith, W. W., Ross, C. A., Dawson, V. L., and Dawson, T. M. Parkinson's disease-associated mutations in

leucine-rich repeat kinase 2 augment kinase activity. *Proceedings of the National Academy of Sciences of the United States of America*, 102(46):16842–16847, 2005. ISSN 0027-8424 1091-6490. doi: 10.1073/pnas.0507360102. URL `http://www.ncbi.nlm.nih.gov/pmc/articles/PMC1283829/`.

[75] Gloeckner, C. J., Kinkl, N., Schumacher, A., Braun, R. J., O'Neill, E., Meitinger, T., Kolch, W., Prokisch, H., and Ueffing, M. The Parkinson disease causing LRRK2 mutation I2020T is associated with increased kinase activity. *Human Molecular Genetics*, 15(2):223–232, 2006. ISSN 0964-6906. doi: 10.1093/hmg/ddi439. URL `http://dx.doi.org/10.1093/hmg/ddi439`.

[76] Jaleel, M., Nichols, R. J., Deak, M., Campbell, D. G., Gillardon, F., Knebel, A., and Alessi, D. R. LRRK2 phosphorylates moesin at threonine-558: characterization of how Parkinson's disease mutants affect kinase activity. *Biochemical Journal*, 405(Pt 2):307–317, 07 2007. doi: 10.1042/BJ20070209. URL `http://www.ncbi.nlm.nih.gov/pmc/articles/PMC1904520/`.

[77] Xiong, Y., Dawson, V. L., and Dawson, T. M. LRRK2 GTPase Dysfunction in the Pathogenesis of Parkinson's disease. *Biochemical Society transactions*, 40(5): 1074–1079, 2012. ISSN 0300-5127 1470-8752. doi: 10.1042/BST20120093. URL `http://www.ncbi.nlm.nih.gov/pmc/articles/PMC3701022/`.

[78] Daniels, V., Vancraenenbroeck, R., Law, B. M., Greggio, E., Lobbestael, E., Gao, F., De Maeyer, M., Cookson, M. R., Harvey, K., Baekelandt, V., and Taymans, J. M. Insight into the mode of action of the LRRK2 Y1699C pathogenic mutant. *J Neurochem*, 116(2):304–15, 2011. ISSN 0022-3042. doi: 10.1111/j.1471-4159.2010. 07105.x.

[79] Li, Y., Liu, W., Oo, T. F., Wang, L., Tang, Y., Jackson-Lewis, V., Zhou, C., Geghman, K., Bogdanov, M., Przedborski, S., Beal, M. F., Burke, R. E., and Li, C. Mutant LRRK2(R1441G) BAC transgenic mice recapitulate cardinal features of Parkinson's disease. *Nature neuroscience*, 12(7):826–828, 2009. ISSN 1097-6256 1546-1726. doi: 10.1038/nn.2349. URL `http://www.ncbi.nlm.nih.gov/pmc/articles/PMC2845930/`.

[80] Ramonet, D., Daher, J. P. L., Lin, B. M., Stafa, K., Kim, J., Banerjee, R., Westerlund, M., Pletnikova, O., Glauser, L., Yang, L., Liu, Y., Swing, D. A., Beal, M. F., Troncoso, J. C., McCaffery, J. M., Jenkins, N. A., Copeland, N. G., Galter, D., Thomas, B., Lee, M. K., Dawson, T. M., Dawson, V. L., and Moore, D. J. Dopaminergic Neuronal Loss, Reduced Neurite Complexity and Autophagic Abnormalities in Transgenic Mice Expressing G2019S Mutant LRRK2. *PLOS ONE*, 6(4):e18568, 2011. doi: 10.1371/journal.pone.0018568. URL `http://dx.doi.org/10.1371%2Fjournal.pone.0018568`.

[81] Maekawa, T., Mori, S., Sasaki, Y., Miyajima, T., Azuma, S., Ohta, E., and Obata, F. The I2020T Leucine-rich repeat kinase 2 transgenic mouse exhibits impaired locomotive ability accompanied by dopaminergic neuron abnormalities. *Mol Neurodegener*, 7:15, 2012. ISSN 1750-1326. doi: 10.1186/1750-1326-7-15.

[82] Yue, M., Hinkle, K., Davies, P., Trushina, E., Fiesel, F., Christenson, T., Schroeder, A., Zhang, L., Bowles, E., Behrouz, B., Lincoln, S., Beevers, J.,

Milnerwood, A., Kurti, A., McLean, P. J., Fryer, J. D., Springer, W., Dickson, D., Farrer, M., and Melrose, H. Progressive dopaminergic alterations and mitochondrial abnormalities in LRRK2 G2019S knock in mice. *Neurobiology of disease*, 78:172–195, 06 2015. doi: 10.1016/j.nbd.2015.02.031. URL `http://www.ncbi.nlm.nih.gov/pmc/articles/PMC4526103/`.

[83] Tong, Y., Pisani, A., Martella, G., Karouani, M., Yamaguchi, H., Pothos, E. N., and Shen, J. R1441C mutation in LRRK2 impairs dopaminergic neurotransmission in mice. *Proc Natl Acad Sci U S A*, 106(34):14622–7, 2009. ISSN 0027-8424. doi: 10.1073/pnas.0906334106.

[84] Garcia-Miralles, M., Coomaraswamy, J., Häbig, K., Herzig, M. C., Funk, N., Gillardon, F., Maisel, M., Jucker, M., Gasser, T., Galter, D., and Biskup, S. No Dopamine Cell Loss or Changes in Cytoskeleton Function in Transgenic Mice Expressing Physiological Levels of Wild Type or G2019S Mutant LRRK2 and in Human Fibroblasts. *PLoS ONE*, 10(4):e0118947, 2015. ISSN 1932-6203. doi: 10.1371/journal.pone.0118947. URL `http://www.ncbi.nlm.nih.gov/pmc/articles/PMC4382199/`.

[85] Cookson, M. R. The role of leucine-rich repeat kinase 2 (LRRK2) in Parkinson's disease. *Nat Rev Neurosci*, 11(12):791–7, 2010. ISSN 1471-003x. doi: 10.1038/nrn2935.

[86] Lin, X., Parisiadou, L., Gu, X. L., Wang, L., Shim, H., Sun, L., Xie, C., Long, C. X., Yang, W. J., Ding, J., Chen, Z. Z., Gallant, P. E., Tao-Cheng, J. H., Rudow, G., Troncoso, J. C., Liu, Z., Li, Z., and Cai, H. Leucine-rich repeat kinase 2 regulates the progression of neuropathology Induced by Parkinson's disease-related Mutant α-synuclein. *Neuron*, 64(6):807–827, 2009. ISSN 0896-6273 1097-4199. doi: 10.1016/j.neuron.2009.11.006. URL `http://www.ncbi.nlm.nih.gov/pmc/articles/PMC2807409/`.

[87] Chen, C. Y., Weng, Y. H., Chien, K. Y., Lin, K. J., Yeh, T. H., Cheng, Y. P., Lu, C. S., and Wang, H. L. (G2019S) LRRK2 activates MKK4-JNK pathway and causes degeneration of SN dopaminergic neurons in a transgenic mouse model of PD. *Cell Death and Differentiation*, 19(10):1623–1633, 10 2012. doi: 10.1038/cdd.2012.42. URL `http://www.ncbi.nlm.nih.gov/pmc/articles/PMC3438494/`.

[88] Lee, B. D., Shin, J.-H., VanKampen, J., Petrucelli, L., West, A. B., Ko, H. S., Lee, Y., Maguire-Zeiss, K. A., Bowers, W. J., Federoff, H. J., Dawson, V. L., and Dawson, T. M. Inhibitors of Leucine Rich Repeat Kinase 2 (LRRK2) Protect Against LRRK2-Models of Parkinson's Disease. *Nature medicine*, 16(9):998–1000, 09 2010. doi: 10.1038/nm.2199. URL `http://www.ncbi.nlm.nih.gov/pmc/articles/PMC2935926/`.

[89] Dusonchet, J., Kochubey, O., Stafa, K., Young, S. M. J., Zufferey, R., Moore, D. J., Schneider, B. L., and Aebischer, P. A rat model of progressive nigral neurodegeneration induced by the Parkinson's disease-associated G2019S mutation in LRRK2. *J Neurosci*, 31(3):907–912, Jan 2011. ISSN 1529-2401 (Electronic); 0270-6474 (Linking). doi: 10.1523/JNEUROSCI.5092-10.2011.

[90] Tsika, E., Nguyen, A. P. T., Dusonchet, J., Colin, P., Schneider, B. L., and Moore, D. J. Adenoviral-mediated expression of G2019S LRRK2 induces striatal pathology

in a kinase-dependent manner in a rat model of Parkinson's disease. *Neurobiol Dis*, 77:49–61, May 2015. ISSN 1095-953X (Electronic); 0969-9961 (Linking). doi: 10.1016/j.nbd.2015.02.019.

[91] Longo, F., Russo, I., Shimshek, D. R., Greggio, E., and Morari, M. Genetic and pharmacological evidence that G2019S LRRK2 confers a hyperkinetic phenotype, resistant to motor decline associated with aging. *Neurobiology of Disease*, 71: 62–73, 11 2014. doi: http://doi.org/10.1016/j.nbd.2014.07.013. URL http://www.sciencedirect.com/science/article/pii/S0969996114002149.

[92] Funayama, M., Li, Y., Tomiyama, H., Yoshino, H., Imamichi, Y., Yamamoto, M., Murata, M., Toda, T., Mizuno, Y., and Hattori, N. Leucine-rich repeat kinase 2 G2385R variant is a risk factor for Parkinson disease in Asian population. *Neuroreport*, 18(3):273–5, 2007. ISSN 0959-4965 (Print) 0959-4965. doi: 10.1097/WNR.0b013e32801254b6.

[93] Di Fonzo, A., Wu-Chou, Y. H., Lu, C. S., van Doeselaar, M., Simons, E. J., Rohé, C. F., Chang, H. C., Chen, R.-S., Weng, Y. H., Vanacore, N., Breedveld, G. J., Oostra, B. A., and Bonifati, V. A common missense variant in the LRRK2 gene, Gly2385Arg, associated with Parkinson's disease risk in Taiwan. *Neurogenetics*, 7(3):133–138, 2006. ISSN 1364-6753. doi: 10.1007/s10048-006-0041-5. URL http://dx.doi.org/10.1007/s10048-006-0041-5.

[94] Rudenko, I. N., Kaganovich, A., Hauser, D. N., Beylina, A., Chia, R., Ding, J., Maric, D., Jaffe, H., and Cookson, M. R. The G2385R Variant of Leucine-Rich Repeat Kinase 2 Associated with Parkinson's Disease is a Partial Loss of Function Mutation. *The Biochemical journal*, 446(1):99–111, 2012. ISSN 0264-6021 1470-8728. doi: 10.1042/BJ20120637. URL http://www.ncbi.nlm.nih.gov/pmc/articles/PMC4667980/.

[95] Ho, D. H., Jang, J., Joe, E. H., Son, I., Seo, H., and Seol, W. G2385R and I2020T Mutations Increase LRRK2 GTPase Activity. *BioMed Research International*, 2016:7917128, 2016. doi: 10.1155/2016/7917128. URL http://www.ncbi.nlm.nih.gov/pmc/articles/PMC4897664/.

[96] Rudenko, I. N., Kaganovich, A., Langston, R. G., Beilina, A., Ndukwe, K., Kumaran, R., Dillman, A. A., Chia, R., and Cookson, M. R. The G2385R risk factor for Parkinson's disease enhances CHIP-dependent intracellular degradation of LRRK2. *Biochemical Journal*, 03 2017. URL http://www.biochemj.org/content/early/2017/03/20/BCJ20160909.abstract.

[97] Ohta, E., Kawakami, F., Kubo, M., and Obata, F. Dominant-negative effects of LRRK2 heterodimers: a possible mechanism of neurodegeneration in Parkinson's disease caused by LRRK2 I2020T mutation. *Biochem Biophys Res Commun*, 430 (2):560–6, 2013. ISSN 0006-291x. doi: 10.1016/j.bbrc.2012.11.113.

[98] Nichols, R. J., Dzamko, N., Morrice, N. A., Campbell, D. G., Deak, M., Ordureau, A., Macartney, T., Tong, Y., Shen, J., Prescott, A. R., and Alessi, D. R. 14-3-3 binding to LRRK2 is disrupted by multiple Parkinson's disease-associated mutations and regulates cytoplasmic localization. *Biochemical Journal*, 430(Pt 3): 393–404, 09 2010. doi: 10.1042/BJ20100483. URL http://www.ncbi.nlm.nih.gov/pmc/articles/PMC2932554/.

[99] Herzig, M. C., Kolly, C., Persohn, E., Theil, D., Schweizer, T., Hafner, T., Stemmelen, C., Troxler, T. J., Schmid, P., Danner, S., Schnell, C. R., Mueller, M., Kinzel, B., Grevot, A., Bolognani, F., Stirn, M., Kuhn, R. R., Kaupmann, K., van der Putten, P. H., Rovelli, G., and Shimshek, D. R. LRRK2 protein levels are determined by kinase function and are crucial for kidney and lung homeostasis in mice. *Human Molecular Genetics*, 20(21):4209–4223, 2011. ISSN 0964-6906 1460-2083. doi: 10.1093/hmg/ddr348. URL http://www.ncbi.nlm.nih.gov/pmc/articles/PMC3188995/.

[100] Baptista, M. A., Dave, K. D., Frasier, M. A., Sherer, T. B., Greeley, M., Beck, M. J., Varsho, J. S., Parker, G. A., Moore, C., Churchill, M. J., Meshul, C. K., and Fiske, B. K. Loss of leucine-rich repeat kinase 2 (LRRK2) in rats leads to progressive abnormal phenotypes in peripheral organs. *PLoS One*, 8(11):e80705, 2013. ISSN 1932-6203. doi: 10.1371/journal.pone.0080705.

[101] Tong, Y., Yamaguchi, H., Giaime, E., Boyle, S., Kopan, R., Kelleher, R. J., and Shen, J. Loss of leucine-rich repeat kinase 2 causes impairment of protein degradation pathways, accumulation of α-synuclein, and apoptotic cell death in aged mice. *Proceedings of the National Academy of Sciences of the United States of America*, 107(21):9879–9884, 05 2010. doi: 10.1073/pnas.1004676107. URL http://www.ncbi.nlm.nih.gov/pmc/articles/PMC2906862/.

[102] Hinkle, K. M., Yue, M., Behrouz, B., Dachsel, J. C., Lincoln, S. J., Bowles, E. E., Beevers, J. E., Dugger, B., Winner, B., Prots, I., Kent, C. B., Nishioka, K., Lin, W. L., Dickson, D. W., Janus, C. J., Farrer, M. J., and Melrose, H. L. LRRK2 knockout mice have an intact dopaminergic system but display alterations in exploratory and motor co-ordination behaviors. *Mol Neurodegener*, 7:25, 2012. ISSN 1750-1326. doi: 10.1186/1750-1326-7-25.

[103] Melrose, H. L., Dächsel, J. C., Behrouz, B., Lincoln, S. J., Yue, M., Hinkle, K. M., Kent, C. B., Korvatska, E., Taylor, J. P., Witten, L., Liang, Y. Q., Beevers, J. E., Boules, M., Dugger, B. N., Serna, V. A., Gaukhman, A., Yu, X., Castanedes-Casey, M., Braithwaite, A. T., Ogholikhan, S., Yu, N., Bass, D., Tyndall, G., Schellenberg, G. D., Dickson, D. W., Janus, C., and Farrer, M. J. Impaired dopaminergic neurotransmission and microtubule-associated protein tau alterations in human LRRK2 transgenic mice. *Neurobiology of Disease*, 40(3):503–517, 2010. ISSN 0969-9961. doi: http://dx.doi.org/10.1016/j.nbd.2010.07.010. URL http://www.sciencedirect.com/science/article/pii/S0969996110002342.

[104] Matta, S., Van Kolen, K., da Cunha, R., van den Bogaart, G., Mandemakers, W., Miskiewicz, K., De Bock, P. J., Morais, V. A., Vilain, S., Haddad, D., Delbroek, L., Swerts, J., Chávez-Gutiérrez, L., Esposito, G., Daneels, G., Karran, E., Holt, M., Gevaert, K., Moechars, D. W., De Strooper, B., and Verstreken, P. LRRK2 Controls an EndoA Phosphorylation Cycle in Synaptic Endocytosis. *Neuron*, 75 (6):1008–1021, 9 2012. doi: http://doi.org/10.1016/j.neuron.2012.08.022. URL http://www.sciencedirect.com/science/article/pii/S0896627312007593.

[105] Thévenet, J., Pescini Gobert, R., Hooft van Huijsduijnen, R., Wiessner, C., and Sagot, Y. J. Regulation of LRRK2 Expression Points to a Functional Role in Human Monocyte Maturation. *PLoS ONE*, 6(6):e21519, 2011. doi:

10.1371/journal.pone.0021519. URL http://www.ncbi.nlm.nih.gov/pmc/articles/PMC3124520/.

[106] Moehle, M. S., Webber, P. J., Tse, T., Sukar, N., Standaert, D. G., DeSilva, T. M., Cowell, R. M., and West, A. B. LRRK2 inhibition attenuates microglial inflammatory responses. *J Neurosci*, 32(5):1602–11, 2012. ISSN 0270-6474. doi: 10.1523/jneurosci.5601-11.2012.

[107] Rudenko, I. N., Chia, R., and Cookson, M. R. Is inhibition of kinase activity the only therapeutic strategy for LRRK2-associated Parkinson's disease? *BMC Medicine*, 10:20–20, 2012. doi: 10.1186/1741-7015-10-20. URL http://www.ncbi.nlm.nih.gov/pmc/articles/PMC3308210/.

[108] Tong, Y., Giaime, E., Yamaguchi, H., Ichimura, T., Liu, Y., Si, H., Cai, H., Bonventre, J. V., and Shen, J. Loss of leucine-rich repeat kinase 2 causes age-dependent bi-phasic alterations of the autophagy pathway. *Molecular Neurodegeneration*, 7: 2–2, 2012. doi: 10.1186/1750-1326-7-2. URL http://www.ncbi.nlm.nih.gov/pmc/articles/PMC3296570/.

[109] Parisiadou, L., Xie, C., Cho, H. J., Lin, X., Gu, X. L., Long, C. X., Lobbestael, E., Baekelandt, V., Taymans, J. M., Sun, L., and Cai, H. Phosphorylation of ERM Proteins by LRRK2 Promotes the Rearrangement of Actin Cytoskeleton in Neuronal Morphogenesis. *The Journal of neuroscience : the official journal of the Society for Neuroscience*, 29(44):13971–13980, 11 2009. doi: 10.1523/JNEUROSCI.3799-09.2009. URL http://www.ncbi.nlm.nih.gov/pmc/articles/PMC2807632/.

[110] Paus, M., Kohl, Z., Ben Abdallah, N. M., Galter, D., Gillardon, F., and Winkler, J. Enhanced dendritogenesis and axogenesis in hippocampal neuroblasts of LRRK2 knockout mice. *Brain Res*, 1497:85–100, 2013. ISSN 0006-8993. doi: 10.1016/j.brainres.2012.12.024.

[111] Andres-Mateos, E., Mejias, R., Sasaki, M., Li, X., Lin, B. M., Biskup, S., Zhang, L., Banerjee, R., Thomas, B., Yang, L., Liu, G., Beal, M. F., Huso, D. L., Dawson, T. M., and Dawson, V. L. Unexpected Lack of Hypersensitivity in LRRK2 Knockout Mice to 1-methyl-4-phenyl-1,2,3,6-tetrahydropyridine (MPTP). *The Journal of neuroscience : the official journal of the Society for Neuroscience*, 29(50):15846–15850, 2009. ISSN 0270-6474 1529-2401. doi: 10.1523/JNEUROSCI.4357-09.2009. URL http://www.ncbi.nlm.nih.gov/pmc/articles/PMC2846613/.

[112] Daher, J. P. L., Pletnikova, O., Biskup, S., Musso, A., Gellhaar, S., Galter, D., Troncoso, J. C., Lee, M. K., Dawson, T. M., Dawson, V. L., and Moore, D. J. Neurodegenerative phenotypes in an A53T α-synuclein transgenic mouse model are independent of LRRK2. *Human Molecular Genetics*, 21(11):2420–2431, 06 2012. doi: 10.1093/hmg/dds057. URL http://www.ncbi.nlm.nih.gov/pmc/articles/PMC3349422/.

[113] Xing, W., Liu, J., Cheng, S., Vogel, P., Mohan, S., and Brommage, R. Targeted disruption of leucine-rich repeat kinase 1 but not leucine-rich repeat kinase 2 in mice causes severe osteopetrosis. *J Bone Miner Res*, 28(9):1962–74, 2013. ISSN 0884-0431. doi: 10.1002/jbmr.1935.

[114] Ness, D., Ren, Z., Gardai, S., Sharpnack, D., Johnson, V. J., Brennan, R. J., Brigham, E. F., and Olaharski, A. J. Leucine-Rich Repeat Kinase 2 (LRRK2)-Deficient Rats Exhibit Renal Tubule Injury and Perturbations in Metabolic and Immunological Homeostasis. *PLoS ONE*, 8(6):e66164, 2013. doi: 10.1371/journal.pone.0066164. URL `http://www.ncbi.nlm.nih.gov/pmc/articles/PMC3682960/`.

[115] Boddu, R., Hull, T. D., Bolisetty, S., Hu, X., Moehle, M. S., Daher, J. P. L., Kamal, A. I., Joseph, R., George, J. F., Agarwal, A., Curtis, L. M., and West, A. B. Leucine-rich repeat kinase 2 deficiency is protective in rhabdomyolysis-induced kidney injury. *Human Molecular Genetics*, 24(14):4078–4093, 07 2015. doi: 10.1093/hmg/ddv147. URL `http://www.ncbi.nlm.nih.gov/pmc/articles/PMC4476452/`.

[116] Daher, J. P. L., Volpicelli-Daley, L. A., Blackburn, J. P., Moehle, M. S., and West, A. B. Abrogation of α-synuclein–mediated dopaminergic neurodegeneration in LRRK2-deficient rats. *Proceedings of the National Academy of Sciences of the United States of America*, 111(25):9289–9294, 2014. ISSN 0027-8424 1091-6490. doi: 10.1073/pnas.1403215111. URL `http://www.ncbi.nlm.nih.gov/pmc/articles/PMC4078806/`.

[117] Biskup, S., Moore, D. J., Rea, A., Lorenz-Deperieux, B., Coombes, C. E., Dawson, V. L., Dawson, T. M., and West, A. B. Dynamic and redundant regulation of LRRK2 and LRRK1 expression. *BMC Neuroscience*, 8:102–102, 2007. ISSN 1471-2202. doi: 10.1186/1471-2202-8-102. URL `http://www.ncbi.nlm.nih.gov/pmc/articles/PMC2233633/`.

[118] Davies, P., Hinkle, K. M., Sukar, N. N., Sepulveda, B., Mesias, R., Serrano, G., Alessi, D. R., Beach, T. G., Benson, D. L., White, C. L., Cowell, R. M., Das, S. S., West, A. B., and Melrose, H. L. Comprehensive characterization and optimization of anti-LRRK2 (leucine-rich repeat kinase 2) monoclonal antibodies. *Biochemical Journal*, 453(Pt 1):101–113, 07 2013. doi: 10.1042/BJ20121742. URL `http://www.ncbi.nlm.nih.gov/pmc/articles/PMC3682752/`.

[119] West, A. B., Cowell, R. M., Daher, J. P., Moehle, M. S., Hinkle, K. M., Melrose, H. L., Standaert, D. G., and Volpicelli-Daley, L. A. Differential LRRK2 Expression in the Cortex, Striatum, and Substantia Nigra in Transgenic and Nontransgenic Rodents. *The Journal of comparative neurology*, 522(11):2465–2480, 08 2014. doi: 10.1002/cne.23583. URL `http://www.ncbi.nlm.nih.gov/pmc/articles/PMC4076169/`.

[120] Atashrazm, F. and Dzamko, N. LRRK2 inhibitors and their potential in the treatment of Parkinson's disease: current perspectives. *Clinical Pharmacology : Advances and Applications*, 8:177–189, 2016. ISSN 1179-1438. doi: 10.2147/CPAA.S102191. URL `http://www.ncbi.nlm.nih.gov/pmc/articles/PMC5076802/`.

[121] Flinn, L., Bretaud, S., Lo, C., Ingham, P. W., and Bandmann, O. Zebrafish as a new animal model for movement disorders. *J Neurochem*, 106(5):1991–7, 2008. ISSN 0022-3042. doi: 10.1111/j.1471-4159.2008.05463.x.

[122] Panula, P., Chen, Y. C., Priyadarshini, M., Kudo, H., Semenova, S., Sundvik, M., and Sallinen, V. The comparative neuroanatomy and neurochemistry of zebrafish

CNS systems of relevance to human neuropsychiatric diseases. *Neurobiol Dis*, 40 (1):46–57, 2010. ISSN 0969-9961. doi: 10.1016/j.nbd.2010.05.010.

[123] Bandmann, O. and Burton, E. A. Genetic zebrafish models of neurodegenerative diseases. *Neurobiol Dis*, 40(1):58–65, Oct 2010. ISSN 1095-953X (Electronic); 0969-9961 (Linking). doi: 10.1016/j.nbd.2010.05.017.

[124] Kalueff, A. V., Gebhardt, M., Stewart, A. M., Cachat, J. M., Brimmer, M., Chawla, J. S., Craddock, C., Kyzar, E. J., Roth, A., Landsman, S., Gaikwad, S., Robinson, K., Baatrup, E., Tierney, K., Shamchuk, A., Norton, W., Miller, N., Nicolson, T., Braubach, O., Gilman, C. P., Pittman, J., Rosemberg, D. B., Gerlai, R., Echevarria, D., Lamb, E., Neuhauss, S. C., Weng, W., Bally-Cuif, L., and Schneider, H. Towards a Comprehensive Catalog of Zebrafish Behavior 1.0 and Beyond. *Zebrafish*, 10(1):70–86, 03 2013. doi: 10.1089/zeb.2012.0861. URL `http://www.ncbi.nlm.nih.gov/pmc/articles/PMC3629777/`.

[125] Kizil, C., Kaslin, J., Kroehne, V., and Brand, M. Adult neurogenesis and brain regeneration in zebrafish. *Dev Neurobiol*, 72(3):429–61, 2012. ISSN 1932-8451. doi: 10.1002/dneu.20918.

[126] Kroehne, V., Freudenreich, D., Hans, S., Kaslin, J., and Brand, M. Regeneration of the adult zebrafish brain from neurogenic radial glia-type progenitors. *Development*, 138(22):4831–41, 2011. ISSN 0950-1991. doi: 10.1242/dev.072587.

[127] Kaslin, J. and Panula, P. Comparative anatomy of the histaminergic and other aminergic systems in zebrafish (Danio rerio). *The Journal of Comparative Neurology*, 440(4):342–377, 2001. ISSN 1096-9861. doi: 10.1002/cne.1390. URL `http://dx.doi.org/10.1002/cne.1390`.

[128] Bretaud, S., Lee, S., and Guo, S. Sensitivity of zebrafish to environmental toxins implicated in Parkinson's disease. *Neurotoxicology and Teratology*, 26(6):857–864, 2004/12// 2004. doi: http://doi.org/10.1016/j.ntt.2004.06.014. URL `http://www.sciencedirect.com/science/article/pii/S0892036204000881`.

[129] Anichtchik, O. V., Kaslin, J., Peitsaro, N., Scheinin, M., and Panula, P. Neurochemical and behavioural changes in zebrafish Danio rerio after systemic administration of 6-hydroxydopamine and 1-methyl-4-phenyl-1,2,3,6-tetrahydropyridine. *Journal of Neurochemistry*, 88(2):443–453, 2004. ISSN 1471-4159. doi: 10.1111/j.1471-4159.2004.02190.x. URL `http://dx.doi.org/10.1111/j.1471-4159.2004.02190.x`.

[130] Bretaud, S., Allen, C., Ingham, P. W., and Bandmann, O. p53-dependent neuronal cell death in a DJ-1-deficient zebrafish model of Parkinson's disease. *Journal of Neurochemistry*, 100(6):1626–1635, 2007. ISSN 1471-4159. doi: 10.1111/j.1471-4159.2006.04291.x. URL `http://dx.doi.org/10.1111/j.1471-4159.2006.04291.x`.

[131] Flinn, L., Mortiboys, H., Volkmann, K., Köster, R. W., Ingham, P. W., and Bandmann, O. Complex I deficiency and dopaminergic neuronal cell loss in parkin-deficient zebrafish (Danio rerio). *Brain*, 132(6):1613–1623, 06 2009. URL `http://dx.doi.org/10.1093/brain/awp108`.

[132] Fett, M. E., Pilsl, A., Paquet, D., van Bebber, F., Haass, C., Tatzelt, J., Schmid, B., and Winklhofer, K. F. Parkin Is Protective against Proteotoxic Stress in a Transgenic Zebrafish Model. *PLoS ONE*, 5(7):e11783, 2010. doi: 10.1371/journal.pone. 0011783. URL `http://www.ncbi.nlm.nih.gov/pmc/articles/PMC2912770/`.

[133] Anichtchik, O., Diekmann, H., Fleming, A., Roach, A., Goldsmith, P., and Rubinsztein, D. C. Loss of PINK1 Function Affects Development and Results in Neurodegeneration in Zebrafish. *The Journal of Neuroscience*, 28(33):8199, 08 2008. URL `http://www.jneurosci.org/content/28/33/8199.abstract`.

[134] Priyadarshini, M., Orosco, L. A., and Panula, P. J. Oxidative Stress and Regulation of Pink1 in Zebrafish (Danio rerio). *PLoS ONE*, 8(11):e81851, 2013. doi: 10.1371/journal.pone.0081851. URL `http://www.ncbi.nlm.nih.gov/pmc/articles/PMC3850071/`.

[135] Flinn, L. J., Keatinge, M., Bretaud, S., Mortiboys, H., Matsui, H., De Felice, E., Woodroof, H. I., Brown, L., McTighe, A., Soellner, R., Allen, C. E., Heath, P. R., Milo, M., Muqit, M. M. K., Reichert, A. S., Köster, R. W., Ingham, P. W., and Bandmann, O. TigarB causes mitochondrial dysfunction and neuronal loss in PINK1 deficiency. *Annals of Neurology*, 74(6):837–847, 01 2014. doi: 10.1002/ana. 23999. URL `http://www.ncbi.nlm.nih.gov/pmc/articles/PMC4154126/`.

[136] Sheng, D., Qu, D., Kwok, K. H., Ng, S. S., Lim, A. Y., Aw, S. S., Lee, C. W., Sung, W. K., Tan, E. K., Lufkin, T., Jesuthasan, S., Sinnakaruppan, M., and Liu, J. Deletion of the WD40 domain of LRRK2 in Zebrafish causes Parkinsonism-like loss of neurons and locomotive defect. *PLoS Genet*, 6(4):e1000914, 2010. ISSN 1553-7404 (Electronic) 1553-7390 (Linking). doi: 10.1371/journal.pgen.1000914. URL `https://www.ncbi.nlm.nih.gov/pubmed/20421934`.

[137] Ren, G., Xin, S., Li, S., Zhong, H., and Lin, S. Disruption of LRRK2 does not cause specific loss of dopaminergic neurons in zebrafish. *PLoS One*, 6(6):e20630, 2011. ISSN 1932-6203 (Electronic) 1932-6203 (Linking). doi: 10.1371/journal. pone.0020630. URL `https://www.ncbi.nlm.nih.gov/pubmed/21698186`.

[138] Prabhudesai, S., Bensabeur, F. Z., Abdullah, R., Basak, I., Baez, S., Alves, G., Holtzman, N. G., Larsen, J. P., and Moller, S. G. LRRK2 knockdown in zebrafish causes developmental defects, neuronal loss, and synuclein aggregation. *J Neurosci Res*, 94(8):717–35, 2016. ISSN 1097-4547 (Electronic) 0360-4012 (Linking). doi: 10.1002/jnr.23754. URL `https://www.ncbi.nlm.nih.gov/pubmed/27265751`.

[139] Lopes da Fonseca, T., Correia, A., Hasselaar, W., van der Linde, H. C., Willemsen, R., and Outeiro, T. F. The zebrafish homologue of Parkinson's disease ATP13A2 is essential for embryonic survival. *Brain Res Bull*, 90:118–126, Jan 2013. ISSN 1873-2747 (Electronic); 0361-9230 (Linking). doi: 10.1016/j.brainresbull.2012.09.017.

[140] Bento, C. F., Ashkenazi, A., Jimenez-Sanchez, M., and Rubinsztein, D. C. The Parkinson's disease-associated genes ATP13A2 and SYT11 regulate autophagy via a common pathway. *Nature Communications*, 7:11803, 2016. doi: 10.1038/ncomms11803. URL `http://www.ncbi.nlm.nih.gov/pmc/articles/PMC4906231/`.

[141] Zancan, I., Bellesso, S., Costa, R., Salvalaio, M., Stroppiano, M., Hammond, C., Argenton, F., Filocamo, M., and Moro, E. Glucocerebrosidase deficiency in zebrafish affects primary bone ossification through increased oxidative stress and reduced Wnt/β-catenin signaling. *Human Molecular Genetics*, 24(5):1280–1294, 03 2015. URL http://dx.doi.org/10.1093/hmg/ddu538.

[142] Keatinge, M., Bui, H., Menke, A., Chen, Y. C., Sokol, A. M., Bai, Q., Ellett, F., Da Costa, M., Burke, D., Gegg, M., Trollope, L., Payne, T., McTighe, A., Mortiboys, H., de Jager, S., Nuthall, H., Kuo, M. S., Fleming, A., Schapira, A. H., Renshaw, S. A., Highley, J. R., Chacinska, A., Panula, P., Burton, E. A., O'Neill, M. J., and Bandmann, O. Glucocerebrosidase 1 deficient Danio rerio mirror key pathological aspects of human Gaucher disease and provide evidence of early microglial activation preceding alpha-synuclein-independent neuronal cell death. *Hum Mol Genet*, 24(23):6640–52, 2015. ISSN 0964-6906. doi: 10.1093/hmg/ddv369.

[143] Milanese, C., Sager, J. J., Bai, Q., Farrell, T. C., Cannon, J. R., Greenamyre, J. T., and Burton, E. A. Hypokinesia and Reduced Dopamine Levels in Zebrafish Lacking β- and γ1-Synucleins. *The Journal of Biological Chemistry*, 287(5):2971–2983, 01 2012. doi: 10.1074/jbc.M111.308312. URL http://www.ncbi.nlm.nih.gov/pmc/articles/PMC3270954/.

[144] Sallinen, V., Torkko, V., Sundvik, M., Reenila, I., Khrustalyov, D., Kaslin, J., and Panula, P. MPTP and MPP$^+$ target specific aminergic cell populations in larval zebrafish. *J Neurochem*, 108(3):719–31, 2009. ISSN 0022-3042. doi: 10.1111/j.1471-4159.2008.05793.x.

[145] Ren, G., Li, S., Zhong, H., and Lin, S. Zebrafish Tyrosine Hydroxylase 2 Gene Encodes Tryptophan Hydroxylase. *The Journal of Biological Chemistry*, 288(31): 22451–22459, 08 2013. doi: 10.1074/jbc.M113.485227. URL http://www.ncbi.nlm.nih.gov/pmc/articles/PMC3829334/.

[146] McPherson, A. D., Barrios, J. P., Luks-Morgan, S. J., Manfredi, J. P., Bonkowsky, J. L., Douglass, A. D., and Dorsky, R. I. Motor Behavior Mediated by Continuously Generated Dopaminergic Neurons in the Zebrafish Hypothalamus Recovers After Cell Ablation. *Current biology : CB*, 26(2):263–269, 01 2016. doi: 10.1016/j.cub.2015.11.064. URL http://www.ncbi.nlm.nih.gov/pmc/articles/PMC4864152/.

[147] Semenova, S. A., Chen, Y. C., Zhao, X., Rauvala, H., and Panula, P. The tyrosine hydroxylase 2 (TH2) system in zebrafish brain and stress activation of hypothalamic cells. *Histochem Cell Biol*, 142(6):619–33, 2014. ISSN 0948-6143. doi: 10.1007/s00418-014-1240-z.

[148] Candy, J. and Collet, C. Two tyrosine hydroxylase genes in teleosts. *Biochim Biophys Acta*, 1727(1):35–44, 2005. ISSN 0006-3002 (Print) 0006-3002. doi: 10.1016/j.bbaexp.2004.11.005.

[149] Chen, Y. C., Priyadarshini, M., and Panula, P. Complementary developmental expression of the two tyrosine hydroxylase transcripts in zebrafish. *Histochem Cell Biol*, 132(4):375–81, 2009. ISSN 0948-6143. doi: 10.1007/s00418-009-0619-8.

[150] Filippi, A., Mahler, J., Schweitzer, J., and Driever, W. Expression of the paralogous tyrosine hydroxylase encoding genes *th1* and *th2* reveals the full complement of

dopaminergic and noradrenergic neurons in zebrafish larval and juvenile brain. *J Comp Neurol*, 518(4):423–38, 2010. ISSN 0021-9967. doi: 10.1002/cne.22213.

[151] Yamamoto, K., Ruuskanen, J. O., Wullimann, M. F., and Vernier, P. Two tyrosine hydroxylase genes in vertebrates: New dopaminergic territories revealed in the zebrafish brain. *Mol Cell Neurosci*, 43(4):394–402, 2010. ISSN 1044-7431. doi: 10.1016/j.mcn.2010.01.006.

[152] Riederer, P. and Laux, G. MAO-inhibitors in Parkinson's Disease. *Experimental Neurobiology*, 20(1):1–17, 2011. ISSN 1226-2560 2093-8144. doi: 10.5607/en.2011. 20.1.1. URL `http://www.ncbi.nlm.nih.gov/pmc/articles/PMC3213739/`.

[153] Waters, C. Catechol-O-Methyltransferase (COMT) Inhibitors in Parkinson's Disease. *Journal of the American Geriatrics Society*, 48(6):692–698, 2000. ISSN 1532-5415. doi: 10.1111/j.1532-5415.2000.tb04732.x. URL `http://dx.doi.org/10.1111/j.1532-5415.2000.tb04732.x`.

[154] Anichtchik, O., Sallinen, V., Peitsaro, N., and Panula, P. Distinct structure and activity of monoamine oxidase in the brain of zebrafish (Danio rerio). *J Comp Neurol*, 498(5):593–610, 2006. ISSN 0021-9967 (Print) 0021-9967. doi: 10.1002/cne.21057.

[155] Alazizi, A., Liu, M. Y., Williams, F. E., Kurogi, K., Sakakibara, Y., Suiko, M., and Liu, M. C. Identification, Characterization, and Ontogenic Study of a Catechol O-methyltransferase from Zebrafish. *Aquatic toxicology (Amsterdam, Netherlands)*, 102(1-2):18–23, 03 2011. doi: 10.1016/j.aquatox.2010.12.016. URL `http://www.ncbi.nlm.nih.gov/pmc/articles/PMC3515678/`.

[156] Jeffery, D. R. and Roth, J. A. Characterization of Membrane-Bound and Soluble Catechol-O-Methyltransferase from Human Frontal Cortex. *Journal of Neurochemistry*, 42(3):826–832, 1984. ISSN 1471-4159. doi: 10.1111/j.1471-4159.1984. tb02755.x. URL `http://dx.doi.org/10.1111/j.1471-4159.1984.tb02755.x`.

[157] Setini, A., Pierucci, F., Senatori, O., and Nicotra, A. Molecular characterization of monoamine oxidase in zebrafish (Danio rerio). *Comparative Biochemistry and Physiology Part B: Biochemistry and Molecular Biology*, 140(1):153–161, 1 2005. doi: https://doi.org/10.1016/j.cbpc.2004.10.002. URL `http://www.sciencedirect.com/science/article/pii/S1096495904003124`.

[158] Schildknecht, S., Pape, R., Meiser, J., Karreman, C., Strittmatter, T., Odermatt, M., Cirri, E., Friemel, A., Ringwald, M., Pasquarelli, N., Ferger, B., Brunner, T., Marx, A., Möller, H. M., Hiller, K., and Leist, M. Preferential Extracellular Generation of the Active Parkinsonian Toxin MPP(+) by Transporter-Independent Export of the Intermediate MPDP(+). *Antioxidants & Redox Signaling*, 23(13): 1001–1016, 11 2015. doi: 10.1089/ars.2015.6297. URL `http://www.ncbi.nlm.nih.gov/pmc/articles/PMC4649766/`.

[159] Pavlidis, M., Sundvik, M., Chen, Y. C., and Panula, P. Adaptive changes in zebrafish brain in dominant–subordinate behavioral context. *Behavioural Brain Research*, 225(2):529–537, 12 2011. doi: https://doi.org/10.1016/j.bbr. 2011.08.022. URL `http://www.sciencedirect.com/science/article/pii/S0166432811006140`.

[160] Sallinen, V., Sundvik, M., Reenila, I., Peitsaro, N., Khrustalyov, D., Anichtchik, O., Toleikyte, G., Kaslin, J., and Panula, P. Hyperserotonergic phenotype after monoamine oxidase inhibition in larval zebrafish. *J Neurochem*, 109(2):403–15, 2009. ISSN 0022-3042. doi: 10.1111/j.1471-4159.2009.05986.x.

[161] Nicotra, A., Pierucci, F., Parvez, H., and Senatori, O. Monoamine Oxidase Expression During Development and Aging. *NeuroToxicology*, 25(1–2):155–165, 1 2004. doi: https://doi.org/10.1016/S0161-813X(03)00095-0. URL `http://www.sciencedirect.com/science/article/pii/S0161813X03000950`.

[162] Kumar, M. J. and Andersen, J. K. Perspectives on MAO-B in aging and neurological disease. *Molecular Neurobiology*, 30(1):77–89, 2004. doi: 10.1385/MN:30:1:077. URL `http://dx.doi.org/10.1385/MN:30:1:077`.

[163] Kok, F. O., Shin, M., Ni, C.-W., Gupta, A., Grosse, A. S., van Impel, A., Kirchmaier, B. C., Peterson-Maduro, J., Kourkoulis, G., Male, I., DeSantis, D. F., Sheppard-Tindell, S., Ebarasi, L., Betsholtz, C., Schulte-Merker, S., Wolfe, S. A., and Lawson, N. D. Reverse Genetic Screening Reveals Poor Correlation between Morpholino-Induced and Mutant Phenotypes in Zebrafish. *Developmental Cell*, 32(1):97–108, 2015. ISSN 1534-5807. doi: http://dx.doi.org/10.1016/j.devcel.2014.11.018. URL `http://www.sciencedirect.com/science/article/pii/S1534580714007357`.

[164] Gerety, S. S. and Wilkinson, D. G. Morpholino artifacts provide pitfalls and reveal a novel role for pro-apoptotic genes in hindbrain boundary development. *Developmental Biology*, 350(2):279–289, 2011. ISSN 0012-1606 1095-564X. doi: 10.1016/j.ydbio.2010.11.030. URL `http://www.ncbi.nlm.nih.gov/pmc/articles/PMC3111810/`.

[165] Bedell, V. M., Westcot, S. E., and Ekker, S. C. Lessons from morpholino-based screening in zebrafish. *Briefings in Functional Genomics*, 10(4):181–188, 2011. ISSN 2041-2649 2041-2657. doi: 10.1093/bfgp/elr021. URL `http://www.ncbi.nlm.nih.gov/pmc/articles/PMC3144740/`.

[166] Place, E. S. and Smith, J. C. Zebrafish *atoh8* mutants do not recapitulate morpholino phenotypes. *PLoS One*, 12(2):e0171143, 2017. ISSN 1932-6203. doi: 10.1371/journal.pone.0171143.

[167] Rossi, A., Kontarakis, Z., Gerri, C., Nolte, H., Holper, S., Kruger, M., and Stainier, D. Y. R. Genetic compensation induced by deleterious mutations but not gene knockdowns. *Nature*, 524(7564):230–233, 2015. ISSN 0028-0836. doi: 10.1038/nature14580http://www.nature.com/nature/journal/v524/n7564/abs/nature14580.html#supplementary-information. URL `http://dx.doi.org/10.1038/nature14580`.

[168] Ahrendt, R. T. *The Lrrk2-deficient Zebrafish Model for Parkinson's Disease - A combination of impaired proliferation and continuous loss of dopaminergic neurons.* PhD thesis, Dresden, Technische Universität, 2011.

[169] Winkler, S., Gscheidel, N., and Brand, M. Mutant generation in vertebrate model organisms by TILLING. *Methods Mol Biol*, 770:475–504, 2011. ISSN 1064-3745. doi: 10.1007/978-1-61779-210-6_19.

[170] den Dunnen, J. T., Dalgleish, R., Maglott, D. R., Hart, R. K., Greenblatt, M. S., McGowan-Jordan, J., Roux, A. F., Smith, T., Antonarakis, S. E., Taschner, P. E. M., on behalf of the Human Genome Variation Society, t. H. V. P., and the Human Genome, O. HGVS Recommendations for the Description of Sequence Variants: 2016 Update. *Human Mutation*, 37(6):564–569, 2016. ISSN 1098-1004. doi: 10.1002/humu.22981. URL `http://dx.doi.org/10.1002/humu.22981`.

[171] Chen, S., Owens, G. C., Makarenkova, H., and Edelman, D. B. HDAC6 Regulates Mitochondrial Transport in Hippocampal Neurons. *PLoS ONE*, 5(5):e10848, 2010. doi: 10.1371/journal.pone.0010848. URL `http://www.ncbi.nlm.nih.gov/pmc/articles/PMC2877100/`.

[172] Grandel, H., Kaslin, J., Ganz, J., Wenzel, I., and Brand, M. Neural stem cells and neurogenesis in the adult zebrafish brain: origin, proliferation dynamics, migration and cell fate. *Dev Biol*, 295(1):263–77, 2006. ISSN 0012-1606 (Print) 0012-1606. doi: 10.1016/j.ydbio.2006.03.040.

[173] Munzel, E. J., Schaefer, K., Obirei, B., Kremmer, E., Burton, E. A., Kuscha, V., Becker, C. G., Brosamle, C., Williams, A., and Becker, T. Claudin k is specifically expressed in cells that form myelin during development of the nervous system and regeneration of the optic nerve in adult zebrafish. *Glia*, 60(2):253–70, 2012. ISSN 0894-1491. doi: 10.1002/glia.21260.

[174] Redd, M. J., Kelly, G., Dunn, G., Way, M., and Martin, P. Imaging macrophage chemotaxis in vivo: studies of microtubule function in zebrafish wound inflammation. *Cell Motil Cytoskeleton*, 63(7):415–22, 2006. ISSN 0886-1544 (Print) 0886-1544. doi: 10.1002/cm.20133.

[175] Untergasser, A., Cutcutache, I., Koressaar, T., Ye, J., Faircloth, B. C., Remm, M., and Rozen, S. G. Primer3—new capabilities and interfaces. *Nucleic Acids Research*, 40(15):e115–e115, 08 2012. doi: 10.1093/nar/gks596. URL `http://www.ncbi.nlm.nih.gov/pmc/articles/PMC3424584/`.

[176] Koressaar, T. and Remm, M. Enhancements and modifications of primer design program Primer3. *Bioinformatics*, 23(10):1289, 2007. doi: 10.1093/bioinformatics/btm091. URL `+http://dx.doi.org/10.1093/bioinformatics/btm091`.

[177] Kyritsis, N., Kizil, C., Zocher, S., Kroehne, V., Kaslin, J., Freudenreich, D., Iltzsche, A., and Brand, M. Acute inflammation initiates the regenerative response in the adult zebrafish brain. *Science*, 338(6112):1353–6, 2012. ISSN 0036-8075. doi: 10.1126/science.1228773.

[178] Sambrook, J. and Russell, D. W. *Molecular Cloning: A Laboratory Manual*. New York, USA, 2001.

[179] Brand, M., Granato, M., and Nüsslein-Volhard, C. Keeping and raising zebrafish. In *Zebrafish: A Practical Approach*. Oxford University Press, Oxford, UK, 2002.

[180] Kimmel, C. B., Ballard, W. W., Kimmel, S. R., Ullmann, B., and Schilling, T. F. Stages of embryonic development of the zebrafish. *Developmental Dynamics*, 203 (3):253–310, 1995. ISSN 1097-0177. doi: 10.1002/aja.1002030302. URL `http://dx.doi.org/10.1002/aja.1002030302`.

[181] Koide, T., Miyasaka, N., Morimoto, K., Asakawa, K., Urasaki, A., Kawakami, K., and Yoshihara, Y. Olfactory neural circuitry for attraction to amino acids revealed by transposon-mediated gene trap approach in zebrafish. *Proceedings of the National Academy of Sciences*, 106(24):9884–9889, 2009. doi: 10.1073/pnas. 0900470106. URL `http://www.pnas.org/content/106/24/9884.abstract`.

[182] Susaki, E. A., Tainaka, K., Perrin, D., Yukinaga, H., Kuno, A., and Ueda, H. R. Advanced CUBIC protocols for whole-brain and whole-body clearing and imaging. *Nat. Protocols*, 10(11):1709–1727, 2015. ISSN 1754-2189. doi: 10.1038/nprot.2015.085http://www.nature.com/nprot/journal/v10/n11/abs/nprot.2015.085.html-supplementary-information. URL `http://dx.doi.org/10.1038/nprot.2015.085`.

[183] Livak, K. J. and Schmittgen, T. D. Analysis of relative gene expression data using real-time quantitative PCR and the 2(-Delta Delta C(T)) Method. *Methods*, 25 (4):402–8, 2001. ISSN 1046-2023 (Print) 1046-2023. doi: 10.1006/meth.2001.1262.

[184] Sievers, F., Wilm, A., Dineen, D., Gibson, T. J., Karplus, K., Li, W., Lopez, R., McWilliam, H., Remmert, M., Söding, J., Thompson, J. D., and Higgins, D. G. Fast, scalable generation of highâquality protein multiple sequence alignments using Clustal Omega. *Molecular Systems Biology*, 7(1), 2011. doi: 10.1038/msb.2011.75.

[185] Altschul, S. F., Gish, W., Miller, W., Myers, E. W., and Lipman, D. J. Basic local alignment search tool. *J Mol Biol*, 215(3):403–10, 1990. ISSN 0022-2836 (Print) 0022-2836. doi: 10.1016/s0022-2836(05)80360-2.

[186] Schindelin, J., Arganda-Carreras, I., Frise, E., Kaynig, V., Longair, M., Pietzsch, T., Preibisch, S., Rueden, C., Saalfeld, S., Schmid, B., Tinevez, J. Y., White, D. J., Hartenstein, V., Eliceiri, K., Tomancak, P., and Cardona, A. Fiji: an open-source platform for biological-image analysis. *Nat Methods*, 9(7):676–82, 2012. ISSN 1548-7091. doi: 10.1038/nmeth.2019.

[187] Ollion, J., Cochennec, J., Loll, F., Escude, C., and Boudier, T. TANGO: a generic tool for high-throughput 3D image analysis for studying nuclear organization. *Bioinformatics*, 29(14):1840–1, 2013. ISSN 1367-4803. doi: 10.1093/bioinformatics/btt276.

[188] Arganda-Carreras, I., Fernandez-Gonzalez, R., Munoz-Barrutia, A., and Ortiz-De-Solorzano, C. 3D reconstruction of histological sections: Application to mammary gland tissue. *Microsc Res Tech*, 73(11):1019–29, 2010. ISSN 1059-910x. doi: 10.1002/jemt.20829.

[189] Team, R. D. C. R: A Language and Environment for Statistical Computing. Vienna, Austria, R Foundation for Statistical Computing., 2015. URL `https://www.R-project.org/`.

[190] Rossiter, D. G. and Loza, A. *Technical Note: Analyzing land cover change with logistic regression in R*. Version 2.4 edition, 2016.

[191] Kelemen, O., Convertini, P., Zhang, Z., Wen, Y., Shen, M., Falaleeva, M., and Stamm, S. Function of alternative splicing. *Gene*, 514(1):1–30, 2 2013. doi:

https://doi.org/10.1016/j.gene.2012.07.083. URL `http://www.sciencedirect.com/science/article/pii/S0378111912009791`.

[192] Spada, F., Haemmer, A., Kuch, D., Rothbauer, U., Schermelleh, L., Kremmer, E., Carell, T., Längst, G., and Leonhardt, H. DNMT1 but not its interaction with the replication machinery is required for maintenance of DNA methylation in human cells. *The Journal of Cell Biology*, 176(5):565–571, 02 2007. doi: 10.1083/jcb.200610062. URL `http://www.ncbi.nlm.nih.gov/pmc/articles/PMC2064015/`.

[193] Egger, G., Jeong, S., Escobar, S. G., Cortez, C. C., Li, T. W. H., Saito, Y., Yoo, C. B., Jones, P. A., and Liang, G. Identification of DNMT1 (DNA methyltransferase 1) hypomorphs in somatic knockouts suggests an essential role for DNMT1 in cell survival. *Proceedings of the National Academy of Sciences of the United States of America*, 103(38):14080–14085, 09 2006. doi: 10.1073/pnas.0604602103. URL `http://www.ncbi.nlm.nih.gov/pmc/articles/PMC1599915/`.

[194] Trabzuni, D., Ryten, M., Emmett, W., Ramasamy, A., Lackner, K. J., Zeller, T., Walker, R., Smith, C., Lewis, P. A., Mamais, A., de Silva, R., Vandrovcova, J., (IP-DGC), I. P. D. G. C., Hernandez, D., Nalls, M. A., Sharma, M., Garnier, S., Lesage, S., Simon-Sanchez, J., Gasser, T., Heutink, P., Brice, A., Singleton, A., Cai, H., Schadt, E., Wood, N. W., Bandopadhyay, R., Weale, M. E., Hardy, J., and Plagnol, V. Fine-Mapping, Gene Expression and Splicing Analysis of the Disease Associated LRRK2 Locus. *PLoS ONE*, 8(8):e70724, 2013. doi: 10.1371/journal.pone.0070724. URL `http://www.ncbi.nlm.nih.gov/pmc/articles/PMC3742662/`.

[195] Van Damme, P., Gawron, D., Van Criekinge, W., and Menschaert, G. N-terminal Proteomics and Ribosome Profiling Provide a Comprehensive View of the Alternative Translation Initiation Landscape in Mice and Men. *Molecular & Cellular Proteomics : MCP*, 13(5):1245–1261, 05 2014. doi: 10.1074/mcp.M113.036442. URL `http://www.ncbi.nlm.nih.gov/pmc/articles/PMC4014282/`.

[196] Stump, M. R., Gong, Q., Packer, J. D., and Zhou, Z. Early LQT2 nonsense mutation generates N-terminally truncated hERG channels with altered gating properties by the reinitiation of translation. *J Mol Cell Cardiol*, 53(5):725–733, Nov 2012. ISSN 1095-8584 (Electronic); 0022-2828 (Linking). doi: 10.1016/j.yjmcc.2012.08.021.

[197] Neu-Yilik, G., Amthor, B., Gehring, N. H., Bahri, S., Paidassi, H., Hentze, M. W., and Kulozik, A. E. Mechanism of escape from nonsense-mediated mRNA decay of human β-globin transcripts with nonsense mutations in the first exon. *RNA*, 17(5):843–854, 05 2011. doi: 10.1261/rna.2401811. URL `http://www.ncbi.nlm.nih.gov/pmc/articles/PMC3078734/`.

[198] Rinne, T., Clements, S. E., Lamme, E., Duijf, P. H. G., Bolat, E., Meijer, R., Scheffer, H., Rosser, E., Tan, T. Y., McGrath, J. A., Schalkwijk, J., Brunner, H. G., Zhou, H., and van Bokhoven, H. A novel translation re-initiation mechanism for the p63 gene revealed by amino-terminal truncating mutations in Rapp-Hodgkin/Hay-Wells-like syndromes. *Human Molecular Genetics*, 17(13):1968–1977, 07 2008. URL `http://dx.doi.org/10.1093/hmg/ddn094`.

[199] Hamid, R., Hedges, L., Austin, E., Phillips, J., Loyd, J., and Cogan, J. Transcripts from a novel BMPR2 termination mutation escape nonsense mediated decay by

downstream translation re-initiation: implications for treating pulmonary hypertension. *Clinical genetics*, 77(3):280–286, 03 2010. doi: 10.1111/j.1399-0004.2009. 01311.x. URL `http://www.ncbi.nlm.nih.gov/pmc/articles/PMC3741656/`.

[200] Paulsen, M., Lund, C., Akram, Z., Winther, J. R., Horn, N., and Møller, L. B. Evidence That Translation Reinitiation Leads to a Partially Functional Menkes Protein Containing Two Copper-Binding Sites. *American Journal of Human Genetics*, 79(2):214–229, 08 2006. URL `http://www.ncbi.nlm.nih.gov/pmc/articles/PMC1559486/`.

[201] Nishikawa, T., Ota, T., and Isogai, T. Prediction whether a human cDNA sequence contains initiation codon by combining statistical information and similarity with protein sequences. *Bioinformatics*, 16(11):960–967, Nov 2000. ISSN 1367-4803 (Print); 1367-4803 (Linking).

[202] Pandey, N., Fahey, M. T., Jong, Y. J. I., and O'Malley, K. L. Sequences Located within the N-Terminus of the PD-Linked LRRK2 Lead to Increased Aggregation and Attenuation of 6-Hydroxydopamine-Induced Cell Death. *PLoS ONE*, 7(9): e45149, 2012. doi: 10.1371/journal.pone.0045149. URL `http://www.ncbi.nlm.nih.gov/pmc/articles/PMC3441673/`.

[203] Zimprich, A., Biskup, S., Leitner, P., Lichtner, P., Farrer, M., Lincoln, S., Kachergus, J., Hulihan, M., Uitti, R. J., Calne, D. B., Stoessl, A. J., Pfeiffer, R. F., Patenge, N., Carbajal, I. C., Vieregge, P., Asmus, F., Muller-Myhsok, B., Dickson, D. W., Meitinger, T., Strom, T. M., Wszolek, Z. K., and Gasser, T. Mutations in LRRK2 cause autosomal-dominant parkinsonism with pleomorphic pathology. *Neuron*, 44(4):601–7, 2004. ISSN 0896-6273 (Print) 0896-6273. doi: 10.1016/j.neuron.2004.11.005.

[204] Chen, W. W., Zhang, X., and Huang, W. J. Role of neuroinflammation in neurodegenerative diseases (Review). *Mol Med Rep*, 13(4):3391–6, 2016. ISSN 1791-2997. doi: 10.3892/mmr.2016.4948.

[205] Pradhan, S. and Andreasson, K. Commentary: Progressive inflammation as a contributing factor to early development of Parkinson's disease. *Experimental Neurology*, 241:148–155, 3 2013. doi: https://doi.org/10.1016/j.expneurol. 2012.12.008. URL `http://www.sciencedirect.com/science/article/pii/S0014488612004566`.

[206] Schapansky, J., Nardozzi, J. D., and LaVoie, M. J. The complex relationships between microglia, alpha-synuclein, and LRRK2 in Parkinson's disease. *Neuroscience*, 302:74–88, 2015. ISSN 0306-4522. doi: 10.1016/j.neuroscience.2014.09.049.

[207] Russo, I., Bubacco, L., and Greggio, E. LRRK2 and neuroinflammation: partners in crime in Parkinson's disease? *J Neuroinflammation*, 11:52, 2014. ISSN 1742-2094. doi: 10.1186/1742-2094-11-52.

[208] Karperien, A., Ahammer, H., and Jelinek, H. F. Quantitating the subtleties of microglial morphology with fractal analysis. *Front Cell Neurosci*, 7:3, 2013. ISSN 1662-5102. doi: 10.3389/fncel.2013.00003.

[209] Stanley, P. L., Steiner, S., Havens, M., and Tramposch, K. M. Mouse skin inflammation induced by multiple topical applications of 12-O-tetradecanoylphorbol-13-acetate. *Skin Pharmacol*, 4(4):262–271, 1991. ISSN 1011-0283 (Print); 1011-0283 (Linking).

[210] Marxreiter, F., Regensburger, M., and Winkler, J. Adult neurogenesis in Parkinson's disease. *Cell Mol Life Sci*, 70(3):459–73, 2013. ISSN 1420-682x. doi: 10.1007/s00018-012-1062-x.

[211] Berwick, D. C. and Harvey, K. LRRK2: an eminence grise of Wnt-mediated neurogenesis? *Front Cell Neurosci*, 7:82, 2013. ISSN 1662-5102. doi: 10.3389/fncel.2013.00082.

[212] Shepard, J. L., Amatruda, J. F., Stern, H. M., Subramanian, A., Finkelstein, D., Ziai, J., Finley, K. R., Pfaff, K. L., Hersey, C., Zhou, Y., Barut, B., Freedman, M., Lee, C., Spitsbergen, J., Neuberg, D., Weber, G., Golub, T. R., Glickman, J. N., Kutok, J. L., Aster, J. C., and Zon, L. I. A zebrafish bmyb mutation causes genome instability and increased cancer susceptibility. *Proc Natl Acad Sci U S A*, 102(37): 13194–9, 2005. ISSN 0027-8424 (Print) 0027-8424. doi: 10.1073/pnas.0506583102.

[213] Milosevic, J., Schwarz, S. C., Ogunlade, V., Meyer, A. K., Storch, A., and Schwarz, J. Emerging role of LRRK2 in human neural progenitor cell cycle progression, survival and differentiation. *Mol Neurodegener*, 4:25, 2009. ISSN 1750-1326. doi: 10.1186/1750-1326-4-25.

[214] Kaslin, J., Kroehne, V., Ganz, J., Hans, S., and Brand, M. Distinct roles of neuroepithelial-like and radial glia-like progenitor cells in cerebellar regeneration. *Development*, 2017. ISSN 0950-1991. doi: 10.1242/dev.144907.

[215] Chen, H., Zhao, E. J., Zhang, W., Lu, Y., Liu, R., Huang, X., Ciesielski-Jones, A. J., Justice, M. A., Cousins, D. S., and Peddada, S. Meta-analyses on prevalence of selected Parkinson's nonmotor symptoms before and after diagnosis. *Translational Neurodegeneration*, 4(1):1, 2015. ISSN 2047-9158. doi: 10.1186/2047-9158-4-1. URL `http://www.ncbi.nlm.nih.gov/pmc/articles/PMC4322463/`.

[216] Schnörr, S. J., Steenbergen, P. J., Richardson, M. K., and Champagne, D. L. Measuring thigmotaxis in larval zebrafish. *Behavioural Brain Research*, 228(2):367–374, 2012. ISSN 0166-4328. doi: http://dx.doi.org/10.1016/j.bbr.2011.12.016. URL `http://www.sciencedirect.com/science/article/pii/S0166432811008758`.

[217] Blaser, R. E., Chadwick, L., and McGinnis, G. C. Behavioral measures of anxiety in zebrafish (Danio rerio). *Behavioural Brain Research*, 208(1):56–62, 2010. ISSN 0166-4328. doi: http://dx.doi.org/10.1016/j.bbr.2009.11.009. URL `http://www.sciencedirect.com/science/article/pii/S0166432809006743`.

[218] Friedberg, I., Nika, K., Tautz, L., Saito, K., Cerignoli, F., Friedberg, I., Godzik, A., and Mustelin, T. Identification and characterization of DUSP27, a novel dual-specific protein phosphatase. *FEBS Letters*, 581(13):2527–2533, 2007. ISSN 1873-3468. doi: 10.1016/j.febslet.2007.04.059. URL `http://dx.doi.org/10.1016/j.febslet.2007.04.059`.

[219] Sangeeta Devi, Y. and Halperin, J. Reproductive actions of prolactin mediated through short and long receptor isoforms. *Molecular and Cellular Endocrinology*, 382(1):400–410, 1 2014. doi: https://doi.org/10.1016/j.mce.2013.09.016. URL `http://www.sciencedirect.com/science/article/pii/S0303720713004073`.

[220] Devi, Y. S., Seibold, A. M., Shehu, A., Maizels, E., Halperin, J., Le, J., Binart, N., Bao, L., and Gibori, G. Inhibition of MAPK by Prolactin Signaling through the Short Form of Its Receptor in the Ovary and Decidua: involvement of a novel phosphatase. *The Journal of Biological Chemistry*, 286(9):7609–7618, 03 2011. doi: 10.1074/jbc.M110.166603. URL `http://www.ncbi.nlm.nih.gov/pmc/articles/PMC3045015/`.

[221] Reinhardt, P., Schmid, B., Burbulla, L. F., Schöndorf, D. C., Wagner, L., Glatza, M., Höing, S., Hargus, G., Heck, S. A., Dhingra, A., Wu, G., Müller, S., Brockmann, K., Kluba, T., Maisel, M., Krüger, R., Berg, D., Tsytsyura, Y., Thiel, C. S., Psathaki, O. E., Klingauf, J., Kuhlmann, T., Klewin, M., Müller, H., Gasser, T., Schöler, H. R., and Sterneckert, J. Genetic Correction of a LRRK2 Mutation in Human iPSCs Links Parkinsonian Neurodegeneration to ERK-Dependent Changes in Gene Expression. *Cell Stem Cell*, 12 (3):354–367, 3 2013. doi: https://doi.org/10.1016/j.stem.2013.01.008. URL `http://www.sciencedirect.com/science/article/pii/S1934590913000118`.

[222] Bravo-San Pedro, J., Niso-Santano, M., Gómez-Sánchez, R., Pizarro-Estrella, E., Aiastui-Pujana, A., Gorostidi, A., Climent, V., López de Maturana, R., Sanchez-Pernaute, R., López de Munain, A., Fuentes, J., and González-Polo, R. A. The LRRK2 G2019S mutant exacerbates basal autophagy through activation of the MEK/ERK pathway. *Cellular and Molecular Life Sciences*, 70(1):121–136, 2013. doi: 10.1007/s00018-012-1061-y. URL `http://dx.doi.org/10.1007/s00018-012-1061-y`.

[223] Gloeckner, C. J., Schumacher, A., Boldt, K., and Ueffing, M. The Parkinson disease-associated protein kinase LRRK2 exhibits MAPKKK activity and phosphorylates MKK3/6 and MKK4/7, in vitro. *Journal of Neurochemistry*, 109(4): 959–968, 2009. ISSN 1471-4159. doi: 10.1111/j.1471-4159.2009.06024.x. URL `http://dx.doi.org/10.1111/j.1471-4159.2009.06024.x`.

[224] Wang, X., Yan, M. H., Fujioka, H., Liu, J., Wilson-Delfosse, A., Chen, S. G., Perry, G., Casadesus, G., and Zhu, X. LRRK2 regulates mitochondrial dynamics and function through direct interaction with DLP1. *Human Molecular Genetics*, 21(9):1931–1944, 05 2012. doi: 10.1093/hmg/dds003. URL `http://www.ncbi.nlm.nih.gov/pmc/articles/PMC3315202/`.

[225] Borman, M. A., Freed, T. A., Haystead, T. A. J., and MacDonald, J. A. The role of the calponin homology domain of smoothelin-like 1 (SMTNL1) in myosin phosphatase inhibition and smooth muscle contraction. *Molecular and cellular biochemistry*, 327(1-2):93–100, 07 2009. doi: 10.1007/s11010-009-0047-z. URL `http://www.ncbi.nlm.nih.gov/pmc/articles/PMC2846773/`.

[226] Hinits, Y., Williams, V. C., Sweetman, D., Donn, T. M., Ma, T. P., Moens, C. B., and Hughes, S. M. Defective cranial skeletal development, larval lethality and

105

haploinsufficiency in Myod mutant zebrafish. *Developmental biology*, 358(1):102–112, 10 2011. doi: 10.1016/j.ydbio.2011.07.015. URL http://www.ncbi.nlm.nih.gov/pmc/articles/PMC3360969/.

[227] Zhang, M., Chen, M., Kim, J. R., Zhou, J., Jones, R. E., Tune, J. D., Kassab, G. S., Metzger, D., Ahlfeld, S., Conway, S. J., and Herring, B. P. SWI/SNF Complexes Containing Brahma or Brahma-Related Gene 1 Play Distinct Roles in Smooth Muscle Development. *Molecular and Cellular Biology*, 31(13):2618–2631, 07 2011. doi: 10.1128/MCB.01338-10. URL http://www.ncbi.nlm.nih.gov/pmc/articles/PMC3133369/.

[228] Black, B. L. and Olson, E. N. Transcriptional control of muscle development by myocyte enhancer factor-2 (MEF2) proteins. *Annu Rev Cell Dev Biol*, 14:167–196, 1998. ISSN 1081-0706 (Print); 1081-0706 (Linking). doi: 10.1146/annurev.cellbio.14.1.167.

[229] Rudnicki, M. A., Schnegelsberg, P. N. J., Stead, R. H., Braun, T., Arnold, H.-H., and Jaenisch, R. MyoD or Myf-5 is required for the formation of skeletal muscle. *Cell*, 75(7):1351–1359, 1993. doi: http://dx.doi.org/10.1016/0092-8674(93)90621-V. URL http://www.sciencedirect.com/science/article/pii/009286749390621V.

[230] Zhou, P., He, A., Pu, W. T., and Bruneau, B. G. *Chapter five - Regulation of GATA4 Transcriptional Activity in Cardiovascular Development and Disease*, volume Volume 100, pages 143–169. Academic Press, 2012. ISBN 0070-2153. doi: https://doi.org/10.1016/B978-0-12-387786-4.00005-1. URL http://www.sciencedirect.com/science/article/pii/B9780123877864000051.

[231] Reyniers, L., Del Giudice, M. G., Civiero, L., Belluzzi, E., Lobbestael, E., Beilina, A., Arrigoni, G., Derua, R., Waelkens, E., Li, Y., Crosio, C., Iaccarino, C., Cookson, M. R., Baekelandt, V., Greggio, E., and Taymans, J.-M. Differential protein–protein interactions of LRRK1 and LRRK2 indicate roles in distinct cellular signaling pathways. *Journal of Neurochemistry*, 131(2):239–250, 2014. ISSN 1471-4159. doi: 10.1111/jnc.12798. URL http://dx.doi.org/10.1111/jnc.12798.

[232] Pellicano, C., Benincasa, D., Pisani, V., Buttarelli, F. R., Giovannelli, M., and Pontieri, F. E. Prodromal non-motor symptoms of Parkinson's disease. *Neuropsychiatric Disease and Treatment*, 3(1):145–152, 2007. ISSN 1176-6328 1178-2021. URL http://www.ncbi.nlm.nih.gov/pmc/articles/PMC2654529/.

[233] Politis, M. and Loane, C. Serotonergic Dysfunction in Parkinson's Disease and Its Relevance to Disability. *TheScientificWorldJournal*, 11:1726–1734, 2011. doi: 10.1100/2011/172893. URL http://www.ncbi.nlm.nih.gov/pmc/articles/PMC3201695/.

[234] Huot, P. and Fox, S. H. The serotonergic system in motor and non-motor manifestations of Parkinson's disease. *Experimental Brain Research*, 230(4):463–476, 2013. doi: 10.1007/s00221-013-3621-2. URL http://dx.doi.org/10.1007/s00221-013-3621-2.

[235] Wile, D. J., Agarwal, P. A., Schulzer, M., Mak, E., Dinelle, K., Shahinfard, E., Vafai, N., Hasegawa, K., Zhang, J., McKenzie, J., Neilson, N., Strongosky, A.,

Uitti, R. J., Guttman, M., Zabetian, C. P., Ding, Y. S., Adam, M., Aasly, J., Wszolek, Z. K., Farrer, M., Sossi, V., and Stoessl, A. J. Serotonin and dopamine transporter PET changes in the premotor phase of *LRRK2* parkinsonism: cross-sectional studies. *The Lancet Neurology*, 16(5):351–359, 04/20 2017. doi: 10.1016/ S1474-4422(17)30056-X. URL `http://dx.doi.org/10.1016/S1474-4422(17) 30056-X`.

[236] Bonifati, V. LRRK2 low-penetrance mutations (Gly2019Ser) and risk alleles (Gly2385Arg)-linking familial and sporadic Parkinson's disease. *Neurochem Res*, 32(10):1700–8, 2007. ISSN 0364-3190 (Print) 0364-3190. doi: 10.1007/s11064-007-9324-y.

[237] Arranz, A. M., Delbroek, L., Van Kolen, K., Guimarães, M. R., Mandemakers, W., Daneels, G., Matta, S., Calafate, S., Shaban, H., Baatsen, P., De Bock, P. J., Gevaert, K., Vanden Berghe, P., Verstreken, P., De Strooper, B., and Moechars, D. LRRK2 functions in synaptic vesicle endocytosis through a kinase-dependent mechanism. *Journal of Cell Science*, 128(3):541–552, 2015. doi: 10.1242/jcs. 158196.

[238] Dias, V., Junn, E., and Mouradian, M. M. The Role of Oxidative Stress in Parkinson's Disease. *Journal of Parkinson's disease*, 3(4):461–491, 2013. ISSN 1877-7171 1877-718X. doi: 10.3233/JPD-130230. URL `http://www.ncbi.nlm.nih.gov/ pmc/articles/PMC4135313/`.

[239] Mallajosyula, J. K., Kaur, D., Chinta, S. J., Rajagopalan, S., Rane, A., Nicholls, D. G., Di Monte, D. A., Macarthur, H., and Andersen, J. K. MAO-B Elevation in Mouse Brain Astrocytes Results in Parkinson's Pathology. *PLoS ONE*, 3(2): e1616, 2008. ISSN 1932-6203. doi: 10.1371/journal.pone.0001616. URL `http: //www.ncbi.nlm.nih.gov/pmc/articles/PMC2229649/`.

[240] Yoles, E., Hauben, E., Palgi, O., Agranov, E., Gothilf, A., Cohen, A., Kuchroo, V., Cohen, I. R., Weiner, H., and Schwartz, M. Protective autoimmunity is a physiological response to CNS trauma. *J Neurosci*, 21(11):3740–8, 2001. ISSN 0270-6474.

[241] Ohnmacht, J., Yang, Y., Maurer, G. W., Barreiro-Iglesias, A., Tsarouchas, T. M., Wehner, D., Sieger, D., Becker, C. G., and Becker, T. Spinal motor neurons are regenerated after mechanical lesion and genetic ablation in larval zebrafish. *Development (Cambridge, England)*, 143(9):1464–1474, 2016. ISSN 0950-1991 1477-9129. doi: 10.1242/dev.129155. URL `http://www.ncbi.nlm.nih.gov/pmc/articles/ PMC4986163/`.

[242] Wright, M. A., Mo, W., Nicolson, T., and Ribera, A. B. In vivo evidence for transdifferentiation of peripheral neurons. *Development (Cambridge, England)*, 137(18):3047–3056, 2010. ISSN 0950-1991 1477-9129. doi: 10.1242/dev.052696. URL `http://www.ncbi.nlm.nih.gov/pmc/articles/PMC2926955/`.

[243] Choi, I., Kim, B., Byun, J. W., Baik, S. H., Huh, Y. H., Kim, J. H., Mook Jung, I., Song, W. K., Shin, J. H., Seo, H., Suh, Y. H., Jou, I., Park, S. M., Kang, H. C., and Joe, E. H. LRRK2 G2019S mutation attenuates microglial motility by inhibiting focal adhesion kinase. *Nature Communications*, 6:8255, 2015. ISSN

2041-1723. doi: 10.1038/ncomms9255. URL `http://www.ncbi.nlm.nih.gov/pmc/articles/PMC4647842/`.

[244] Crane, P. K., Gibbons, L. E., Dams-O'Connor, K., Trittschuh, E., Leverenz, J. B., Keene, C. D., Sonnen, J., Montine, T. J., Bennett, D. A., Leurgans, S., Schneider, J. A., and Larson, E. B. Association of Traumatic Brain Injury With Late-Life Neurodegenerative Conditions and Neuropathologic Findings. *JAMA Neurol*, 73 (9):1062–9, 2016. ISSN 2168-6149. doi: 10.1001/jamaneurol.2016.1948.

[245] Cruts, M., Theuns, J., and Van Broeckhoven, C. Locus-specific mutation databases for neurodegenerative brain diseases. *Hum Mutat*, 33(9):1340–4, 2012. ISSN 1059-7794. doi: 10.1002/humu.22117.

[246] Nuytemans, K., Theuns, J., Cruts, M., and Van Broeckhoven, C. Genetic etiology of Parkinson disease associated with mutations in the SNCA, PARK2, PINK1, PARK7, and LRRK2 genes: a mutation update. *Hum Mutat*, 31(7):763–80, 2010. ISSN 1059-7794. doi: 10.1002/humu.21277.

Glossary

6-OHDA	6-HydroxyDopAmine
AD	Alzheimer's Disease
aTIS	alternative Translation Initiation Site
BrdU	5-bromo-2'-deoxyuridine
CA	CatecholAmine/CatecholAminergic
cDNA	complementary DNA
CI	Confidence Interval
Comt	Catechol-O-methyl transferase
CRISPR/Cas9	Clustered Regularly Interspaced Short Palindromic Repeats/CRISPR associated protein 9
cTIS	canonical Translation Initiation Site
CUBIC	Clear, Unobstructed Brain/Body Imaging Cocktails and Computational analysis; see Table 3.4
DAPI	4',6-diamidino-2-phenylindole, dihydrochloride
DEG	Differentially-Expressed Gene
DEPC	DiEthylPyroCarbonate; see Table 3.4
DIG	DIGoxigenin
DIG-AP	DIG-Alkaline Phosphatase conjugated
DMSO	DiMethyl SulphOxide; see Table 3.4
DNA	DeoxyriboNucleic acid
dpf	days post-fertilisation
DUSP	DUal Specific Phosphatase
EDAC	N-Ethyl-N'-(3-DimethylAminopropyl)Carbodiimide hydrochloride; see Table 3.4
EDTA	EthyleneDinitriloTetraAcetic acid; see Table 3.4
ENU	N-Ethyl-N-NitrosoUrea

ERK	Extracellular signal-Regulated Kinase
EtOH	Ethanol; see Table 3.4
FDR	False Discovery Rate
FFW	Fish Facility Water
for	forward primer
gDNA	genomic DNA
GOF	gain of function
GO	Gene Ontology
hpf	hours post-fertilisation
Hyb+	Hybridisation+ Buffer; see Table 3.4
Hyb−	Hybridisation− Buffer; see Table 3.4
i-PrOH	Isopropanol; see Table 3.4
IHC	ImmunoHistoChemistry
IPA	Ingenuity Pathway Analysis
ISH	*in situ* hybridisation
LOF	loss of function
LRRK2	Leucine Rich Repeat Kinase 2
MAB	Maleic Acid Buffer; see Table 3.4
MABT	MAB-Tween 20; see Table 3.4
Mao	Monoamine oxidase
MAP(K)n	Mitogen Activated Protein $(\text{Kinase})_n$
MEF	Myocyte-specific Enhancer Factor
MESAB	ethyl 3-aminobenzoate methanesulfonate; see Table 3.4
MetOH	Methanol; see Table 3.4
MO	Morpholino
mo	months old
MPDP$^+$	1-Methyl-4-Phenyl-2,3-DihydroPyridinium
MPP$^+$	1-Methyl-4-PhenylPyridinium
MPTP	1-Methyl-4-Phenyl-1,2,3,6-TetrahydroPyridine

MYOD	MYOgenic Differentiation
mz	maternal zygotic
NBT/BCIP	Nitro Blue Tetrazolium chloride/5-Bromo-4-Chloro-3-Indolyl Phosphate, toluidine salt
NGS	Normal Goat Serum; see Table 3.4
NHS	N-HydroxySuccinimide; see Table 3.4
NMD	Nonsense-Mediated Decay
o/n	overnight
OR	Odds Ratio
ORF	Open Reading Frame
PB	Phosphate Buffer; see Table 3.4
PBS	Phosphate Buffer Saline; see Table 3.4
PBST	PBS-Tween 20; see Table 3.4
PBSTx	PBS-Triton X-100; see Table 3.4
PCNA	Proliferating Cell Nuclear Antigen
PCR	Polymerase Chain Reaction
PD	Parkinson's Disease
PFA	Paraformaldehyde; see Table 3.4
pHH3	phosphoHistone H3
PTC	Premature Termination Codon
rev	reverse primer
RFLP	Restriction Fragment Length Polymorphism
RNA	RiboNucleic Acid
RT	Room Temperature
RT-(q)PCR	Reverse Transcriptase-(quantitative) PCR
s.d.	standard deviation
sgRNA	single guide RNA
SMARCA	SWI/SNF-related, Matrix-associated, Actin-dependent Regulator of Chromatin
SMTLN	SMooTheLiN

SSC   see Table 3.4

Ta annealing temperature

TAE   Tris base, EDTA, Acetic acid; see Table 3.4

TALEN   Transcription Activator-Like Effector Nucleases

TCM   TriChloroMethane; see Table 3.4

TH   Tyrosine hydroxylase

TILLING   Targeting Induced Local Lesions in Genomes

TPA   12-O-TetradecanoylPhorbol 13-Acetate

TUNEL   Terminal deoxynucleotidyl transferase dUTP Nick End Labeling

wt wild-type

Erklärung entsprechend §5.5 der Promotionsordnung/Declaration according to §5.5 of the doctorate regulations

Hiermit versichere ich, dass ich die vorliegende Arbeit ohne unzulässige Hilfe Dritter und ohne Benutzung anderer als der angegebenen Hilfsmittel angefertigt habe; die aus fremden Quellen direkt oder indirekt übernommenen Gedanken sind als solche kenntlich gemacht. Die Arbeit wurde bisher weder im Inland noch im Ausland in gleicher oder ähnlicher Form einer anderen Prüfungsbehörde vorgelegt.

Die Dissertation wurde im Zeitraum vom 1 Nov, 2012 bis 20 Mai, 2017 verfasst und von Prof. Dr. Michael Brand, Center for Regenerative Therapies Dresden betreut.

Meine Person betreffend erkläre ich hiermit, dass keine früheren erfolglosen Promotionsverfahren stattgefunden haben.

Ich erkenne die Promotionsordnung der Fakultät für Mathematik und Naturwissenschaften, Technische Universität Dresden an.

I herewith declare that I have produced this paper without the prohibited assistance of third parties and without making use of aids other than those specified; notions taken over directly or indirectly from other sources have been identified as such. This paper has not previously been presented in identical or similar form to any other German or foreign examination board.

The thesis work was conducted from 1 Nov, 2012 to 20 May, 2017 under the supervision of Prof. Dr. Michael Brand at Center for Regenerative Therapies Dresden.

I declare that I have not undertaken any previous unsuccessful doctorate proceedings.

I declare that I recognise the doctorate regulations of the Fakultät für Mathematik und Naturwissenschaften of the Technische Universität Dresden.

Datum/Date: .... Unterschrift/Signature: ....